Fakultät für Medizin

Klinik und Poliklinik für Innere Medizin II

Translational Applications of a Modified Organoid Culture System from Pancreatic Cancer Patients

Zahra Dantes

Vollständiger Abdruck der von der Fakultät für Medizin der Technischen Universität München zur Erlangung des akademischen Grades eines

Doctor of Philosophy (Ph.D.)

genehmigten Dissertation.

Vorsitzender: Prof. Dr. Dr. Stefan Engelhardt

Betreuer/in: TUM Junior Fellow Dr. Maximilian Reichert

Prüfer der Dissertation:

1. Prof. Dr. Roland M. Schmid

2. apl. Prof. Dr. Güralp O. Ceyhan

Die Dissertation wurde am 15.01.2019 bei der Fakultät für Medizin der Technischen Universität München eingereicht und durch die Fakultät für Medizin am 16.07.2019 angenommen.

I would like to dedicate this doctoral thesis to the memory of our patients.

Abbreviations

2D - Two-Dimensional

3D - Three-Dimensional

5-FU - 5-Fluorouracil

AUC- Area Under the Curve

bFGF - basic Fibroblast Growth Factor

BPE - Bovine Pituitary Extract

BRCA 1,2,3 - BReast Cancer 1,2,3

CDKN2A - Cyclin-Dependent Kinase Inhibitor 2A

Chr. - Chromosome

CNV - Copy Number Variation

Conc. - Concentration

CRISPR - Clustered Regularly Interspaced Short Palindromic Repeats

CYP3A5 - Cytochrome P450 Family 3 Subfamily A Member 5

DAB - 3,3'-diaminobenzidine

ddPCR - digital droplet Polymerase Chain Reaction

DMEM - Dulbecco's Modified Eagle's Medium

ECM - Extracellular Matrix

EGF - Epidermal Growth Factor

EHS - Engelbreth-Holm-Swarm

EMT - Epithelial-Mesenchymal Transition

EUS-FNAs - Endoscopic Ultrasound-guided Fine Needle Aspirations

FBS - Fetal Bovine Serum

^{18}F-FDG - Fluorodeoxyglucose

FDR - False Discovery Rate

FFPE - Formalin-Fixed Paraffin-Embedded

FGF 10 - Fibroblast Growth Factor

FM - Freezing Medium

FNA - Fine Needle Aspiration

GEMMs - Genetically Engineered Mouse Models

GFR - Growth Factor Reduced

GSEA - Gene Set Enrichment Analysis

hFNA - Human FNA

hRT - Human Resected Tumor

IC-50 - Half Maximal Inhibitory Concentration

IF - Immunofluorescence

IHC - Immunohistochemistry

KRAS - Kirsten Rat Sarcoma viral oncogene homolog

KRT81 - Keratin 81

MAF - Mutant Allele Frequency

MBq - Megabecquerel

Min. - Minutes

MRI - Magnetic Resonance Imaging

MSCT - Multi-Slice Computed Tomography

NFM - Normal Feeding Medium

NFMm - Normal Feeding Medium modified

NET- Neuroendocrine Tumor

NGS - Next Generation Sequencing

OR - Operation Room

OS - Overall Survival

PanIN - Pancreatic Intraepithelial Neoplasia

PARP - Poly (ADP-Ribose) Polymerase

PBS - Phosphate-Buffered Saline

PC - Pancreatic Cancer

PCR - Polymerase Chain Reaction

PDAC - Pancreatic Ductal Adenocarcinoma

PDGF - Platelet-Derived Growth Factor

PDO - Patient-Derived Organoid

PDO-SN - PDO-Supernatant

PDOX - Patient Derived Organoid Xenograft

PDX - Patient-Derived Xenograft

Pdx1 - Pancreatic and duodenal homeobox

Pen/Strep (P/S) - Penicillin-Streptomycin

PET - Positron-Emission-Tomography

PFA - Paraformaldehyde

PFS - Progression-Free Survival

PGE-2 - Prostaglandin E2

PT - Primary Tumor

Ptf1a - Pancreas transcription factor 1 subunit alpha

Res. - Resection

RNA-seq. - RNA sequencing

ROCK - Rho-associated protein kinase

RPM - Revolutions Per Minute

R-Spo - R-Spondin

RT- Room Temperature

SC - Subcutaneously

SMAD4 - Mothers against decapentaplegic homolog 4

α-SMA - alpha Smooth Muscle Actin

SN - Supernatant

STI - Soybean Trypsin Inhibitor

TGF-β - Transforming Growth Factor beta

TP53 - Tumor Protein p53

Vs. - Versus

WES - Whole Exome Sequencing

WT - Wild Type

Table of Contents

List of tables

SUMMARY

For the year 2030, it is estimated that the number of cancer deaths caused by pancreatic ductal adenocarcinoma (PDAC) will surpass colorectal and breast cancer. One of the main reasons for this development, besides demographic changes, is resistance to chemotherapy. Because of the molecular and morphological tumor heterogeneity leading to dismal responses to chemotherapeutic approaches and diverse clinical outcomes, better and efficient strategies for personalized assays are urgently needed. To this end, a living patient-derived organoid (PDO) biobank was established. Utilizing three-dimensional organoid culture derived from 39 surgical specimens and 41 endoscopic ultrasound-guided fine needle aspirations (EUS-FNA), the PDO repository was generated with a take rate of 97% from surgical specimens and 75% from EUS-FNAs.

Due to the immense costs of established organoid media supplements, a more cost-effective alternative media composition was generated that can be used to generate pancreatic cancer patient-derived organoids (PDOs) from PDAC patients successfully. The new established media was called normal feeding media modified (NFMm) and was validated to the established NFM media (Boj et al., 2015) using multilayered bioassays assessing take rate, proliferation, viability, morphology. PDOs were also compared based on orthotopic transplantation (patient-derived organoid xenografts; PDOX), whole-exome and RNA sequencing and most importantly sensitivity towards chemotherapy. Interestingly, the PDOs generated with NFMm media were comparable with PDOs generated with NFM media in all settings.

The PDOs withstand freeze-thaw cycles and functional assays can be implemented within 2-6 weeks post-isolation. Drug-screens were performed using conventional chemotherapeutic drugs such as gemcitabine, 5-fluorouracil (5-fu), oxaliplatin, cisplatin, carboplatin, irinotecan, paclitaxel and bortezomib. Most importantly, drug screens of PDOs revealed that PDOs mirror the intertumoral heterogeneity and correlate with clinical parameters. For instance, patients, whose corresponded PDOs were resistant towards gemcitabine, displayed a mean progression-free survival (PFS) of 50 days compared to the expected PFS of 180 days. Whereas, patients with gemcitabine-sensitive PDOs showed a mean PFS of 200 days.

Additional evidence which underscores the fact that PDO serves as predictive model system in terms of treatment response as well as mimicking the biology of PDAC *in situ* was a patient with *PALB2* germline mutation. It has been demonstrated that mutations in DNA-repair genes (*BRCA1*, *BRCA2*, *PALB2*) display increased sensitivity towards platinum-based chemotherapy and PARP inhibition. Indeed, one study patient with familial pancreatic cancer due to a *PALB2*

germline mutation showed an outstanding clinical response towards a platinum-based chemotherapy. PDOs that have been derived after therapy have been treated with PARP inhibitors. Remarkably, this *PALB2*-mutated organoid line showed a significant response to olaparib whereas *PALB2*-wildtype organoids showed no response even at the highest concentration.

In this study, PDOs were also used as model system for diagnosis, genetic characterization as well as drug screening platform in a rapid and clinically relevant time-frame. In this PDO repository, the cytology and/or histology of 42% of EUS-FNA samples with established PDOs failed to designate a definitive diagnosis. The next aim was to investigate the potential of PDO technology as a diagnostic tool, which could be able to maximize the information that could be extracted from a single biopsy. Findings of this study could clearly indicate the remarkable potential of PDO technology to generate enough material from very small starting material (few tumor cells) that were undetectable by cytology as well from EUS-FNAs with a negative cytology (cytology negative-PDOs) to perform functional *in vivo* assays. For instance, the cytology negative-PDOs could give rise to tumors upon orthotopic transplantation in nude mice (PDOX). Furthermore, primary tumor (PT), PDOs and PDOXs could be subtyped by IHC staining based on HNF1A- and KRT81- expression. Notably, the cytology negative-PDOs displayed the mutational profile of PDAC as well as other additional genetic mutations.

Most importantly, the next aim was to reduce the time required for the PDO-augmented diagnosis and molecular characterization of PDAC, which is one of the most challenging tasks in this field. The hypothesis was that the cell-free-DNA (cfDNA) is released from PDOs very soon after PDO isolation, which could be used to detect mutations of the corresponding PDAC patient which might be potentially druggable. To this end, cfDNA of the PDO supernatant (PDO-SN) was subjected to digital-droplet PCR (ddPCR) as well as next generation sequencing (NGS) for genomic characterization. Interestingly, performing sequencing on cfDNA from PDO-SN could retrieve the same mutational profile of corresponding PT and PDO suggesting that cfDNA in PDO supernatant can serve as valuable resource for precision medicine in pancreatic cancer.

Taken together, this novel established organoid culture system appears to be predictive for clinical response. In addition, the modified and affordable culture protocol makes this model system accessible to the entire scientific community in the field of pancreatic cancer and might be useful clinically at a large scale. Findings of this study also suggest that generating PDOs from a single EUS-FNA enhances the diagnostic accuracy and allows molecular subtyping and drug testing which can be achieved in a swift and practicable fashion with implications in clinical practice.

I. Clinical challenges in pancreatic cancer

1.1. The high and growing number of deaths from pancreatic cancer

Pancreatic ductal adenocarcinoma (PDAC) accounts for over 90% of pancreatic cancers and is one of the most aggressive solid tumors (Garrido-Laguna and Hidalgo, 2015) with the lowest five-year survival rate of 8% for cancers (Siegel et al., 2018). Despite advancements in pancreatic cancer research, the number of pancreatic cancer related deaths is dramatically on the rise and PDAC is projected to be the second cause of cancer-related deaths after lung cancer by 2030 (Rahib et al., 2014; Quante et al., 2016) (Fig. 1). The reasons for this alarming development of pancreatic cancer besides demographic changes are dependent on several factors such as late diagnosis, fast progression of the tumor leading to metastasis to other organs, resistance to chemotherapy, as well as a lack of targeted therapeutic approaches (Oberstein and Olive, 2013; Rahib et al., 2014). In order improve the outcomes of PDAC, an early diagnosis is mandatory and in addition more effective therapies are urgently required (Hidalgo et al., 2015).

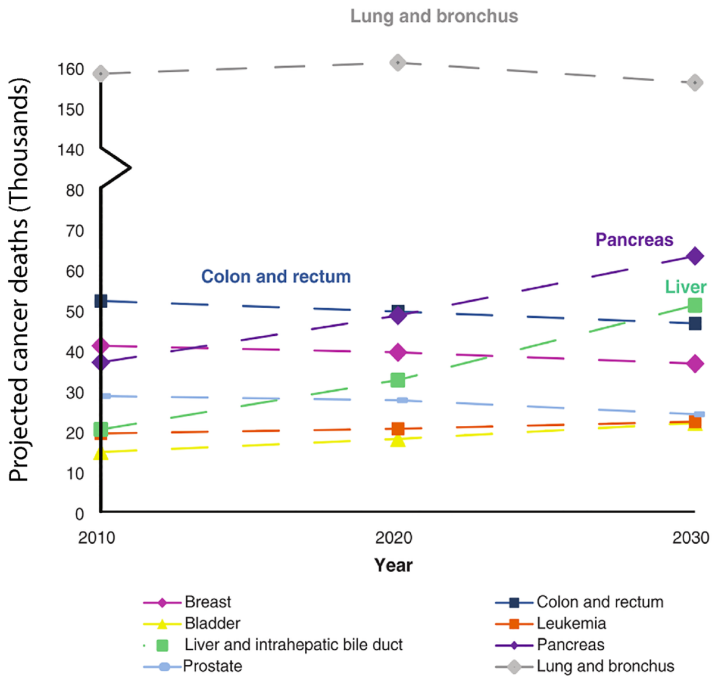

Figure 1. Death projections of the most common cancer related deaths (taken from Rahib et al., 2014).

1.2. Genetic heterogeneity

Genetically, PDAC is a very complex disease due to a high variety of mutations and this genetic heterogeneity of pancreatic cancer is one of the important factors causing conventional therapies to fail. Compared to mutations observed in other solid cancers, the mutations present in PDAC patients rarely exceed a frequency beyond a few percent (Fig. 2), and in addition, the most frequently mutated candidates in PDAC such as *KRAS*, *TP53*, *CDKN2A* and *SMAD4* are not druggable to this date (Cowley et al., 2013). Therefore, individualized treatment strategies might be the only way to improve patient survival.

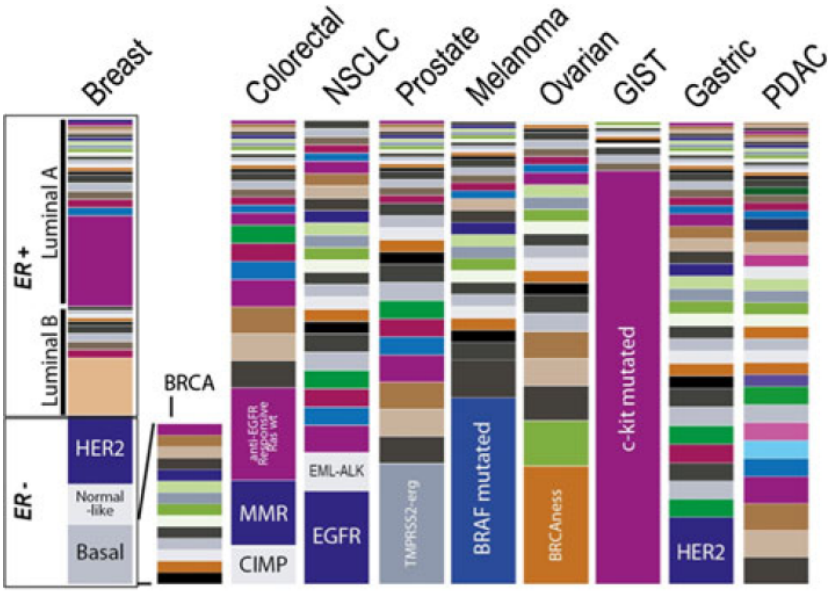

Figure. 2. Sub-classification of divergent cancers based on molecular phenotypes (taken from Cowley et al., 2013).

II. Current chemotherapeutic options for pancreatic cancer patients

Since 1997 and for more than a decade, gemcitabine has been the first-line of treatment for advanced PDAC (Burris et al., 1997). The advantage of gemcitabine in comparison to fluorouracil (5-FU) has been reported in many studies. An increase in median overall survival (OS) in patients treated with gemcitabine versus 5-FU patients (5.65 months vs. 4.41 months) was observed by Burris et al. In addition, gemcitabine patients showed a survival rate of 18% vs.

2% survival rate in 5-FU patients at 12 months. Furthermore, gemcitabine was well tolerated (Burris et al., 1997). Combining gemcitabine with additional cytotoxic drugs such as oxaliplatin (Louvet et al., 2005; Poplin et al., 2009; Ruess et al., 2017), Irinotecan (Rocha Lima et al., 2004; Stathopoulos et al., 2006; Ruess et al., 2017), cisplatin (Colucci et al., 2002; Heinemann et al., 2006; Colucci et al., 2010; Ruess et al., 2017) or pemetrexed (Oettle et al., 2005; Ruess et al., 2017) did not increase the OS in unselected populations and have not been integrated into clinical routines. In 2011, FOLFIRINOX, which is a multidrug regimen combination of fluorouracil, irinotecan, oxaliplatin and leucovorin, increased OS as well as progression free survival (PFS) compared to gemcitabine (11.1 versus (vs.) 6.8 months and 6.4 months vs. 3.3 months respectively) (Ychou et al., 2003; Conroy et al., 2011). In 2013, a significant response regarding combination treatment of nab-paclitaxel (albumin-bound paclitaxel) and gemcitabine was observed (Von Hoff et al., 2013). An improvement in the median overall survival (mOS) as well as PFS (8.5 months vs. 6.7 months and 5.5 months vs. 3.7 months respectively) was noted in patients treated with nab-paclitaxel combined with gemcitabine compared to patients who were treated with gemcitabine alone (Von Hoff et al., 2013).

III. Pancreatic cancer subtypes

Because of the high inter- and intra-tumoral heterogeneity present in pancreatic cancer, it cannot be recognized and treated as one disease (Torres and Grippo, 2018)

Subtyping of pancreatic cancer has made a significant progress over the past 5 years (Torres and Grippo, 2018) . Based on expression of transcription factors and downstream targets or the distribution of structural rearrangements, pancreatic cancer has been classified into four main molecular subtypes (Du et al., 2017).

Collisson subtyping was the first molecular subtyping in 2011. By performing combined analysis of the transcriptional profiles of primary PDAC samples from different studies, in addition to the human and mouse PDAC cell lines, they identified three subtypes including: classical, quasi-mesenchymal (QM), and exocrine-like. Regarding drug response and identifying predictive biomarkers, they could show that the classical subtype PDAC cell line is more dependent on *KRAS* compared to the QM-PDA cell line, indicating that the classical subtype might get the most benefit from KRAS-directed therapy. In addition, they also could show that the quasi-mesenchymal PDAC cell lines were more sensitive to gemcitabine, whereas the classical subtype cell lines show a high sensitivity towards erlotinib (Collisson et al., 2011; Du et al., 2017).

In 2015, Moffitt and colleagues could separate the epithelial compartment from the stromal compartment using virtual microdissection. By investigating the tumor- and stroma-specific gene expression, they could classify PDAC into four distinict subtypes with prognostic relevance. These subtypes include: classical and basal-like tumor subtypes and normal and activated stromal subtypes. Basal-like and classical tumors have been observed in both normal and activated stromal subtypes, and therefore 4 molecular PDAC subtypes were identified: classical tumor and normal stroma, classical tumor and activated stroma, basal-like tumor and normal stroma, basal-like tumor and activated stroma. Furthermore, they also could show that patients with the activated stromal subtype or basal-like tumor subtype have a worse median survival time and 1-year survival rate than those with the normal stromal subtype or classical tumor subtype. In contrast to that, patients with basal-like tumors showed a better response to adjuvant therapy (Moffitt et al., 2015; Du et al., 2017).

Importantly, we could also apply Moffitt subtyping to our PDOs and show the classical and basal subtype which was also showed by Tiriac and colleagues (Tiriac et al., 2018a).

Another PDAC subtyping based on integrated genomic analysis of 456 PDAC tumors was identified by Bailey et al. These subtypes include squamous, pancreatic progenitor, immunogenic and aberrantly differentiated endocrine exocrine (ADEX), on the basis of the differential expression of transcription factors and downstream targets which are important in lineage specification and differentiation during pancreas development and regeneration. The squamous subtype was determined to be an independent prognostic factor for poor survival (Bailey et al., 2016; Du et al., 2017).

In 2015, Waddell and colleagues performed whole-genome sequencing and copy number variation (CNV) analysis of PDACs and they could show a high commonness of chromosomal rearrangements. Based on structural variations, PDAC was subtyped into 4 subtypes including subtype 1 which is called stable (≤50 structural variation), subtype 2 is a locally rearranged subtype (significant focal events on one or two chromosomes), subtype 3 or scattered subtype (moderate range of non-random chromosomal damage as well as less than 200 structural variation events) and subtype 4 or unstable (large number of structural variation events, more than 200). This genomic instability indicates defects in DNA maintenance, and therefore suggests sensitivity to DNA-damaging agents (Waddell et al., 2015; Du et al., 2017).

In 2016, an additional type of PDAC subtyping was reported (Noll et al., 2016). Noll and colleagues identified two markers including HNF1A and KRT81, enabling stratification of tumors into different subtypes by immunohistochemistry. These known different subtypes show diverse

overall survival and different sensitivity towards treatment. Exocrine-like subtype displayed resistance to tyrosine kinase inhibitors and paclitaxel, and this phenotype is mediated by cytochrome P450 3A5 (CYP3A5) which metabolizes these compounds in tumors of the exocrine-like subtype and is regulated by HNF4A and NR1I2 expression. In addition, CYP3A5 helps to develop an acquired drug resistance in QM and classical PDAC and is highly expressed in many other malignancies. The basal expression of CYP3A5 is mediated by hepatocyte nuclear factor 4 alpha (HNF4A), whereas drug-induced CYP3A5 upregulation is controlled by the nuclear receptor NR1I2. Finally, their findings suggested CYP3A5 as a predictor for the therapy response and as a tumor cell-autonomous detoxification system that must be controlled in order to prevent the drug resistance (Noll et al., 2016; Du et al., 2017).

Interestingly, in this project we could also apply the abovementioned subtyping to the primary tumors and PDOs, as well as PDOXs, and we were able to demonstrate different subtypes.

IV. Pre-clinical models of PDAC

Despite our immense understanding of PDAC biology, disease initiation and progression, translation of this information from bench to bedside in order to improve the patient outcome is lacking. All improvements thus far were based on toxicity escalation by oncologists and not scientifically driven, therefore they led to limited success in improving treatments. Consequently, pre-clinical models that can be used to generate hypotheses that can then be tested in the clinic are required. To this end, an appropriate model system which can recapitulate the human disease is urgently needed, since many cancer models very poorly mimic the parental tumor from which they are derived (Drost and Clevers, 2018).

4.1. *In vivo* models of PDAC

4.1.1. Genetically engineered mouse models (GEMMs)

PDAC is distinguished by four common mutated genes comprising of *KRAS*, *TP53*, *CDKN2A* and *SMAD4.* In order to mimic the biology of PDAC in mice, mutations were therefore introduced into mice via genetic engineering techniques that can either activate or silence gene expression (Moreira et al., 2018). Virtually all GEMMs utilize *KRAS* and *TP53* mutations. Pancreas-specific cre-lines (e.g., *Pdx1*-Cre or *Ptf1a*-Cre) in combination with a mutant allele of

Kras^{G12D} and loss of *TP53* (Hingorani et al., 2003; Hingorani et al., 2005; Moreira et al., 2018) are applied to generate the most common mouse models of PDAC resembling the human disease with a high accuracy. GEMMs offer an excellent approach to study disease progression from early stages (even pancreatic intraepithelial neoplasia (PanIN)) through to primary and metastatic PDAC (Perez-Mancera et al., 2012). Some benefits of this model include the spontaneous developments of the tumor, the preservation of the interaction between tumor and stroma and investigation the biology of metastasis, since GEMMs harbor an intact immune system. Although GEMMs act as powerful tools to increase our knowledge of tumor biology as well as to investigate disease initiation and progression, they are often high cost- and time-consuming to breed (Moreira et al., 2018). In addition, the mutations of targeted genes have been introduced into the germline of the mouse, whereas in human tumors they develop somatically (Moreira et al., 2018). Furthermore, although GEMMs of PDAC display a desmoplastic stroma, they do not represent the extreme levels observed in human pancreatic cancer. Of real concern is the fact that the difference might have an important impact on the biology as well as the response to therapy in GEMMs especially in the setting of preclinical therapeutic studies (Westphalen and Olive, 2012).

4.1.2. Xenografts

As prefix “XENO” denotes something foreign, the xenograft model describes a graft of tissue or cells which are taken from a donor of one species and are grafted into a recipient of another species.

Xenograft mouse models of pancreatic cancer achieve tumor generation by transplantation of either cancer cells or implanting of the patient tumors orthotopically or ectopically into immune-compromised mice.

4.1.2.1. Generation of xenografts from cell-lines

Xenograft generation based on cell-lines involves the injection of human cancer cell lines orthotopically or ectopically (usually subcutaneously (sc)) into immune-deficient mice that facilitates generation of a tumor in a three-dimensional (3D) structure which better mimics human tumors (Hwang et al., 2016). The advantage of this model compared to *in vitro* cell lines is a better representation of the human tumors due to recruiting of host stromal microenvironment, however difficulties regarding therapeutic responses and fidelity in several studies have been reported (Voskoglou-Nomikos et al., 2003; Peterson and Houghton, 2004; Philip et al., 2010; Kondo et al., 2011). An important factor that might contribute to the lack of predictive therapeutic responses of

xenografts is the lack of interaction of human neoplastic cells with the immune cells (Frese and Tuveson, 2007).

4.1.2.2. Patient-derived tumor xenografts (PDTX)

It has been reported that PDTX models predict therapeutic responses better than traditional xenografts (Hwang et al., 2016). Since in PDTX the freshly resected tumor specimens are directly orthotopically or ectopically (usually subcutaneously) transplanted into immune-deficient mice, they represent a faithful spectrum of individual tumor (Tentler et al., 2012; Jung et al., 2016). PDTX grow progressively, preserving their original genetic and histological profiles and conserving partially their parental tumor heterogeneity (Daniel et al., 2009; Jin et al., 2010; Tentler et al., 2012). Despite all advantages, there are several caveats for using xenografts as preclinical models for human cancers. The disadvantages include the lack of tumor-immunity and the fact that the tumor-host interaction is not always conserved across species (Caponigro and Sellers, 2011). Furthermore, PDTX establishment require a large amount of tissue and it is time and cost consuming (Rubio-Viqueira et al., 2006; Wang et al., 2017). Most importantly, utilizing PDTX for testing drugs especially in the field of pancreatic cancer is very time consuming, because even for the first generation of PDTX approximately 6 months would be required (Rubio-Viqueira et al., 2006; Hwang et al., 2016).

4.2. *In vitro* models of PDAC

4.2.1. Monolayer cell lines (two-dimensional (2D) cultures)

In adherent two-dimensional (2D) cultures, cells grow as a monolayer on a plastic surface in a culture flask or in a flat petri dish (Breslin and O'Driscoll, 2013).

The first human PDAC cell line was established in 1963 (Dobrynin, 1963) and since then numerous PDAC cell lines have been generated from human as well as murine tumors (Moreira et al., 2018).

In general, working with cell lines has several advantages compared to the other cancer models such as easy propagation, growing in simple media (therefore cheaper) and allowing high-throughput drug screens. However, monolayer cell lines suffer from various limitations.

Firstly, most of the studies in the field of PDAC research were performed based on utilizing a restricted number of cell lines (15 PDAC cell lines) (Ruckert et al., 2012) which do not

recapitulate the entire mutational profile of PDAC patients. In addition, since many cell lines have been established from metastatic sites as well as fast growing tumors, both primary PDAC as well as slow growing tumors were underrepresented (Hwang et al., 2016). Furthermore, the culture and maintenance of normal pancreatic ductal cells in 2D culture is very challenging, making the comparison between normal and tumor cells mostly impossible (Moreira et al., 2018). Secondly, since 2D cell lines grow as monolayer, they lose the structural organization as well as functional differentiation which is represented in vivo (Froeling et al., 2010). Thirdly, because of the absence of a tumor microenvironment and other cell types (fibroblasts, endothelial cells, immune cells, adipocytes and nerves), cell-cell and cell-matrix interactions will not be recapitulated (Moreira et al., 2018). Fourthly, it has been reported in many studies that 2D cell lines show a different expression profile compared to the primary tumor as well as xenografts (Deer et al., 2010; Gadaleta et al., 2011) suggesting growth of aggressive sub-clones (Gillet et al., 2013). In addition to the loss of tumor heterogeneity in 2D culture, genetic drift has been also reported (Deer et al., 2010).

4.2.2. Three-dimensional (3D) cultures

The introduction of *in vitro* three-dimensional (3D) culturing of normal cells as well as their malignant correspondent was introduced as early as the 1970s (Rimann and Graf-Hausner, 2012). Since few years a person-specific 3D culture termed organoids, “organ buds in a dish”, by Hans Clevers was developed (Clevers, 2016). The organoid technology involves growing of cells which are isolated directly from primary tissues, pluripotent stem cells (PSCs), induced pluripotent stem cells (iPSCs), pluripotent embryonic stem cells (ESCs) and organ-restricted adult stem cells (ASCs) in a 3D structure (Clevers, 2016). Organoids have the potential for self-renewal and self-organization, while maintaining the characteristics of the primary tissue from which they were derived including both appearance and function. Recapitulating the tumor heterogeneity by organoids make them a model that surpasses established cell lines. Furthermore, organoids are not as time-consuming and expensive as PDTXs. Organoids can be frozen and thawed for many passages, while keeping the genetic stability of the primary tumor (Huch et al., 2015; Blokzijl et al., 2016). The isolated cells from tissue are embedded in a matrix. Different laboratories use different kinds of matrices and media conditions.

In 3D culture methods, the cells are either cultured inside of matrix or on top of matrix. The matrix prevents attachment of cells to the bottom of the plate and additionally allowing interaction of the cells by providing a physical structure upon which they can grow. The matrix recapitulates the environment of the extracellular matrix (ECM) *in vivo* (Gurski et. al., 2010). The most common

matrices that are used for the culturing of pancreatic organoids are collagen and Matrigel (Baker et al., 2016).

Out of 26 types of collagen, the most common ones used in tissue culture include types I and IV (Baker et al., 2016). Collagen type I exists either as recombinant protein or is isolated from a biological source (e.g. rat tail) and is the most abundant collagen in human body which can be found in many tissues such as bone, tendon, skin interstitial connective tissues (Gelse et al., 2003). On the other hand, the most common collagen in the basal lamina of normal tissues such as pancreatic epithelium is type IV collagen (Gelse et al., 2003; Baker et al., 2016) which regulates cell adhesion, migration and differentiation of epithelial cells (Khoshnoodi et al., 2008). Progression of PDAC is associated with breakdown of existing basement membrane and with increased production of type I collagen as the most common extracellular matrix present in PDAC tumors leading to a desmoplastic reaction (Shields et al., 2012; Baker et al., 2016).

Matrigel which is a gelatinous protein secreted from murine Engelbreth-Holm-Swarm (EHS) tumors, promotes cell differentiation (Kleinman and Martin, 2005). In addition to the high level of collagen type IV, laminin and enactin in Matrigel (Kleinman and Martin, 2005), there are more than 1800 proteins identified in Matrigel such as various growth factors including epidermal growth factor (EGF), basic fibroblast growth factor (bFGF), transforming growth factor beta (TGF-β), and platelet-derived growth factor (PDGF) (Vukicevic et al., 1992; Baker et al., 2016). Since growth factors in Matrigel might influence the cellular behavior, a modified version of Matrigel which is a growth factor-reduced (GFR) is available allowing researchers to control growth factor levels in their cultures (Taub et al., 1990; Baker et al., 2016).

The first 3D organoids were generated from the small intestine of mice (Sato et al., 2009). Following this, organoid technology was applied to other gastrointestinal organs including stomach, liver, colon and other organs (Barker et al., 2010; Huch et al., 2013a; Sato and Clevers, 2013). Huch and colleagues introduced this technology in pancreatic tissue in 2013 (Huch et al., 2013b) and following this in 2015, the first 3D organoid model of PDAC patients (Boj et al., 2015) was established. Boj and colleagues embedded murine as well as human pancreatic cells into Matrigel and could show that normal and tumor pancreatic organoids recapitulate the corresponding primary tissue in both species. Furthermore, they reported that the pancreatic organoids demonstrate ductal markers whereas markers for acinar and endocrine lineages are absent. Additionally, the orthotopic transplantation of tumor organoids into immunocompromised mice was described which displayed the progression from PanIN lesions to pancreatic ductal adenocarcinoma, illustrating a fascinating model for studying cancer progression (Boj et al., 2015). By performing RNA-sequencing and mass spectrometry in murine organoids, the correlation of gene expression and proteomic profiles with pancreatic tumor progression was also

demonstrated (Boj et al., 2015), underscoring the fact that the organoids could recapitulate the primary tissue from different aspects.

Another group (laboratory of Dr. Muthuswamy) generated organoids from pancreatic exocrine progenitors of human pluripotent stem cells. In their method, the cells, media and 5% Matrigel was plated on top of a Matrigel bed. The organoids represented a similar gene expression profile compared to the human pancreas including similar expression of pancreatic markers (NKX6.1, PTF1A). Furthermore, higher expression of progenitor markers (PDX1, NKX6.1) was shown. On the other hand, lower expression markers of islet and acinar (NKX2.2 and GATA4 respectively) were described (Huang et al., 2015).

The Skala laboratory developed another method to study not only organoids but also fibroblasts. The media was supplemented with 10% FBS, 1% penicillin-streptomycin, and 10-ng/mL epidermal growth factor receptor. Interestingly, the conditioned media allowed the culture of both cell types including tumor cells and fibroblasts in both species including human and murine (Walsh et al., 2016).

In another study, Kuo and colleagues described an air-liquid interface methodology which utilizes an inner collagen gel containing transwell with direct air exposure. In particular this approach allows growth of organoids as epithelial/mesenchymal hybrids without any requirement for exogenous growth factor supplementation (Li et al., 2014).

Despite all of the advantages of organoid technology, this technique also has some caveats. PDO culturing is generally costly due to the matrix as well as different growth factors in the media. The handling of PDOs requires expert practices. Due to the high inter-patient heterogeneity in pancreatic cancer patients, each established PDO grows differently leading to a diverse time-frame which is needed for performing functional assays such as drug screening.

V. Applications of organoids as a platform for disease modelling, biobanks, drug testing and personalized medicine

Generating patient-derived organoids (PDOs) from different organs gives researchers a great possibility to study a variety of diseases as well as different treatment options. So far human organoids from different organs have been established and they can recapitulate the corresponding organ that they are derived from and can be applied to study different diseases.

Organoids can also be genetically manipulated (Broutier et al., 2016) and combining the organoid technology with CRISPR/Cas 9 system gave researchers a great chance to model and study oncogenes and mutational signatures in an *ex vivo* system (Drost et al., 2016; Drost et al., 2017).

The existence of subpopulations of tumor cells with genotypic and phenotypic diversity leading to diverse biological functions within the same tumor of a patient, or between the same tumor from different patients are called intra-tumor and inter-tumor heterogeneity, respectively. Cancer heterogeneity plays an important role in clonal and mutational evolution, disease progression, drug resistance (Jin et al., 2018) and many targeted therapies have failed due to the cancer heterogeneity (Russo et al., 2016) In addition, because of high inter-patient heterogeneity differences in response from person to person can be observed (Dutta et al., 2017). Several different studies including our study have shown that the intra-tumor heterogeneity of primary tumor tissue is maintained in the matched organoid culture not only at the beginning, but also across different passages of organoids (Schutte et al., 2017; Weeber et al., 2017). The inter-tumoral heterogeneity is also preserved in organoids leading to differences in growth rate as well as drug response.

The organoid cultures generated from different tissues recapitulated the genetic and heterogenous phenotype of the morphology of original cancer cells in the primary tumor tissue from which they were derived (van de Wetering et al., 2015; Weeber et al., 2015; Pauli et al., 2017) and by using them as a research platform for drug screens prior to the treatment of the patient they might contribute to a tremendous breakthrough in personalized medicine. However, similar to all cancer models, genetic drift and clonal dynamics should be taken into consideration (Jin et al., 2018). It should be mentioned that the composition of the media can have influences on the genetic spectrum of organoids (Fujii et al., 2016). For example, removal of some growth factors from media such as Wnt, R-spondin I, EGF, and Noggin favors the outgrowth of mutated clones (Drost et al., 2015; Matano et al., 2015).

Since PDOs mimic the pathophysiology of their corresponding organs in a highly similar manner, organoids can be used as a valuable platform for disease modeling, to study biological processes such as cell behavior not only in a single cell type but also in co-culture with other cells of the tumor-microenvironment such as fibroblasts and immune cells, and to study oncogenes by inducing different mutations, tissue repair and improving drug development.

Three dimensional organoids provide a valuable tool and a research platform to discover many aspects of different types of cancer from basic to translational research. PDOs can be used as a platform to identify the sensitivity towards different targeted therapeutics (Cantrell and Kuo, 2015).

In 2013, Dekkers and colleagues used organoids as a research platform for the diagnosis and treatment of cystic fibrosis (Dekkers et al., 2013).

In 2015, the first biobank of organoids from healthy and tumor tissue of colorectal cancer patients (paired organoids) was described (van de Wetering et al., 2015). They performed high-throughput drug screens on PDOs in order to identify the gene-drug association and stratification markers for personalized treatment. Their findings illustrated the suitability of patient-derived organoids (PDOs) for drug testing in a personalized treatment approach.

In 2015, an organoid culturing from biopsy specimens of colorectal cancer (CRC) patients with an 18G needle was described (Weeber et al., 2015).

Since 3D organoids offer a very valuable platform for testing chemotherapeutic drugs, Walsh and colleagues in 2016 developed a method which uses the optical metabolic imaging (OMI) to evaluate the metabolic changes due to the drug on the cellular level. In their study, they assessed the drug response not only in the organoids but also in fibroblasts (Walsh et al., 2016).

In 2016, Kumar and colleagues showed the importance of MAPK-interacting protein kinase inhibitors (CGP 57380) with PDAC organoids by utilizing the colony formation measurement in individual organoids suggesting that organoids could be used for testing drug sensitivity (Kumar et al., 2016; Baker et al., 2016; Jin et al., 2018).

In 2017, another biobank of CRC-organoids was established (Schutte et al., 2017).

Recently in 2017, Pauli and colleagues established tumor organoids either from surgical specimens or biopsy materials from different types of tumors including prostate, bladder, ureter, kidney, stomach, pancreas, colon, rectum, esophagus, brain and soft tissue as well as some epithelial and mesenchymal cancers. They performed high-throughput drug screening on cells derived from tumors and validated their results by using PDOs and PDX models. They combined the drug screening data with genomic data to guide personalized medicine (Pauli et al., 2017).

Another study by Vlachogiannis and colleagues in 2018 established a living biobank from metastatic, heavily pretreated colorectal and gastroesophageal cancer patients recruited in phase 1/2 clinical trials. They compared the drug-screen responses in PDOs, PDOX and corresponding patients and could indicate that PDOs can recapitulate patient responses in the clinic and be implemented in personalized medicine programs (Vlachogiannis et al., 2018).

In 2018, Tiriac and colleagues generated an organoid biobank from pancreatic cancer patients and compared the treatment response of PDOs with patient response which showed a high concordance (Tiriac et al., 2018a).

This advanced technology gives us the possibility to generate organoids not only from resected tumors, but also from very limited starting material such as endoscopic fine-needle aspiration or biopsy samples (Boj et al., 2016).

Miserably, more than 80% of pancreatic cancer patients are not eligible for surgery and consequently would not benefit from surgery which is the only curative option (Ryan et al., 2014). Generation of organoids from EUS-guided FNA (endoscopic ultrasound-guided fine needle aspiration) biopsies is a major breakthrough in discovering the understudied population of PDAC patients. In 2018, Tiriac and colleagues generated a biobank of PDOs from PDAC patients, performed with a 22-gauge FNB needle for organoid generation (Tiriac et al., 2018b).

One of the main focuses in the clinical research of pancreatic cancer could be rapid generation of PDOs from all patients who undergo EUS-guided FNA for initial diagnosis, enabling testing different drugs for each patient in a reasonable and clinically relevant time-frame, and therefore allowing physicians to apply a more precise treatment option for each individual patient (Tiriac et al., 2018b). Since it has been shown that PDOs recapitulate the drug sensitivity of the patient, they present a promising platform for personalized medicine (Tiriac et al., 2018a).

VI. Aims and research objectives

6.1. Establishing a PDAC patient-derived organoid (PDO) biobank and characterizing a subset of PDOs by performing drug screens and sequencing (WES and RNA)

In order to be able to generate PDOs from PDAC patients, firstly, the organoid technology was established. Then, an organoid biobank was created by enrolling 80 patients into the PDO-repository and a subset of PDOs were further characterized. Samples were obtained either as a resection tumor from patients who underwent surgery or a fine-needle-aspiration from patients who were submitted to the endoscopy suite for initial diagnosis. In order to accomplish this, the following aims were developed:

6.1.1. Establishing and culturing of organoids from resected samples of PDAC patients

6.1.2. Establishing and culturing of organoids from EUS-FNA samples of PDAC patients

6.1.3. Establishing a living PDO biobank from PDAC patients

6.1.4. Characterizing PDOs on the genomic level by performing whole exome sequencing (WES)

6.1.5. Characterizing PDOs on the transcriptomic level by performing RNA sequencing

6.1.6. Establishing a 96-well based therapeutic platform to investigate the sensitivity and resistance of PDOs towards different chemotherapeutic agents

6.1.7. Discovering the gemcitabine-dependent signature by combining the therapeutic sensitivity of PDOs towards gemcitabine and transcriptomic profile of corresponding PDOs

6.1.8. Comparing the clinical response of patients with PDO's response

6.2. Establishing a cost-effective culture method for human pancreatic organoids (NFMmodified)

Organoid technology is an expensive culture technique therefore another aim of this project was to develop a new culture media in order to make this technique affordable and therefore accessible to a larger group of scientists. In order to achieve this aim, a new media named Normal Feeding Media modified (NFMm) was established and compared to basic media (NFM) which was published by the group of Dr. Tuveson based on following experiments:

6.2.1. Comparison of morphology and viability in both media conditions (NFM vs. NFMm)

6.2.2. Comparison of PDOs treated with both media conditions based on proliferation and apoptosis by immunofluorescence staining (Ki67/ToPro and Cleaved-cas3/ToPro)

6.2.3. Investigating the role of media on the chemotherapeutic sensitivity or resistance

6.2.4. *In vivo* imaging of transplanted PDOs treated with 2 media conditions (NFM vs. NFMm) by PET/MRI imaging modalities

6.2.5. Comparison of tumor initiation capacity of PDOs cultured with NFM vs. NFMm media

6.2.6. Comparison of IHC-subtyping in Patient-derived organoid xenografts (PDOX) from PDOs cultured with NFM vs. NFMm media

6.2.7. Comparison of PDOs cultured with both media conditions based on RNA-sequencing

6.2.8. Comparison of PDOs cultured with different media conditions based on whole-exome-sequencing (WES)

6.3. Utilizing patient-derived organoids from fine needle aspiration as diagnostic and therapeutic research platforms for personalized medicine in pancreatic ductal adenocarcinoma

Since the cytology and histopathology for a subset of established FNA-PDOs was negative, the next aim of this project was to characterize these negative PDOs. In order to achieve this aim, the following steps were planned:

6.3.1. Identifying the histopathology status of PDOs generated from EUS-guided FNAs

6.3.2. Investigating the ability of negative-cytology PDOs to induce tumor by orthotopic transplantation of negative-cytology PDOs into athymic Nude mice (PDOX generation)

6.3.3. Further investigation of primary tumor (when available), PDOs and corresponding PDOXs based on histology and subtyping

6.3.4. Characterization of PDOs on the genomic level by performing next generation sequencing (NGS)

6.3.5. Performing digital-droplet-PCR (ddPCR) on the supernatant (cfDNA) of PDOs to detect *KRAS* mutation

6.3.6. Applying NGS to PDO supernatant (cfDNA) for detecting the mutational profile of PDAC

MATERIALS AND METHODS

All centrifugation steps for organoids were performed at 1000 rpm at 4°C for 5 minutes. For the cell culture procedures all centrifugation steps were performed using Centrifuge 5702R (Eppendorf).

I. *In Vitro* Experiments

1.1. Isolation and culture of organoids

1.1.1. Isolation of organoids from wild type (wt) and tumor mice

First of all, the organoid technology had to be established. In order to establish this technology pancreatic cells were firstly isolated from wild type and CKP (*Pdx1- Cre*; *Kras* $^{LSL\text{-}G12D/+}$, *p53* $^{loxP/loxP}$) mice as this mouse model develops an aggressive tumor of pancreas. The normal and tumor cells from murine pancreas was isolated and cultured as previously published (Boj et al., 2015).

Briefly, after euthanizing the mice, the pancreas was quickly harvested and washed in wash media (Table 1). Then the pancreas was minced into small pieces in a Petri-dish (1-2 mm). The fragments were transferred into a 15-ml falcon tube. In order to remove the fat, the falcon was incubated at room temperature (RT) for 1-2 minutes. After aspiration of the supernatant, the pancreas fragments were digested with the digestion media (Table 2) for approximately 1 hour. During the digestion, the falcon was placed in a rotator in the incubator at 37ºC. After the digestion, the falcon was centrifuged at 1000 rpm at 4°C for 5 minutes (min). Following centrifugation, the supernatant was aspirated and 1.5 ml TrypLE (Life Technologies) was added to the pellet. The digestion with TrypLE was done for additional 5 minutes while the falcon was placed in the waterbath at 37ºC.

After the digestion was done, 6.5 ml washing media was added to the falcon and centrifuged. After aspiration of the supernatant the pellet was resuspended in Growth Factor Reduced (GFR) Matrigel (Corning). 50 µl of the mixture of Matrigel and the cells was plated in each well of a 24-well plate. After 20 min when the Matrigel had solidified, the full feeding media was added to the well (Table 3).

1.1.2. Isolation of organoids from pancreatic cancer patients with resected tumors - Pancreatic cancer (PDAC) patient-derived organoids (PDOs)

The procedure for the isolation of organoids from pancreatic cancer patients is somewhat similar to the isolation of organoids from mice pancreas with some differences. After receiving the call from the operation room (OR), the sample was picked up. The normal and tumor samples were taken by the pathologist and transferred to the lab in a 15-ml falcon tube containing wash media (Table 4). The rest of the procedure was done under the hood in the tissue culture laboratory.

First of all, the samples were washed with cold wash media, then centrifuged and the supernatant was aspirated. Following this the sample was transferred to a Petri-dish on ice and was minced into small pieces (1-2 mm). After harvesting all fragments from the Petri-dish to the 15-ml falcon tube, the sample was centrifuged, and the supernatant was aspirated. Following centrifugation, the sample was incubated with 2 ml Red Blood Cell lysis buffer (ACK lysis buffer, Life Technologies) on ice for 10-15 minutes in order to lyse blood cells. Following lysis of blood cells, 6 ml wash media was added to the sample and centrifugation was performed. Then sample was incubated with the digestion media (Table 5) for 1.5-3 hours. Afterwards the sample was further digested with TrypLE for additional 5 minutes. After the tissue fragments have been digested, the sample was washed and centrifuged, the supernatant was aspirated, and the pellet was mixed with Matrigel and 50 µl of mixture of Matrigel and cells was plated in each well of a 24-well plate. The plate was placed in the incubator and after 20 minutes of incubation, 500 µl of warm human feeding media (Table 6) was added to each well.

1.1.3. Isolation of cells from pancreatic cancer patients with resected tumors and two-dimensional (2D) culturing

In order to isolate the cells from resected tumors and 2D culturing, the sample has been treated exactly based on what is described above (section 1.1.2.) until and including when there was a pellet. Then the pellet was mixed with 8 ml normal feeding media modified (NFMm; table 10) and cultured in a 10-cm-plate.

1.1.4. Isolation of PDOs from a single endoscopic ultrasound– guided fine needle aspiration (EUS-FNA)

After receiving the call from Endoscopy, the sample was quickly picked up and the procedure of organoid isolation was started within 15 min after biopsy. First of all, washing and centrifugation were performed. Then the supernatant was discarded, and the sample was incubated with Red Blood Cell lysis buffer (ACK lysis buffer, Life Technologies) on ice for 10-15 min. After lysis of blood cells, the wash media (Table 4) was added to the falcon and followed by centrifugation. The sample was cut into small pieces. When the sample was very small there was no enzymatic digestion needed, in case the sample was large, a short enzymatic digestion (5-10 min) with TrypLE was done. Then the sample was washed and centrifuged. The supernatant was aspirated, and the pellet was mixed with Matrigel and 50 µl of the mixture of Matrigel and cells was plated in each well of a 24-well plate. After incubation of the plate for 20 minutes, 500 µl of warm human feeding media (Table 6) was added to each well.

1.2. Media preparation

1.2.1. Preparing wash, splitting, digestion and feeding media

Table 1. Murine wash/splitting media

Component	Company	Volume
DMEM	Life Technologies	485 ml
100x Pen/Strep	Life Technologies	5 ml
100x GlutaMax	Life Technologies	5 ml
Hepes (1M)	Life Technologies	5 ml

Table 2. Murine digestion media

Component	Company	Volume
Wash media	-	10 ml
Collagenase Type V	Sigma	10 mg

Table 3. Murine feeding media

Component	Company	Volume
Splitting media	-	18 ml
R-Spon I- conditioned medium	-	2 ml
B27 supplement (50x)	Life Technologies	400 µl
N- acetylcysteine (500mM)	Sigma	50 µl
Nicotinamide (1M)	Sigma	200µl
mNoggin (100 µg/ml)	PeproTech	20 µl
hFGF-10 (100 µg/ml)	PeproTech	20 µl
A83-01 (0.5mM)	Tocris	2 µl
mEGF (100 µg/ml)	Life Technologies	20 µl
hGastrin I (10µM)	Sigma	4 µl
Y-27632* (10.5 mM)	Sigma	20 µl

*Y-27632 (Rho Kinase (ROCK) inhibitor) is only used when organoids are first isolated and thawed.

Table 4. Human wash/splitting media

Component	Company	Volume
Advanced DMEM/F12	Life Technologies	489 ml
100x GlutaMax	Life Technologies	5 ml
Hepes (1 M)	Life Technologies	5 ml
Primocin™ (50 mg/ml)	Invivogen	1 ml

Table 5. Human digestion media

Component	Company	Volume
Human wash/splitting Media	-	8 ml
Collagenase Type II	Life Technologies	40 mg
OR		
Collagenase Type V	Sigma	8 mg

Table 6. Human feeding media

Component	Company	Volume
Splitting media	-	8 ml
R-Spon I-conditioned medium*	-	2 ml
Wnt3a- conditioned medium**	-	10 ml
B27 supplement (50x)	Life Technologies	400 µl
N- acetylcysteine (500mM)	Sigma	50 µl
Nicotinamide (1M)	Sigma	200 µl
mNoggin (100 µg/ml)	PeproTech	20 µl
hFGF-10 (100 µg/ml)	PeproTech	20 µl
A83-01(0.5mM)	Tocris	2 µl
mEGF (100 µg/ml)	Life Technologies	20 µl
hGastrin I (10µM)	Sigma	4 µl
Y-27632*** (10.5 mM)	Sigma	20 µl
Prostaglandin E2 (PGE2) (1M)****	Tocris	2 µl

*R-Spon I-conditioned medium: sometimes instead of conditioned media, commercial R-Spon (R&D Systems) was used in a final concentration of 500 ng/ml.

** Wnt3a- conditioned medium: sometimes instead of Wnt3a- conditioned medium, Commercial Wnt3a (R&D Systems) was used in a final concentration of 100 ng/ml.

***Y-27632 (Rho Kinase (ROCK) inhibitor) is only used when organoids are first isolated and thawed.

****Prostaglandin E2 (PGE2): is only used for human normal organoids.

1.2.2. Preparing WNT-conditioned media

1 cryovial L-wnt3a cell-line was thawed and mixed with the growing media (Table 7), centrifuged and the pellet was mixed with 25 ml growing media and cultured in a 175 cm^2 flask with Zeocin for selection. Zeocin (Life Technologies) was added in a final concentration of 125 µg/ml. When the flask was confluent, the cells were split into 6 x 175 cm^2 flasks in growing media with FBS (5%) and Zeocin was added to one flask only. No Zeocin was added to other flasks. When the cells without Zeocin were confluent, the cells were trypsinized and the cells were pooled in 600 ml growing medium without Zeocin and cultured in 30 x 150 cm^2 dishes (20 ml per dish). The cells were incubated in the incubator for 1 week. After 1 week the medium was harvested

and aliquoted into 50-ml falcon tubes. The medium was spun down for 5 min at 1500 rpm in order to remove the floating cells. Then the medium was filtered through 0.22 µM filter. The procedure was repeated with the flask containing Zeocin.

Table 7. Growing medium for Wnt-3a and R-Spondin I (R-Spo I) conditioned medium

Component	Company	Volume
DMEM	Life Technologies	470 ml
100% FBS	Life Technologies	25 ml
100x Pen/Strep	Life Technologies	5 ml

1.2.3. Preparing R-Spondin-conditioned media

1 vial of 293-HA-RspoI-Fc from Calvin Kuo was thawed and cultured in growing medium (Table 7) with zeocin (300 µg/ml) in a 175 cm^2 flask. After the cells were confluent, the cells were split into 6 x 175 cm^2 flasks with growing medium and Zeocin was added to only 1 flask but no Zeocin was added to the other flasks. When the flasks with growing media without Zeocin were confluent, the growing medium was removed and replaced with 50 ml conditioning medium (Table 8). After one week of incubation the medium was harvested, spun down for 5 min at 1500 rpm. Then the medium was filtered through 0.2 µM filter. The medium was aliquoted and stored in -20 °C. The procedure was repeated with the flask containing Zeocin.

Table 8. Conditioning medium for R-spondin I

Component	Company	Volume
Advanced DMEM/F12	Life Technologies	485 ml
100x Pen/Strep	Life Technologies	5 ml
100x GlutaMax	Life Technologies	5 ml
Hepes (1M)	Life Technologies	5 ml

1.3. Splitting of organoids

1.3.1. Preparing Fire-polished pipettes for splitting of PDOs

Fire polished pipettes were used for the splitting and freezing of organoids. The glass Pasteur Pipettes (Brand) were fire-polished by rotating the end of the pipettes in fire using a Bunsen burner which made the opening of the glass pipette narrow and therefore breaking up the organoids was possible.

1.3.2. Splitting

The medium was aspirated and 500 µl ice-cold corresponding splitting media (Table 1 and table 4) was added to the well. The Matrigel and organoids have been resuspended well with the splitting media and transferred into a 15-ml falcon tube and centrifuged at 1000 rpm at 4°C for 5 min. Afterwards, the supernatant was removed until 1 ml of the splitting media remained. Using the fire polished pipettes, the organoids were pipetted up and down several times. Then the falcon tube was filled with the splitting media and centrifuged at 1000 rpm at 4°C for 5 min. After aspiration of the supernatant, the pellet was resuspended with the Matrigel and 50 µl of the mixture of organoids and Matrigel was seeded in each well of a 24-well plate. After solidification of the Matrigel, 500 µl corresponding warm feeding media was added in each well. The ratio of splitting of murine organoids was between 1:3-1:4, however for human organoids the ratio of splitting in each individual line was very different due to the high heterogeneity of pancreatic cancer patients.

1.4. Splitting of cells in 2D culture

The medium was aspirated, and the plate was washed with PBS twice. Then 1 ml trypsin was added to the plate and incubated for 5 minutes. Following incubation, 2 ml soybean trypsin inhibitor (STI; 250µg/ml) was added to the plate and resuspended well and transferred into a 15-ml falcon tube. The plate was further washed with 8 ml PBS and transferred into the falcon tube and centrifuged for 5 min at 1000 rpm. Then the supernatant was removed, and the pellet was mixed with required amount of media and cultured in different number of 10-cm plates (8 ml in each plate).

1.5. Freezing of organoids

For freezing, the organoids have been treated exactly based on what is described in the splitting step of organoids (section 1.3.2.) until and including the second wash step when there was a pellet. Then the pellet was resuspended in 1 ml Recovery Cell Culture Freezing Medium (Life Technologies) per each cryovial. Then the cryovial was placed in Mr. Frosty Freezing container and transferred into -80°C.

1.6. Freezing of 2D cell-lines

For freezing, the cells have been treated exactly based on what is described in the splitting step of 2D cells (section 1.4) until there was a pellet. Then the pellet was resuspended in 1 ml Recovery Cell Culture Freezing Medium (Life Technologies) per 1 cryovial. Then the cryovial was placed in Mr. Frosty Freezing container and transferred into -80°C.

1.7. Thawing of organoids and 2D cell-lines

In order to thaw the organoids, the cryovial was transferred from liquid nitrogen to the tissue culture lab quickly. The cryovial was thawed quickly in a waterbath. Then the cryovial was transferred to a 15-ml falcon tube containing 8 ml splitting media. The falcon was centrifuged. Regarding organoids, the pellet was mixed with the required amount of Matrigel and plated as it is described in the splitting step of organoids (section 1.3.2.). Whereas the pellet of 2D cell lines was resuspended in the corresponding medium (Table 10) and transferred into a 10-cm-plate.

1.8. Pharmacotyping/drug testing of organoids

1.8.1. Single cell isolation from PDOs

In order to perform the drug screening on PDOs, single cells had to be isolated from organoids. First of all, Matrigel had to be digested and the structure of organoids had to be disrupted. For this approach, the organoids were harvested and transferred into 15-ml falcon tubes pre-filled with 8 ml splitting media. Then the falcon was centrifuged, the supernatant was aspirated until 1 ml of the supernatant left. Following this the organoids were further broken with fire-polished-pipettes, the falcon was filled with splitting media and centrifuged again, the SN was aspirated, and the pellet was mixed with 500 µl of TryPle, transferred to a reaction tube and placed in the Thermomixer for 10-15 min. Following this, the reaction tube was transferred into a 15-ml

falcon and filled with splitting media. The falcon was centrifuged, the SN was aspirated, the pellet was mixed with 1ml media and cells were counted with Neubauer Chamber slide.

1.8.2. Drug screening of PDOs

The therapeutic agents: gemcitabine, 5-fluorouracil (5-FU), oxaliplatin, cisplatin, carboplatin, irinotecan, paclitaxel were provided by the Pharmacy at Klinikum rechts der Isar, Technical University of Munich. Bortezomib was purchased from LC-Laboratories (Woburn, MA, USA) (Table 9). Each drug screen for each individual PDO-line was repeated at least 3 times. In order to perform drug screening on PDOs, the white 96-well plates (Corning, cat.no. 3610) were firstly coated with mixture of Matrigel and PBS in a ratio of 1:4. Then 1000 cells per well in the mixture of Matrigel (10µl) and medium (80µl) (based on type of experiment, NFM or NFMm) were plated in each well. Serial dilution of the drugs was prepared in 7 different concentrations and each concentration (Conc.) was added in triplicate. The plates were incubated with the drugs for 3-5 days based on the growth of different PDOs. After incubation, the plates were analyzed.

Table 9. Chemotherapeutic agents

Drug	Stock Conc.	Highest Conc.
Gemcitabine	80 µM	200 nM
Paclitaxel	70,26 µM	100 nM
Cisplatin	3,33 mM	200 µM
Oxaliplatin	12,58 mM	50 µM
5-FU	1000 µM	1000 nM
Irinotecan	34,09 mM	50 µM
Carboplatin	26,9 mM	200 µM
Bortezomib	100 µM	100 nM

1.8.3. Measuring cell viability

The cell viability measurement was performed by using CellTiter-Glo® 3D Cell Viability Assay (Promega). First of all, the CellTiter-Glo was thawed and was transferred to a Bio-Pure™ pipetting reservoir and 100 µl of the solution was added to each well of the 96-well-plate with a

multi pipette. The plates were incubated on a shaker for additional 20 min and then were measured using Fluostar Optima (BMG Labtech) on the luminescence setting for 96- well plates.

1.8.4. Data analysis

The average of the triplicate data per concentration was measured and was normalized to the control. The rest of analysis and graph plotting was performed using GraphPad Prism 7.

Using GraphPad Prism, IC-50 was calculated. By placing the IC-50 value of each individual PDO in the percentile calculator, PDOs were grouped into resistant (more than 75% percentile), intermediate (between 25% and 75%) and sensitive (less than 25% percentile)

The area under the curve (AUC) was calculated using GraphPad Prism 7. By dividing the AUC value by the maximum area normalized AUC was measured. The range of normalized AUC is between 0 and 1.

1.9. Establishing a cost-effective culture method of human pancreatic organoids (NFMmodified)

One aim of this project was to reduce the costs for PDO isolation, since the media compositions for culturing of organoids are very expensive. Therefore, a new culture media was established in order to make this technique affordable and therefore accessible to a larger group of scientists. The established new media was called Normal Feeding Media modified (NFMm) and compared the basic NFM media, which was published by the group of Dr. Tuveson (Boj et al., 2015), based on morphology, viability,, drug screening, RNA sequencing and whole exome sequencing. PDOs were also compared based on orthotopic transplantation by generation of patient-derived organoid xenografts (PDOX). The components of NFMm media are listed in the following table (Table 10).

Table 10. Established Normal Feeding Media modified (NFMm)

Component	Company	Volume
DMEM/F-12 (1:1) [1x] – F-12	Life Technologies™	200 ml
R-Spon I-conditioned medium*	-	50 ml
Wnt3a- conditioned medium**	-	250 ml
Nu Serum™ IV	Corning	25 ml
Penicillin-Streptomycin	Life Technologies™	5 ml
ITS™+ Premix	Corning,	2,5 ml
Bovine pituitary extract (15.8 µg/ml)	Life Technologies™	791 µl
3,3´,5-Triiodo-L-Thyronine(50µM)	PeproTech	50 µl
mEGF (100 µg/ml)	Invitrogen™	100 µl
Dexamethasone (100 nM)	Sigma-Aldrich®	5 µl
Choleratoxin (1mg/ml)	Sigma-Aldrich®	50 µl
D-(+)-Glucose (MW: 180, 16 g/mol)	Sigma®	2,5 g
Nicotinamide (MW: 122,12 g/mol)	Sigma®	0,66 g
A83-01(0.5mM)	Tocris	50 µl
Y-27632*** (10.5 mM)	Sigma	500 µl
Soybean Trypsin Inhibitor, STI****	Life Technologies™	50 mg

*R-Spon I-conditioned medium: sometimes instead of conditioned media, commercial R-Spon (R&D Systems) was used in a final concentration of 500 ng/ml.

** Wnt3a-conditioned medium: sometimes instead of Wnt3a- conditioned medium, Commercial Wnt3a (R&D Systems) was used in a final concentration of 100 ng/ml.

***Y-27632 (Rho Kinase Inhibitor) is only used when organoids are first isolated and thawed.

****STI: using STI is optional.

II. Patient cohort and clinical responses

The informed consent forms were signed by all patients who were enrolled in this study based on the institutional review board (IRB) project-number 207/15 and 1946/07 of the Technical University Munich and EK451122014 in Dresden. Samples were either received as EUS-FNA from endoscopy suite at Klinikum rechts der Isar, Technical University Munich (41 samples) or as resection specimens from the Surgical Departments at the Klinikum rechts der Isar (34 samples) or University Hospital Carl Gustav Carus, Technical University Dresden (5 samples).

EUS-FNA was done for initial diagnosis. One additional needle pass (second pass) with a 19, 20 or 22-gauge FNA needle was performed for the 3D organoid-biobank.

The patients were assessed for clinical course, chemotherapy regimen (as adjuvant, neoadjuvant or palliative chemotherapy), re-admissions and mortality. Progression free survival (PFS) was measured based on either progression under palliative or adjuvant chemotherapy (according to RECIST criteria) or until relapse after surgical resection.

III. *In Vivo* Experiments

3.1. Patient-derived-organoid xenografts (PDOXs)

All animal experiments and care were in accordance with the guidelines of institutional committees and approved by the local authority, Regierung von Oberbayern, project-number: 55.2-1-54-2532.0-54-2016.

3.1.1. PDOX generation by orthotopic transplantation of PDOs into immunocompromised mice

In order to evaluate how Patient-derived-organoids (PDOs) would behave *in Vivo*, PDOs were orthotopically transplanted into athymic nude mice (Nc(NCr)-Foxn1^{nu}).

First of all, the single cells from PDOs were isolated, as it has already been described in section 1.6.1. Then single cells were counted and depending on the growth rate of PDOs and type of experiment, different numbers of cells (300000-600000) were mixed with 50 µl Matrigel

and orthotopically transplanted into athymic nude mice (Nc(NCr)-Foxn1^{nu}). After 50 days, the tumor was monitored by PET and MRI imaging. Then the mice were euthanized, and the pancreas was harvested for histology analysis. In addition to the pancreas, other organs e.g. liver, spleen, lung, intestine, lymph-nodes, peritoneum were also harvested to see whether the tumor had metastasized or not.

3.1.2. *In vivo* monitoring of the tumor by PET (Positron-emission tomography) and MRI (Magnetic resonance imaging) imaging

The animals were kept in constantly warm conditions and anesthetized with isoflurane (1,5% O2, 2% Isoflurane). Then the animals were imaged consecutively using the Siemens Inveon microPET/CT (Siemens Healthcare, Erlangen, Germany) and 7T MRI (MR901 Agilent, GE, AVANCE III HD electronics, Bruker, 31 mm inner diameter volume coil, RAPID Biomedical). In order to prevent deformation during the transport between imaging and allowing for precise fusion of PET and MRI, the abdomen was immobilized with a rapidly setting mold (Cho et al., 2009) using the MR-compatible material alginate (Creato Alginat Abformmasse, Zitzmann Zentrale, Wehr, Germany). 10-15 MBq 18F-FDG was injected intravenously (IV) after a CT scan and dynamic PET data were acquired in list mode for 50 min. All PET measurements were corrected for physical decay, dead time and non-uniformity of microPET response and the images were reconstructed using the 3D ordered subset expectation maximization (OSEM) algorithm. T2-weighted MRI was performed after PET/CT acquisition using a Rapid Imaging with Refocused Echoes sequence (RARE, TE/TR/FA=42.7 ms /20000 ms/ 90º). For anatomical T2weighted (T2w) imaging mice were kept in the prone position after the PET imaging to ensure co-registration and scanned at the 7T MRI system with the H-1 volume resonator coil. A coronary multi-slice T2-w RARE sequence (resolution 0.2×0.2×0.4 mm3, TE = 45,5 ms, TR > 5s) was applied for tumor detection.

IV. Histology

4.1. Fixation of PDOs

In order to perform the immunofluorescence (IF) and immunohistochemistry (IHC) staining of organoids, the organoids have been plated in 4-well-chamber slide (Thermo Fisher Scientific) which makes the separation of the chamber from the slide possible. 50 µl of the mixture of

organoid and Matrigel was seeded in each well of a 4-well-chamber slide and the organoids were allowed to grow until they reached a confluency of 50-60%. The media was discarded and organoids were washed with PBS + with a PH of 7.4 (Table 11) twice. Then the organoids were fixed with 4% PFA for 30 minutes on a rocker. After fixation, the staining procedure was performed.

4.2. Immunofluorescence staining of PDOs

The staining procedure is similar to what has been described previously (Reichert et al., 2013). Firstly, the PDOs were washed with PBS^+ three times for 1 min per wash. Secondly, they were washed with PBS^+ twice for 5 min per wash. Then the wells were incubated with 500 µl permeabilization solution (Table 12) with gentle rocking for 30 min at room temperature (RT). Afterwards the first antibody (table 13) was diluted in permeabilization solution and the organoids were incubated with 500 µl of permeabilization/antibody solution overnight at 4°C. The next day, the antibody solution was removed, and the wells were washed with permeabilization solution for 1 min at RT. Then the wells were washed three times for 10 min per wash at RT. Afterwards the desired secondary antibody and DAPI (1:1000) were diluted in permeabilization solution, added to each well and incubated overnight at 4°C. The next day, the samples were washed with permeabilization solution for 1 min at RT. Afterwards the samples were washed with permeabilization solution three times,10 min per wash. The last washing was done with PBS^+ twice for 5 min each time. Then the chamber was removed, and few drops (3-4) of fluorescent mounting medium SlowFade Diamond Antifade Mountant (Life Technologies) were placed on the slide and a coverslip (Thermo scientific) was placed on top. The slides were imaged with Leica SP8 confocal microscope.

Table 11. PBS+ for IF staining

Component	Company	Volume
PBS (1x)	Life Technologies	485 ml
$CaCl_2$ (147 g/mol)	Sigma	100 mg
$MgCl_2$ (203,3 g/mol)	Roth	470 mg

Table 12. Permeabilization solution for IF staining

Component	Company	Volume
PBS^{+}	-	50 ml
Cold-water fish skin gelatin	Sigma	0.35 g
Triton X-100	Sigma	250 µl

Table 13. Primary antibodies for IF staining of PDOs

Antibody	Company	Dilution
Rabbit anti-Ki67	Abcam	1:500
Mouse anti-E-cadherin	BD Transduction Lab	1:500
Rabbit Cleaved Caspase-3	Cell signalling	1:500
TO-Pro-3 Iodide	ThermoFisher	1:1000
Alexa Flour 647 Phalloidin	ThermoFisher	1:40
DAPI	Sigma	1:1000

4.3. Immunohistochemistry staining of primary tumors, PDOs and PDOXs

Cell pellets from the FNA were routinely processed, PDOs were fixed in 4% neutral buffered formalin for 1 hour and PDOXs for a minimum of 48 hours, dehydrated under standard conditions (Leica ASP300S, Wetzlar, Germany) and embedded in paraffin. With a rotary microtome (HM355S, ThermoFisher Scientific, Waltham, USA), serial 2µm thin sections were prepared, and subjected to histological and immunohistochemical analysis. Based on standard protocols for routine diagnostics, Hematoxylin-Eosin (H&E) staining was performed on deparaffinized sections with Eosin and Mayer's Hematoxylin.

Immunohistochemistry of PDOs and primary tumors (PTs) was done on a BenchMark XT automated stainer (Ventana, Tucson, AZ) with an HNF1A (Santa Cruz 8986), KRT81 (Santa Cruz 100929) and c-MYC (clone Y69, Abcam 32072) antibody using the ultraVIEW DAB Detection Kit (all reagents from Ventana, Tucson, AZ). Briefly, the sections were deparaffinized with EZ Prep at 75°C and 76°C, heat pretreated in Cell Conditioning 1 (CC1) for antigen retrieval at 76°C – 100°C and then incubated with the primary antibodies diluted in antibody diluent (Dilution: 1:200, 1:250 and 1:50 for HNF1A, KRT81 and c-MYC respectively) at 37°C after inactivation of the endogenous peroxidase using UV-inhibitor for 4 min at 37°C. The slides were incubated with a

HRP Universal Multimer for 8 min. Antibody binding was detected using DAB as chromogen and counterstained with hematoxylin for 8 min with subsequent bluing in bluing reagent for 4 min. Then the slides were dehydrated manually by alcohol washes of increasing concentration (70%, 96%, 100%) and xylene and coverslipped using Pertex® mounting medium (Histolab, Gothenburg, Sweden, 00801).

By using a Bond RXm system (Leica, Wetzlar, Germany, all reagents from Leica), immunohistochemistry of PDOXs was performed with primary antibodies against HNF1A (Santa Cruz 8986), KRT81 (Santa Cruz 100929). Briefly the slides were deparaffinized using deparaffinization solution, pretreated with Epitope retrieval solution 1 (corresponding to citrate buffer pH6). The primary antibodies were diluted (Dilution: 1:50, 1:200 for HNF1A and KRT81 respectively) and applied for 15 min. Antibody binding was detected with a polymer refine detection kit without post primary reagent and visualized with DAB as a dark brown precipitate. Counterstaining was performed with hematoxylin. Slides were then dehydrated manually by alcohol washes of increasing concentration (70%, 96%, 100%) and xylene and cover slipped using Pertex® mounting medium (Histolab, Gothenburg, Sweden, 00801). For KTR81-staining, Vector M.O.M. Kit was used to reduce the background staining specifically. A positive control was included in each run. The stained slides were evaluated by board certified pathologists blinded to the clinical information. The percentage and color intensity of the positive tumor cells regarding different antibodies were documented. PDACs were subtyped according to criteria published previously (Table 14) (Muckenhuber et al., 2018). Additionally, stained slides were scanned automatically (Leica Biosystems, Wetzlar, Germany, AT-2) and the Aperio Imagescope software (version 12.3, Leica Biosystems, Wetzlar, Germany) was used for acquisition of representative images.

Table 14. The criteria for IHC analysis regarding PDAC subtyping

Subtype	
1	HFN1A negative or slight; KRT81 ≤30% positive tumor cells = double-negative subtype (classical subtype)
2	HFN1A negative or slight; KRT81 >30% positive tumor cells = KRT81-posistive subtype (quasi-mesenchymal subtype)
3	HFN1A moderate or strong; KRT81 ≤30% positive tumor cells = HFN1A-positive subtype (exocrine-like subtype)
4	HFN1A moderate or strong; KRT81 >30% positive tumor cells = unclassifiable/double-positive subtype

Intensity	
0	Negative
1	Slight
2	Moderate
3	Strong

V. Molecular biology

5.1. DNA isolation from PDOs and blood

The PDOs were harvested from four to six wells of a 24-well plate for DNA extraction. DNA isolation was conducted using the QIAamp DNA Mini Kit (Qiagen, Cat. No. 51304) according to manufacturer's instructions.

5.2. Library preparation and whole exome sequencing

The Agilent SureSelect Human All Exon V6 kit was used for exome-enrichment, following the manufacturer's instructions. Samples were sequenced on an Illumina HiSeq 4000 system. Downstream bioinformatic analysis followed the "GATK Best Practices". After trimming of reads, using Trimmomatic 0.33, reads were mapped to the GRCh38.p12 reference genome using BWA-MEM 0.7.12. Picard tools 1.13 was used to mark PCR duplicates. Single nucleotide variants were called using Mutect2 from GATK 4.0.0.0. All potential somatic mutations with coverage < 10 in tumor or normal, mutant allele frequency < 10%, less than 3 variant reads in tumor or more than 0 variant reads in normal were filtered out. SNVs were annotated using SNPeff 4.1. CopywriteR 2.6.1.2 was used for the detection of copy number variations, using the default settings.

5.3. Next generation library preparation and DNA sequencing

DNA isolation from PDOs was conducted using the AllPrep DNA/RNA/miRNA Universal Kit (Qiagen, Cat. No. 80224) based on manufacturer's instructions. In order to extract DNA from formalin-fixed and paraffin embedded (FFPE) samples, eight 8 µm thick sections of FFPE tumor specimens were deparaffinized and digested with Proteinase K overnight. For one cytological sample (ID 42), laser microdissection was performed using a Leica LMD6 system according to the recommendation of the manufacturer.

Using the Maxwell 16 RSC extraction system (Promega, Madison, USA), automated extraction of nucleic acids was performed. DNA concentration was fluorometrically determined using the QuBit 3.0 system (Thermo Fisher Scientific, Waltham, USA) and DNA quality was additionally tested by a qPCR assay (RNAseP assay, Thermo Fisher Scientific) as described previously (Endris et al., 2013). Using the FFPE direct kit (Thermo Fisher Scientific), DNA from the laser-microdissected sample was isolated. In brief, 10 µl of transfer solution was directly added to the laser-microdissected tissue areas for cell lysis and mixed by pipetting. After addition of 21 µl Direct Reagent the mixture was incubated at 65°C in a thermocycler followed by up to 30 min at 20°C. The DNA was quantified by QuBit measurement.

For one case (ID-42) the PDO-supernatant was used for DNA extraction using the Maxwell® RSC ccfDNA Plasma Kit (Promega) according to the manufacturer's instructions for isolating cell free DNA (cfDNA). Libraries were prepared applying the AmpliSeq™ Comprehensive Cancer Panel (AmpliSeq™ CCP, Thermo Fisher Scientific) consisting of four primer pools for amplification of 15992 amplicons covering almost the complete exonic regions of 409 cancer-related genes. Semiconductor sequencing was performed as previously described (Pfarr et al., 2017a) on an Ion S5XL sequencing system using the Ion Chef 540 sequencing chemistry and a 540 Chip.Raw sequencing data was processed in the Torrent Suite Software (version 5.8.0) and alignment against the human genome (version hg19) using TMAP algorithm. The build-in plugins „variantCaller" (version 5.8.0.19), and „coverageAnalysis" (version 5.8.0.8) were used for variant calling and to generate the coverage data.

Variant annotation was performed by a custom built variant annotation pipeline using ANNOVAR (Wang et al., 2010). Variants were visualized using the Integrative Genomics Viewer Browser (IGV, http://www.broadinstitute.org/igv/) and were checked for germline or somatic origin using COSMIC (catalogue of somatic mutations in cancer) (Forbes et al., 2015) dbSNP, and the ExAC (Lek et al., 2016). Identification of copy number variations (amplifications and deletions) was performed for each sample and amplicons using the coverage data summary generated by the Torrent Suite software using a four-step algorithm as previously described (Endris et al., 2013; Pfarr et al., 2017b).

5.4. RNA isolation from tissue and PDOs

The PDOs were harvested from four to six wells of a 24-well plate for RNA extraction. RNA isolation was conducted using the AllPrep DNA/RNA/miRNA Universal Kit (Qiagen, Cat. No. 80224) based on manufacturer's instructions. RNA concentration was measured with a Qubit 2.0 Fluorometer (Invitrogen).

5.5. Library preparation and RNA sequencing

Library preparation for bulk 3'-sequencing of poly(A)-RNA was performed as described previously (Parekh et al., 2016). Briefly, cDNA was generated with a Maxima RT polymerase (Thermo Fisher) of each sample barcoded full-length using oligo-dT primer containing barcodes, unique molecular identifiers (UMIs) and an adapter. Addition of a template switch oligo (TSO) resulted in extension of 5' ends of the cDNAs and full-length cDNA was amplified with a primer binding to the TSO-site and the adapter. cDNA was tagmented with the Nextera XT kit (Illumina) and only the 3'-end-fragments were finally amplified using primers with Illumina P5 and P7 overhangs. In comparison to Parekh et al. the P5 and P7 sites were exchanged to allow sequencing of the cDNA in read1 and barcodes and UMIs in read2 to achieve a better cluster recognition. The library was sequenced on a NextSeq 500 (Illumina) with 75 cycles for the cDNA and 16 cycles for the barcodes and UMIs.

The minor human reference genome release GRCh38.p12 including all haplotypes and patches was used as reference for mapping the raw read data with Dropseq tools v1.13 (Macosko et al., 2015). Gencode annotation release v28 was used to determine read counts per gene. The resulting m X n count matric (m genes, n samples) was imported into R v 3.3 and further processed with DESeq2 v1.8. Prior downstream analysis lowly expressed genes (genes exhibit less than 10 reads across all samples used for analysis) were removed and the data was subsequently rlog transformed with a parametric fit and varying experimental design matrices. Differential expression analysis was performed and genes with an adjusted p-adjusted <= 0.05 were considered to be significantly regulated. Moffit Classifier Genes were used for sample subtyping. Therefore, the rlog transformed expression levels of these genes were z-transformed and hierarchically clustered using the euclidian distance as distance metric and the ward method for cluster agglomeration. Genes were ranked according to the formula -log10 (p-value)*Foldchange for each gene. These rankings were used as input for the preranked GSEA tool. IC-50 values were categorized as it is described in section 1.8.1. Categorized drug responses were used as covariate in the design matrix and differential expression between all possible group comparisons were determined. The significance level alpha for this analysis was set to 0.05. Scatter plots show the rlog transformed expression values. Heatmaps display the z-transformed expression values.

5.6. Quantification of KRAS mutations using digital droplet polymerase chain reaction (ddPCR)

The supernatant of PDOs (PDO-SN) was harvested and submitted to our collaborators at the Institute of Clinical Chemistry and Pathobiochemistry at Klinikum rechts der Isar for detection and quantification of *KRAS* mutations (G12D, G12V, and G12R) using droplet digital polymerase chain reaction (ddPCR). DNA was extracted from 1 ml of PDO-SN using QIAamp UltraSens Virus Kit (Qiagen) and quantified using a Qubit 2.0 fluorometer (Thermo Fisher Scientific).

In order to detect the *KRAS* mutation one fifth of the extracted DNA was used as input for ddPCR on a QX200 Droplet Digital PCR (ddPCR) system with automated droplet generation (Bio-Rad Laboratories). Reactions were carried out in ddPCR 96-well plates (#12001925, Bio-Rad). Each well contained 10.5 µl of ddPCR Supermix for Probes (no dUTP; Bio-Rad), 1.05 µl of target-specific primers (900 nmol/l), 1.05 µl of target-specific probe (250 nmol/l), 1.05 µl of MseI restriction enzyme (New England Biolabs), 1.05 µl of water, and 6.3 µl of sample DNA, for a total volume of 21 µl. Target assays were G12D (dHsaCP2000001, dHsaCP2000002, Bio-Rad), G12V (dHsaCP2000005, dHsaCP2000006, Bio-Rad), and G12R (dHsaCP2000009, dHsaCP20000010, Bio-Rad). Positive controls (gBlocks, synthetic DNA with the amplicon sequence and KRAS mutation or KRAS wildtype), NTC (purified, nuclease-free water), and negative controls (10 ng gDNA, genomic DNA from peripheral blood leukocytes of healthy subjects) were included on every plate for each assay.

Plates were sealed, spun down and loaded into the droplet generator. Immediately after droplet generation, 96-well plates containing droplet-partitioned samples were sealed and PCR was carried out on a C1000 Touch Thermal Cycler (Bio-Rad) using the following cycling protocol: enzyme activation at 95°C for 10 minutes followed by 40 cycles of 94°C for 30 seconds (for denaturation) and 55°C for 60 seconds (for annealing/extension), followed by a final 10 minute incubation at 98°C (for enzyme deactivation). Ramp rate was 2°C per second. Plates were then kept at 4°C. All samples were measured in duplicates (two wells).

Plates were read on a QX200 droplet reader (Bio-Rad). Raw droplet fluorescence intensity values were exported from QuantaSoft droplet reader software v1.7.4 (Bio-Rad). Custom scripts were used to import the intensity values into R (version 3.4.4; http://www.r-project.org) and to quantify concentrations of KRAS mutant and KRAS wildtype DNA. Target concentrations c were calculated for each well from the number of positive droplets Np and negative droplets Nn and the average droplet volume V = 0.85 nanoliter based on Poisson distribution statistics using the formula $c = (\ln(Np + Nn) - \ln(Nn))/V$, where ln is the natural logarithm. The number of partitions

(droplets) per reaction was 16855 on average (range 11837 to 21738, standard deviation (SD) 2743). With a droplet volume of 0.85 nl reported by Bio-Rad, the effective reaction size (total volume of partitions measured) was 14.3 µl on average (range 10.1 to 18.5 µl, SD 2.3 µl).

RESULTS

I. Establishing a PDAC patient-derived organoid (PDO) biobank and characterizing a subset of PDOs by performing drug screens and sequencing (WES and RNA)

1.1. Generation of Organoids from tumor mice

In order to establish the organoid technology, first of all, organoids from CKP (*Pdx1- Cre*; *Kras* $^{LSL\text{-}G12D/+}$*, p53* $^{loxP/loxP}$) mice were isolated and cultured. As it is shown (Fig. 1), organoids form a hollow structure with different sizes.

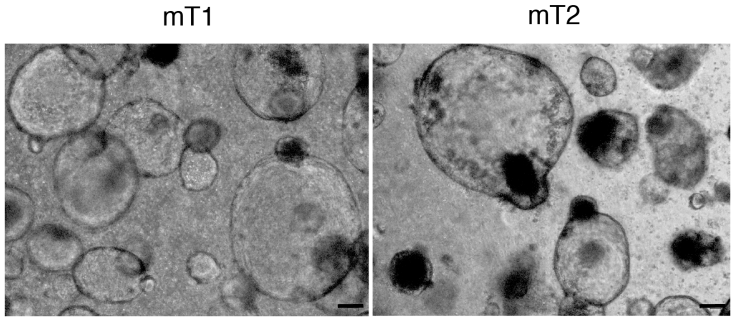

Figure 1. Representative images of organoids isolated from CKP (*Pdx1- Cre; Kras*$^{G12D/+}$*;* *p53*$^{loxP/loxP}$) mice, 7 days post-isolation. mT: murine tumor. Scale bars, 50 μM.

1.2. PDAC Organoid Technology: From bedside to bench and back to bedside in real-time

Establishing the organoid technology from pancreatic cancer patients was performed according to the workflow represented in figure 2 (Fig. 2). After receiving the call from operation room (OR) or endoscopy suite and obtaining the sample either as a surgical resection (Res.) or fine-needle aspiration (FNA), the following steps were performed. After dissociation of the samples following enzymatic digestion and isolating single cells, the samples were embedded into Matrigel, indexed, expanded and stored in liquid nitrogen. Following this, functional assays including drug-screening, whole- exome-sequencing (WES), RNA-sequencing (RNA-seq.), and orthotopic transplantation (patient-derived organoid xenograft, PDOX) were performed. In the

long-term perspective, the aim of such an approach is to provide the oncologist with the results to better direct patient therapy and personalized patient treatment.

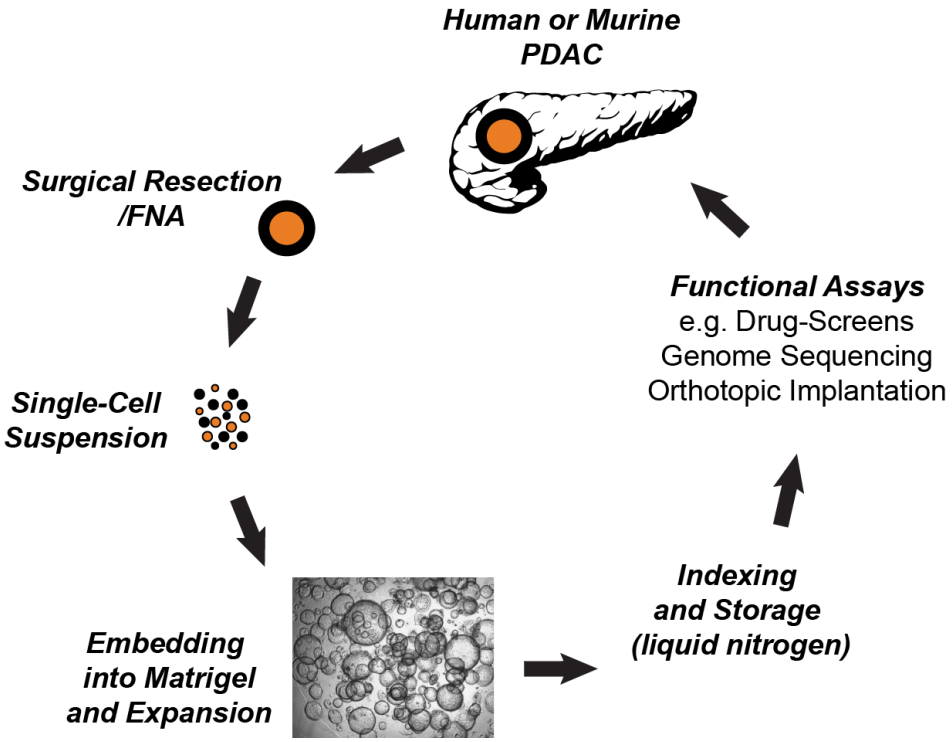

Figure 2. Workflow of PDO generation from resected samples and EUS-guided FNAs and performing functional assays including drug screens, whole-exome-sequencing, RNA-sequencing and generation of patient-derived organoid xenograft (PDOX). (modified from von Figura and Reichert, 2018).

Morphologically, individual organoids look very similar, even across species shown in figure 1 by murine pancreatic cancer derived organoids (Fig. 1 and Fig. 3). Figure 3 A displays the growth of a single organoid from a pancreatic cancer patient over time. Organoids can proliferate and can be expanded for further functional analysis (Fig. 3 B).

A

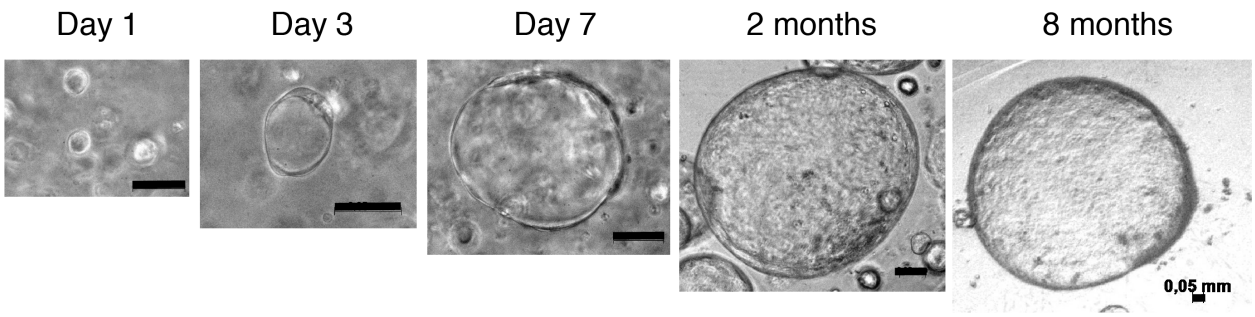

B

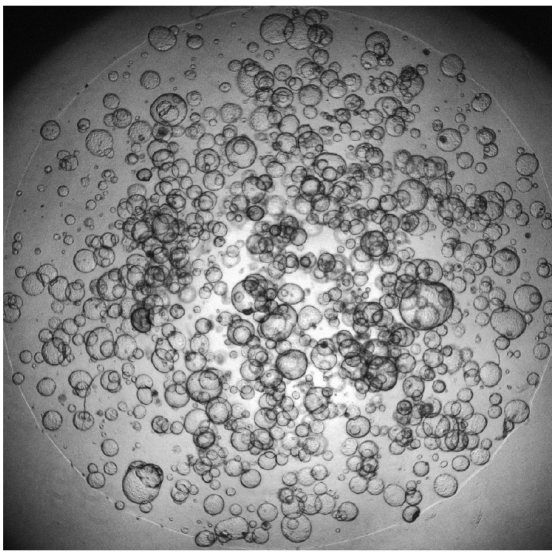

Figure 3. **A**. Phase contrast images of the growth of an individual organoid from a pancreatic cancer patient over time. Scale bars, 50 μM. **B**. A representative image of *in vitro* expansion of patient derived organoids (PDOs) grown in 1 well of a 24-well plate.

1.3. Assembling a living PDO biobank from pancreatic cancer patients

The first aim of this project was to establish the organoid technology and the generation and characterization of a living pancreatic cancer patient-derived-organoid (PDO) biobank. As it was mentioned above, samples were obtained either as a surgical resection from OR or as FNA from endoscopy suite. In this study, 80 patients were enrolled (Table 15). Most cases were diagnosed as pancreatic ductal adenocarcinoma (PDAC), however there were some patients who were diagnosed for other diseases e.g. IPMN, PanIN, lymphoma, neuroendocrine-tumor (NET) and pancreatitis.

Patient ID	Specimen	Histopathology	PDO Isolation
PDO 1	FNA	no histo	
PDO 2	FNA	no histo	
PDO 3	resection	PDAC	
PDO 4	resection	PDAC	
PDO 5	FNA	PDAC (suspicious)	
PDO 6	resection	insulinoma	
PDO 7	resection	PDAC	
PDO 8	resection	PDAC	
PDO 9	resection	PDAC	
PDO 10	FNA	negative	
PDO 11	resection	PDAC	
PDO 12	resection	PDAC	
PDO 13	resection	pancreatitis, acute	
PDO 14	resection	PDAC	
PDO 15	resection	PDAC	
PDO 16	resection	pancreatitis, acute	
PDO 17	resection	IPMN	
PDO 18	resection	PDAC	
PDO 19	FNA	PDAC	
PDO 20	resection	PDAC	
PDO 21	FNA	Lymphoma	
PDO 22	resection	PanIN	
PDO 23	resection	PDAC	
PDO 24	resection	PDAC	
PDO 25	resection	PDAC	
PDO 26	resection	IPMN	
PDO 27	resection	IPMN	
PDO 28	FNA	PDAC	
PDO 29	resection	PDAC	
PDO 30	resection	PDAC	
PDO 31	resection	PDAC, liver met	
PDO 32	resection	PanIN	
PDO 33	resection	PDAC	
PDO 34	FNA	PDAC	
PDO 35	FNA	PDAC	
PDO 36	resection, ascitis	PDAC	
PDO 37	FNA	IPMN	
PDO 38	FNA	PDAC	
PDO 39	FNA	negative	
PDO 40	FNA	negative	

Patient ID	Specimen	Histopathology	PDO Isolation
PDO 41	resection	IPMN	
PDO 42	FNA	PDAC	
PDO 43	FNA	negative	
PDO 44	FNA	PDAC	
PDO 45	FNA	negative	
PDO 46	FNA	negative	
PDO 47	FNA	negative	
PDO 48	resection	IPMN	
PDO 49	FNA	negative	
PDO 50	resection	IPMN	
PDO 51	FNA	negative	
PDO 52	FNA	negative	
PDO 53	FNA	PDAC	
PDO 54	resection	PDAC	
PDO 55	FNA	PDAC	
PDO 56	FNA	PDAC	
PDO 57	resection	PDAC	
PDO 58	FNA	NET	
PDO 59	resection	PDAC, liver met	
PDO 60	resection	PDAC, liver met	
PDO 61	resection	PDAC	
PDO 62	resection	PDAC, liver met	
PDO 63	resection	PDAC	
PDO 64	FNA	IPMN	
PDO 65	FNA	negative	
PDO 66	FNA	negative	
PDO 67	FNA	no histo	
PDO 68	FNA	no histo	
PDO 69	FNA	negative	
PDO 70	FNA	negative	
PDO 71	FNA	PDAC	
PDO 72	FNA	no histo	
PDO 73	FNA	PanIN (suspicious)	
PDO 74	FNA	PDAC	
PDO 75	FNA	PDAC	
PDO 76	FNA	PDAC (suspicious)	
PDO 77	FNA	PDAC (suspicious)	
PDO 78	FNA	PDAC (suspicious)	
PDO 79	resection	PDAC	
PDO 80	resection	PDAC	

Table 15. Living organoid biobank from pancreatic cancer patients
Successful PDO isolation: green-color, unsuccessful PDO isolation: pink-color.

After generation of PDOs, individual lines were subjected to functional assays. The organoids generated from resection tumors were in general growing faster than the organoids established from FNAs. In phase contrast images, the PDOs from resection tumors could make larger spheroids than PDOs from FNAs especially at early passages (Fig. 4). An important reason could be the larger amount of starting material in resected samples. Organoids could also be generated from metastatic sites. In our PDO library there are four PDOs that were generated from liver metastases (in collaboration with University Hospital Carl Gustav Carus, Technical University Dresden). PDOs generated from liver metastases look morphologically different. They could build round, empty spheroids or spheroids which are filled with cells (Fig. 4-right panel, top) In some

cases when the normal tissue was available, organoids were generated from normal tissue. This is especially critical for comparative studies including WES, synthetic lethality studies (the normal cells of a given patient should be less sensitive to the treatment than the tumor cells), as well as modeling PDAC progression by introducing defined genetic modifications.

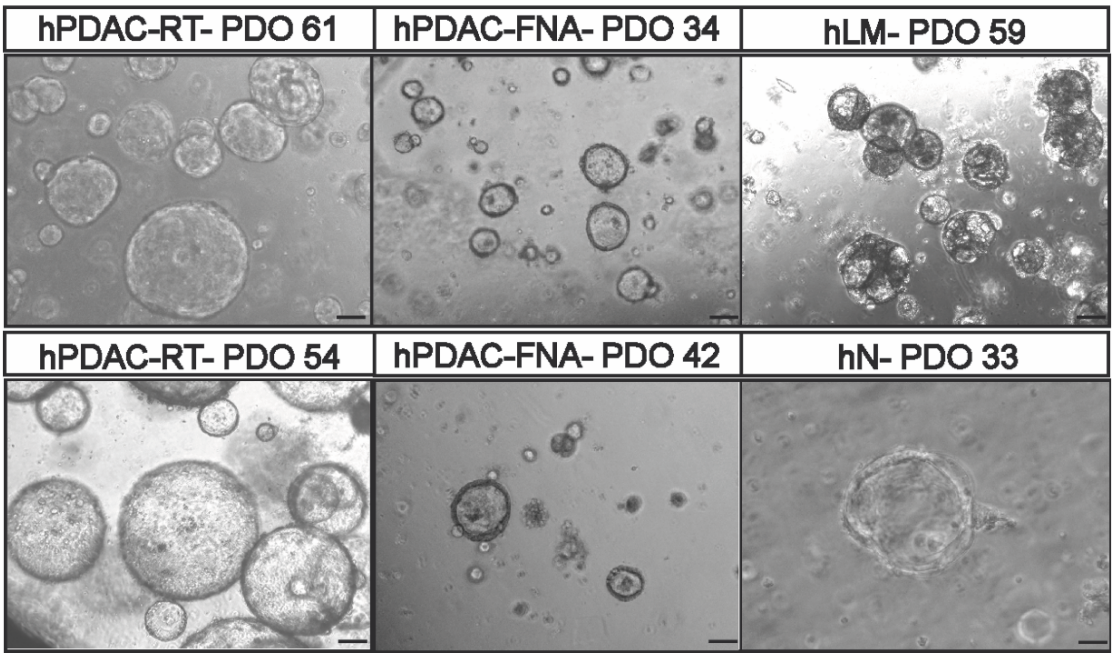

Figure 4. Representative phase-contrast images of PDOs. The left panel show PDOs generated from surgical resection, the middle panel illustrates PDOs from FNAs and on the right side, the upper panel shows PDO from liver metastasis and the lower panel illustrates normal human organoids. Scale bars, 50 µM.

1.4. Comparing PDOs with the matched primary tumors on the genomic level by performing whole-exome-sequencing (WES)

In order to determine whether PDOs represent the genomic characteristics of the matched primary tumor, the DNA from PDOs and matched primary tumor tissue was subjected to whole-exome-sequencing (WES). In general, PDOs maintained the genomic characteristics of the matched primary tumor (PT). By comparing the mutant allele frequency (MAF) of the most known mutated candidates in PDAC (Fig. 5 A) an increasing of the frequency of mutations in PDO compared to the primary tumor could be also noticed, underscoring the high cancer cell purity of the PDOs. For example, in *TP53* and *SMAD4* the MAF was only 6% and 5% respectively in the primary tumor, most likely due to the substantial stromal content. In the PDO however, which is composed of only tumor cells, we could show that both *TP53* and *SMAD4* were homozygously

mutated (Fig. 5 A). We evaluated the copy number profiles of the respective genetic loci for *TP53*, where we detected loss of parts of chromosome (chr.) 17 (Fig. 5 B, B48-PDO). Most likely, the observed homozygous allele frequencies are therefore due to a single nucleotide mutation on one chromosome/haplotype, and subsequent loss of the wild-type allele due to loss of heterozygosity (LOH), which is visualized in Figure 5 C.

By looking at copy number variations (CNVs) (Fig. 5 B) an increasing of the amplifications (green arrows) and deletions (blue arrows) of different parts of chromosomes in the PDO compared to the primary tumor could also be observed.

A

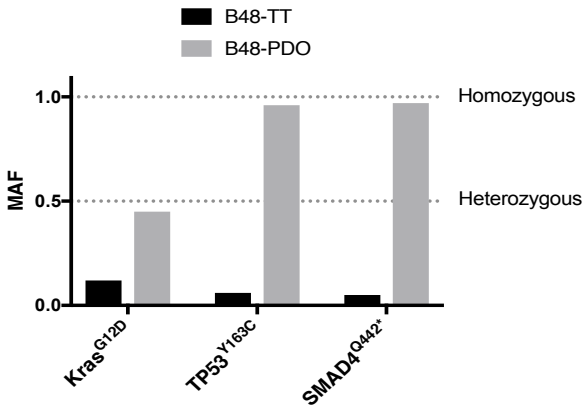

B

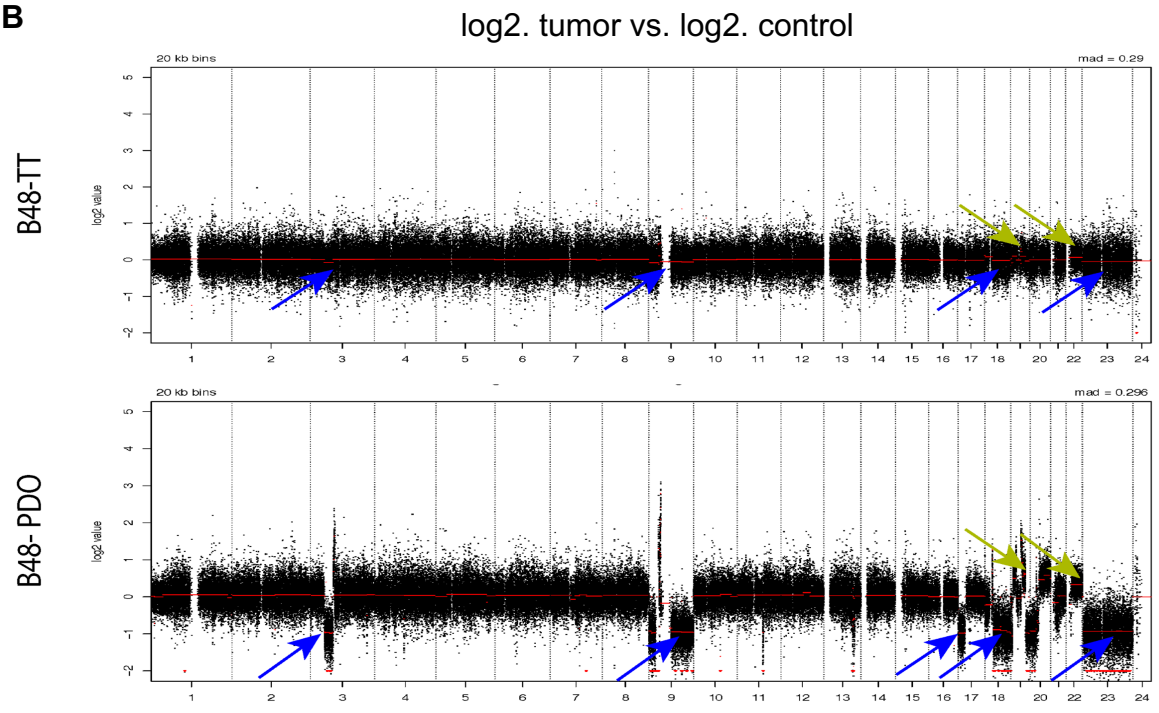

C

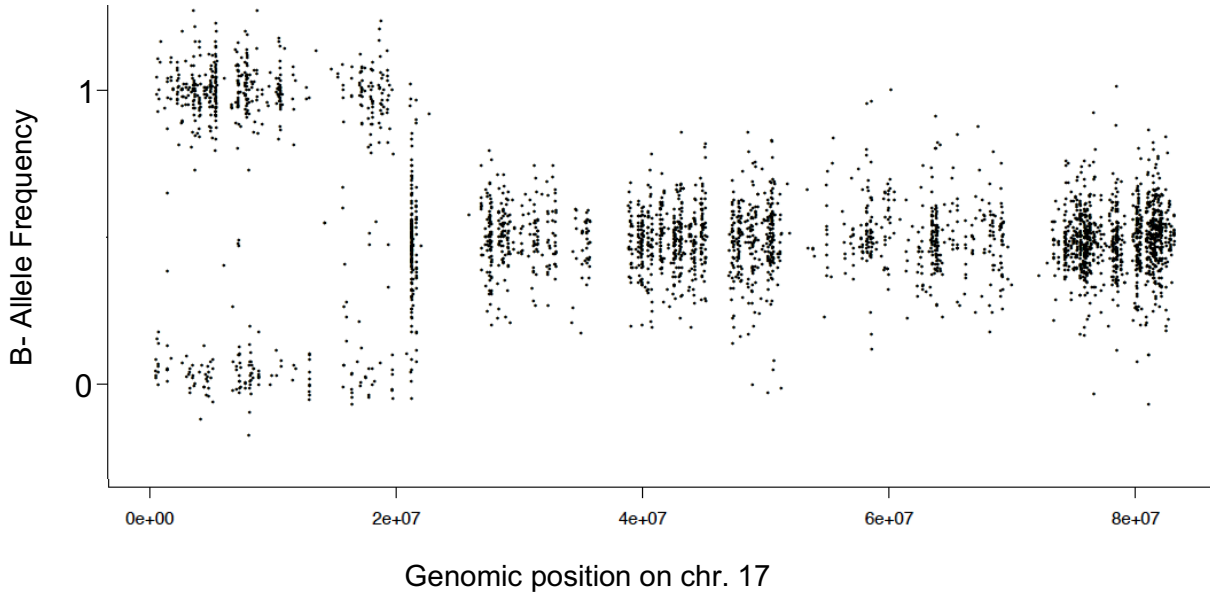

Figure 5. PDOs preserve the genomic characterization of the matched primary tumor. **A**. MAF of *KRAS*, *TP53* and *SMAD4* in primary tumor compared to the matched PDO. **B**. Copy number variation (CNV) of the primary tumor and matched PDO 48. Green arrows and blue arrows show amplification and deletion of chromosomes respectively. **C**. Loss of heterozygosity (LOH) of *TP53* on chromosome 17.

1.5. Comparing PDOs with paired 2D-cultures as well as matched primary tumors on the genomic level by performing whole-exome-sequencing (WES)

Furthermore, in order to investigate the genomic mutations in PDO versus PT and 2D culture, PDO and 2D cultures from the same patient were established, DNA was extracted and submitted to WES. We extracted all mutations in coding genes, leading to amino acid changes ("missense and nonsense mutations") in PT, PDO and 2D culture (ID 48) (Fig. 6). The number of missense and nonsense mutations was higher in PDO compared to the primary tumor (50 vs. 14). PT and PDO also shared 27 mutations. It should be mentioned that the most known mutated candidates in PDAC (*KRAS*, *TP53* and *SMAD4* and *CDKN2A*) were included in the shared genes between PDO and primary tumor. Interestingly, there was no common mutation between 2D culture and PT, nor for 2D culture and PDO. Another example was PDO 3, which showed 101 mutated genes (by filtering for missense and nonsense mutations) in PDO whereas illustrating 36 genes in 2D culture. The number of shared mutated genes was 5% (Supplementary Fig. 1).

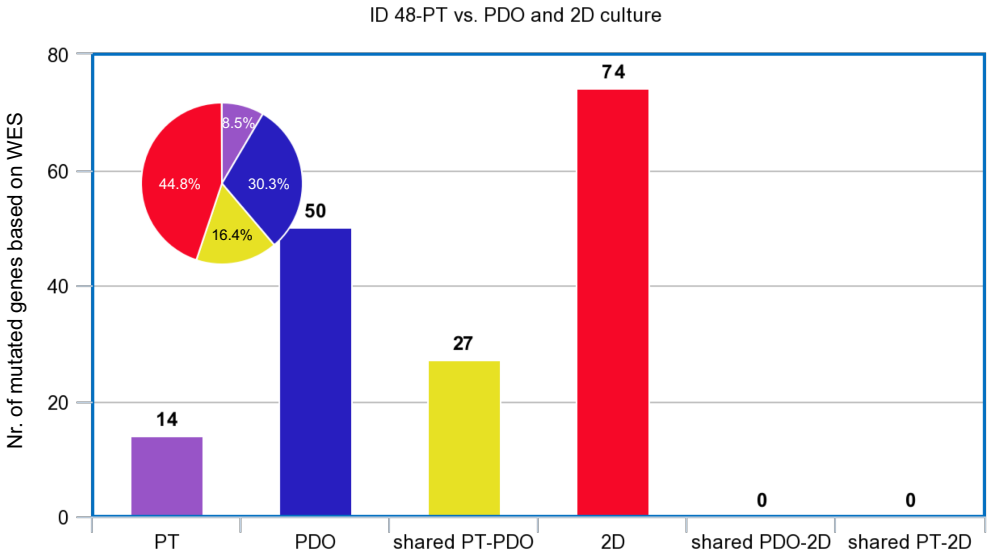

Figure 6. Number of unique as well as shared mutated genes in PDAC within the PT, 2D and PDO. The pie chart shows the percentage of missense and nonsense mutations for PT (8.5%), PDO (30.3%), 2D culture (44.8%) as well as shared genes between PT and PDO (16.4%). The bar graphs show the missense and nonsense mutations for PT (14), PDO (50), shared PT-PDO (27), 2D culture (74), shared PDO-2D (0) and shared PT-2D (0).

1.6. Characterizing the genomic profile of an individual PDO upon passages *in vitro*

In order to investigate whether PDOs maintain their genomic characteristics over passages, a low passage (LP, passage 20) and a high passage (HP, passage 50) of PDO 25 with an interval of 30 passages were subjected to WES. Interestingly, there was not any difference regarding MAF of known mutated candidates in PDAC (*KRAS*, *TP53*) as well as *TGFBR1* (Fig. 7 A). On the CNV level, also no difference regarding amplification or deletion of different parts of chromosomes could be seen (Fig. 7 B).

A

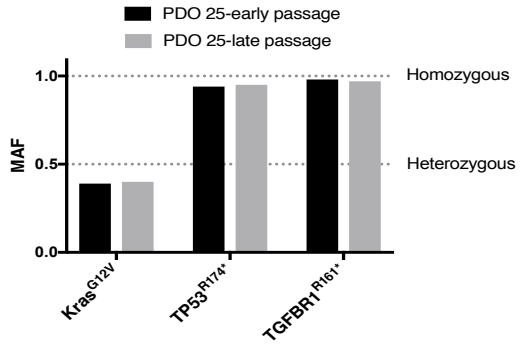

B

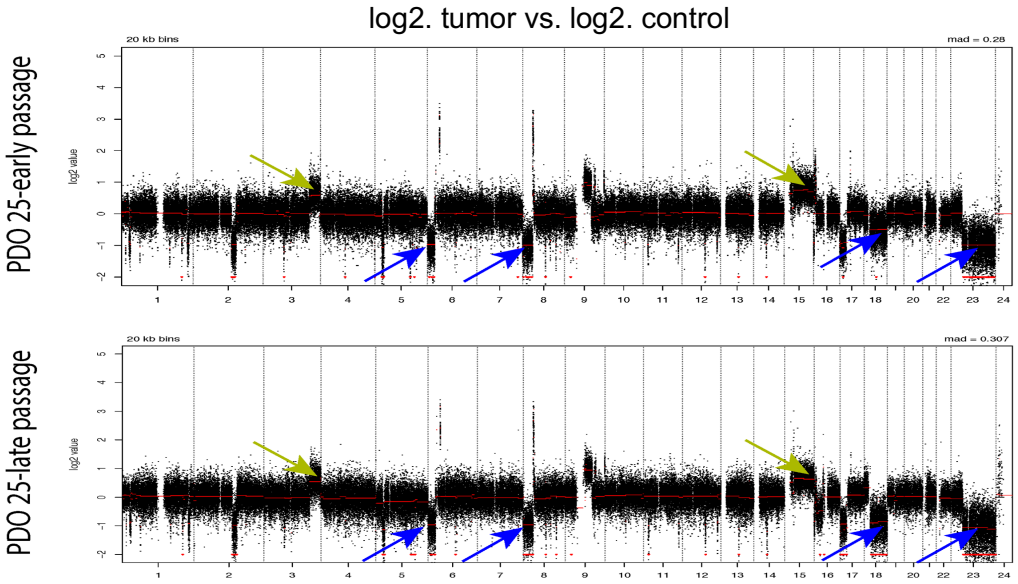

Figure 7. PDOs maintain their genomic characteristics over passages. **A**. MAF of *KRAS*, *TP53* and *TGFBR1* of PDO 25 at low and high passages. **B**. CNV of PDO 25 with a low passage (PDO-LP) and a high passage (PDO-HP). Green arrows and blue arrows show amplification and deletion of chromosomes respectively.

Furthermore, by comparing missense and nonsense mutations in low passage PDO versus high passage PDO, 15 mutations were only found in PDO-LP, 43 in PDO-HP and 51 mutations were identified in both low and high passage samples (Fig. 8). Of note, the most common mutated candidates in PDAC were shared in both passages.

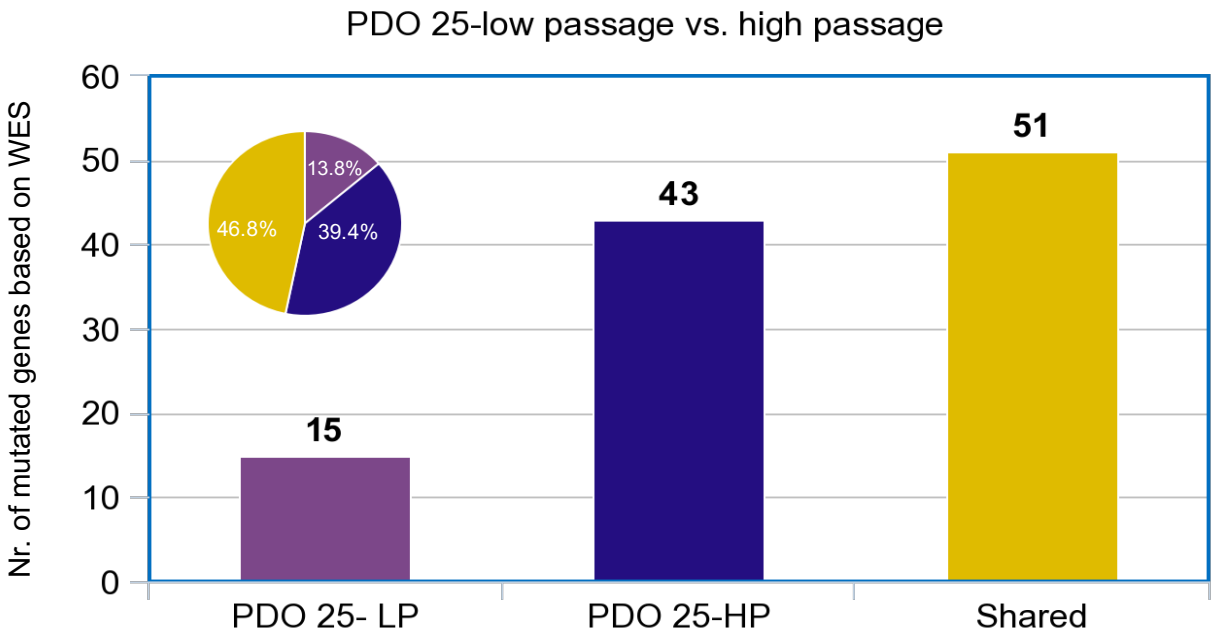

Figure 8. Pie chart shows the percentage of amino-acid changing mutations for PDO-LP (13.8 %), PDO-HP (39.4 %) as well as shared mutations between PDO-LP and PDO-HP (46.8 %). The bar graphs illustrate the number of missense and nonsense mutations for PDO-LP (15), PDO-HP (43) and shared mutations between LP and HP-PDO (51).

1.7. PDO subtyping based on transcriptomic profiling

PDOs were characterized on the transcriptomic level by performing RNA-sequencing. The screening was conducted in two different batches (Fig. 9 A, right panel: first sequencing run and left panel: second sequencing run). Unsupervised clustering of gene expression based on RNA sequencing data of PDOs was conducted with published signature lists from Moffitt (Moffitt et al., 2015) (Fig. 9 A).

By unsupervised clustering of the results, seven out of 15 PDOs showed higher expression of genes from classical subtype (Fig. 9 A, blue box) and were therefore classified as classical subtype (Fig. 9 B). Five out of 15 PDOs demonstrated a basal-like subtype (Fig. 9 B). By unsupervised clustering for 3 PDOs, it was not clear to which subtype they belong which made assigning a class to these PDOs (PDO 27, 48 and 54) impossible (Fig. 9 A, green box and Fig. 9 B).

For the PDOs that could be classified (n=12), 59% of PDOs (7/12) showed a classical subtype and 41% of PDOs (5/12) demonstrated a basal-like subtype (Fig. 9 C).

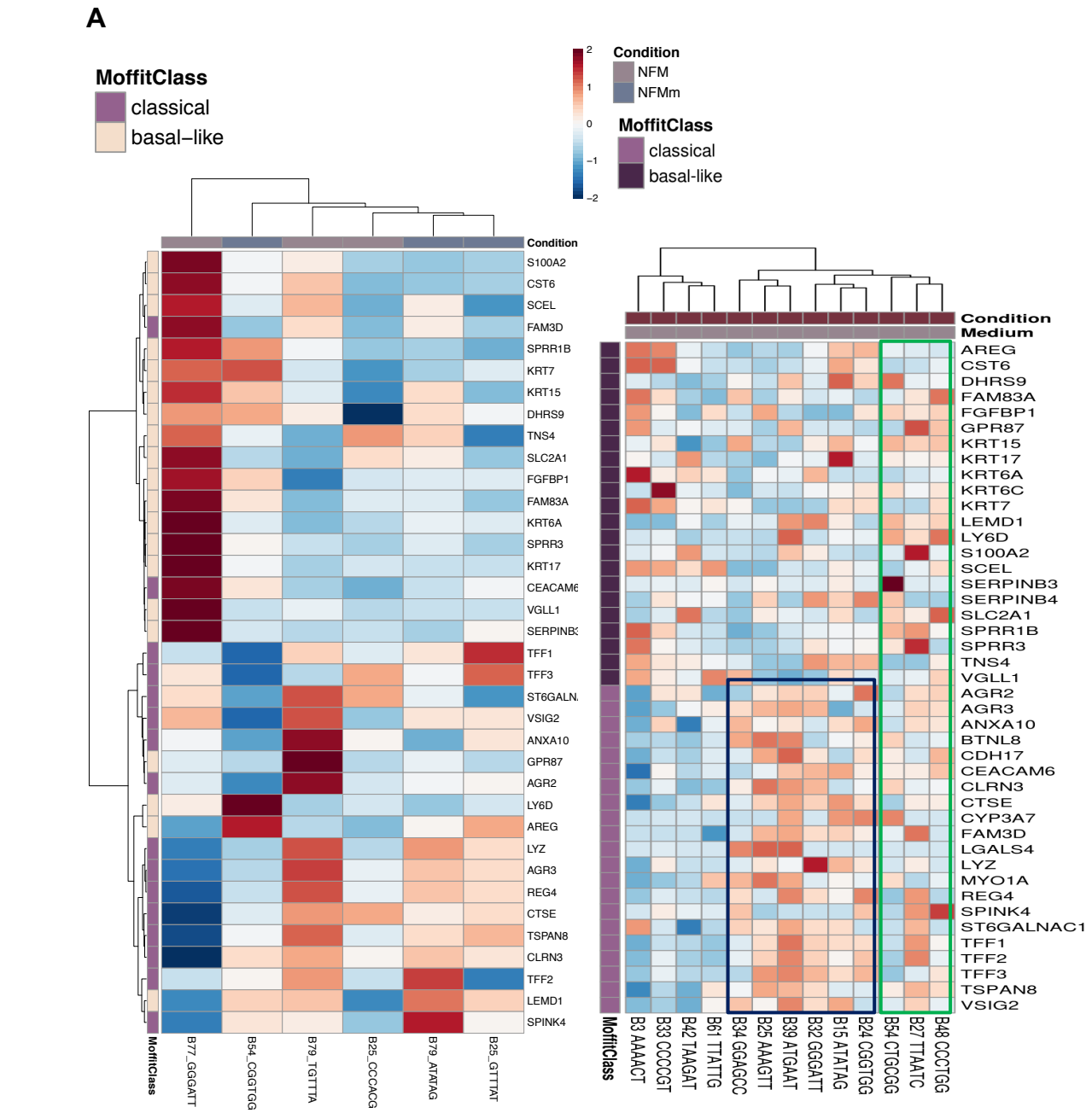
A
MoffitClass
classical
basal–like
Condition
NFM
NFMm
MoffitClass
classical
basal-like
Condition
S100A2
CST6
SCEL
FAM3D
SPRR1B
KRT7
KRT15
DHRS9
TNS4
SLC2A1
FGFBP1
FAM83A
KRT6A
SPRR3
KRT17
CEACAM6
VGLL1
SERPINB3
TFF1
TFF3
ST6GALN
VSIG2
ANXA10
GPR87
AGR2
LY6D
AREG
LYZ
AGR3
REG4
CTSE
TSPAN8
CLRN3
TFF2
LEMD1
SPINK4
MoffitClass
B77_GGGATT
B54_CGGTGG
B79_TGTTTA
B25_CCCACG
B79_ATATAG
B25_GTTTAT
Condition
Medium
AREG
CST6
DHRS9
FAM83A
FGFBP1
GPR87
KRT15
KRT17
KRT6A
KRT6C
KRT7
LEMD1
LY6D
S100A2
SCEL
SERPINB3
SERPINB4
SLC2A1
SPRR1B
SPRR3
TNS4
VGLL1
AGR2
AGR3
ANXA10
BTNL8
CDH17
CEACAM6
CLRN3
CTSE
CYP3A7
FAM3D
LGALS4
LYZ
MYO1A
REG4
SPINK4
ST6GALNAC1
TFF1
TFF2
TFF3
TSPAN8
VSIG2
MoffitClass
B3 AAAACT
B33 CCCCGT
B42 TAAGAT
B61 TTATTG
B34 GGAGCC
B25 AAAGTT
B39 ATGAAT
B32 GGGATT
B15 ATATAG
B24 CGGTGG
B54 CTGCGG
B27 TTAATC
B48 CCCTGG
B
PDO
3
33
42
77
61
15
24
25
32
34
79
39
27
48
54
Moffitt-subtype
Classcial
Basal-like
n.c.
C
41%
59%
Classical
Basal-like
Total=12

Figure 9. A. Transcriptomic profiling of PDOs indicates different subtypes (classical and basal-like) based on Moffitt subtype. Blue box illustrates the expression of genes in classical subtype. The green box shows the expression of genes in PDOs which could not be classified (PDO 27,48 and 54). **B.** The color-coded chart summarizes the results of 2 heatmaps (from 2 sequencing batches) in figure A: classical (blue-color), basal-like (red-color) and not-classified/not-subtyped PDOs (gray-color). **C.** The pie chart shows proportion of classical PDOs (59%) vs. basal-like PDOs (41%).

1.8. Characterizing of PDOs vs. paired 2D cultures on the transcriptomic level by performing RNA-sequencing

In order to investigate the difference between PDOs and 2D cultures on the RNA level, the RNA from PDO and paired 2D cultures was extracted and submitted for RNA-sequencing. PDOs and 2D culture from the same patient showed considerably variation of gene expression (Fig. 10).

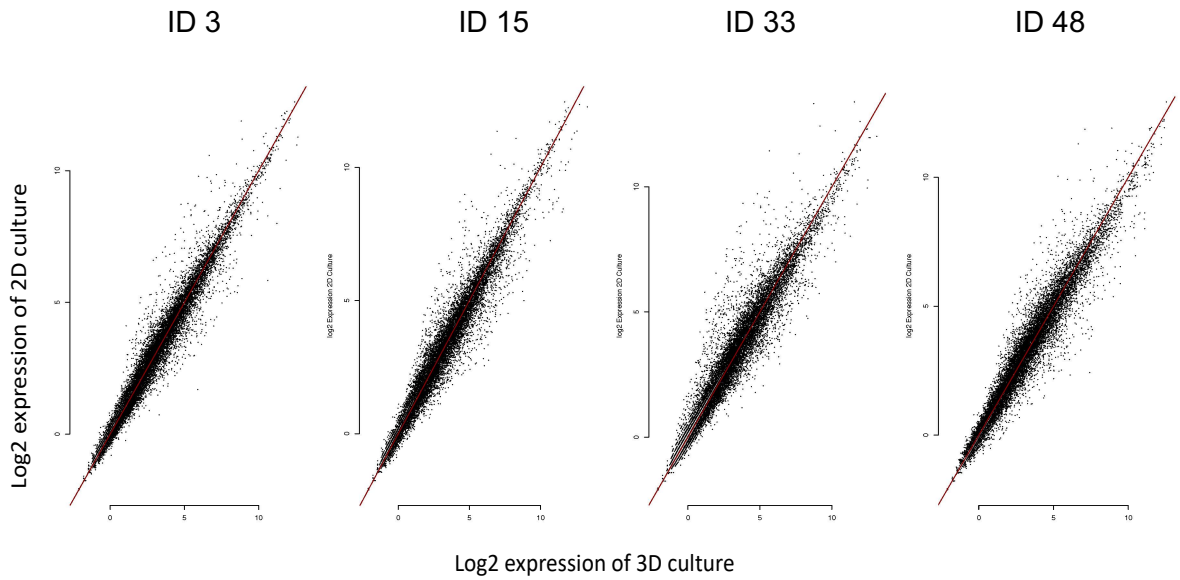

Figure 10. The scatter plots show the log2 expression of genes in PDOs (3D culture) (X-axis) versus log2 expression of genes in 2D culture (Y-axis). The red line indicates the bisecting line. Samples from the same patient (PDO and 2D culture) show varying expression across the whole intensity range.

This variation between PDO and paired 2D culture might be at least partly attributed to different signaling pathways as discovered by gene set enrichment analysis (GSEA). Differential expression analysis between PDOs and 2D cultures revealed large expression difference for 975

genes (Fig. 11 A). Most importantly genes involved in epithelial-mesenchymal transition (EMT) were differentially expressed (Fig. 11 B).

A **B**

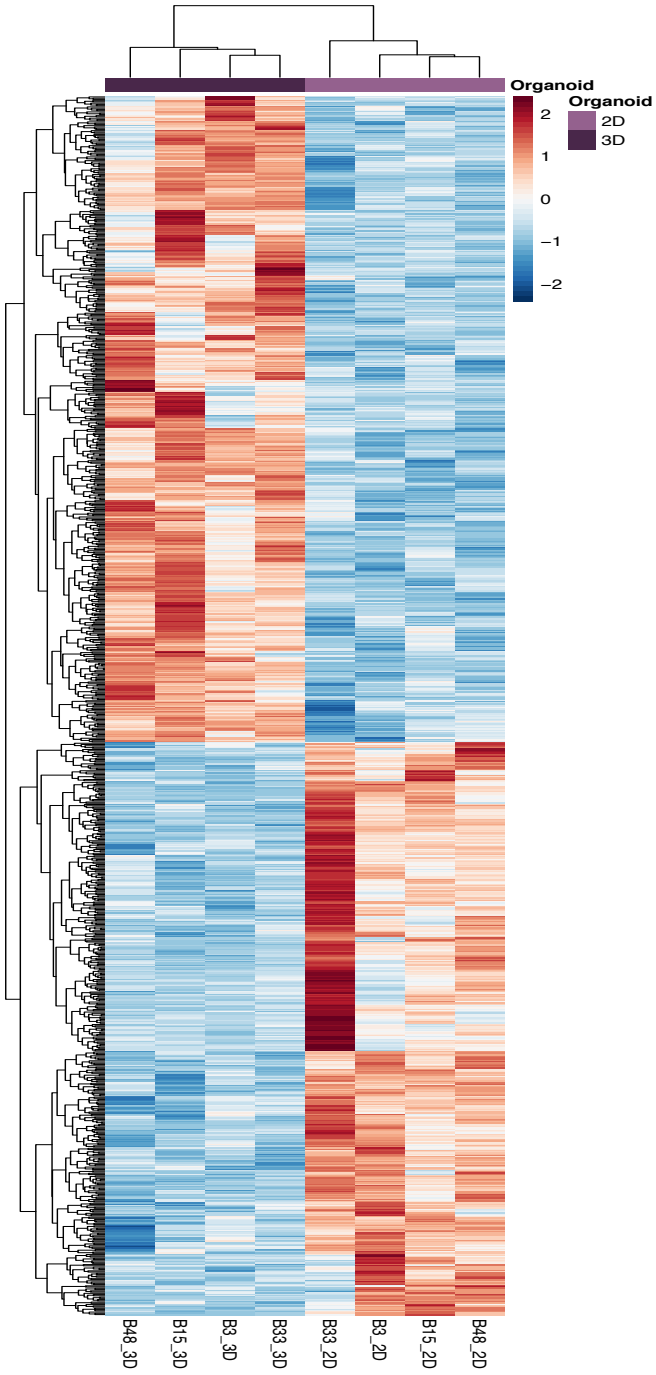

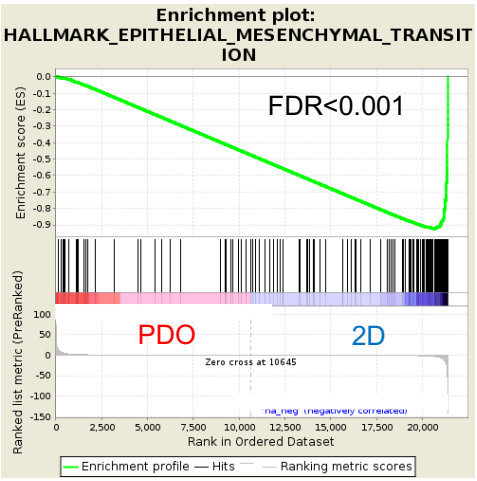

Figure 11. A. Heatmap illustrates the gene expression profile of PDOs versus 2D culture. **B.** GSEA analysis of expression patterns of 2D vs. 3D samples revealed EMT as most significant pathway in 2D culture.

1.9. Pharmacotyping/drug testing of PDOs

Because the genomic information alone is often not ample to identify critical pharmacotherapeutic vulnerabilities with high certainty, PDOs were treated with different standard chemotherapeutic drugs. Drug screening using 8 different chemotherapeutic drugs including gemcitabine, oxaliplatin, cisplatin, carboplatin, 5-fluorouracil (5-fu), paclitaxel, irinotecan and bortezomib was performed. Phase-contrast images of PDOs under treatment were made (Fig. 12). Three up to five days after treatment the cell viability was measured using CellTitre-Glo Luminescent cell viability assay based on ATP levels. Regarding drug response, an intertumoral heterogeneity between different organoid lines could be observed (Fig. 13).

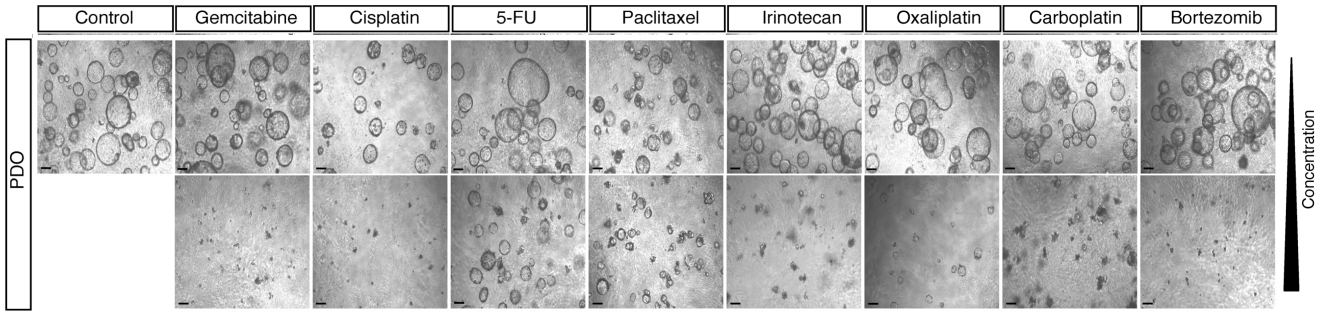

Figure 12. Pharmacotyping of PDOs. Morphology of PDOs before and after treatment in brightfield microscopy. Scale bars represent 50 µm. The upper panel shows control-PDO and PDOs treated with the lowest concentration of the drugs. The lower panel displays PDOs treated with the highest concentration of each indicated drug. Scale bars represent 50 µm.

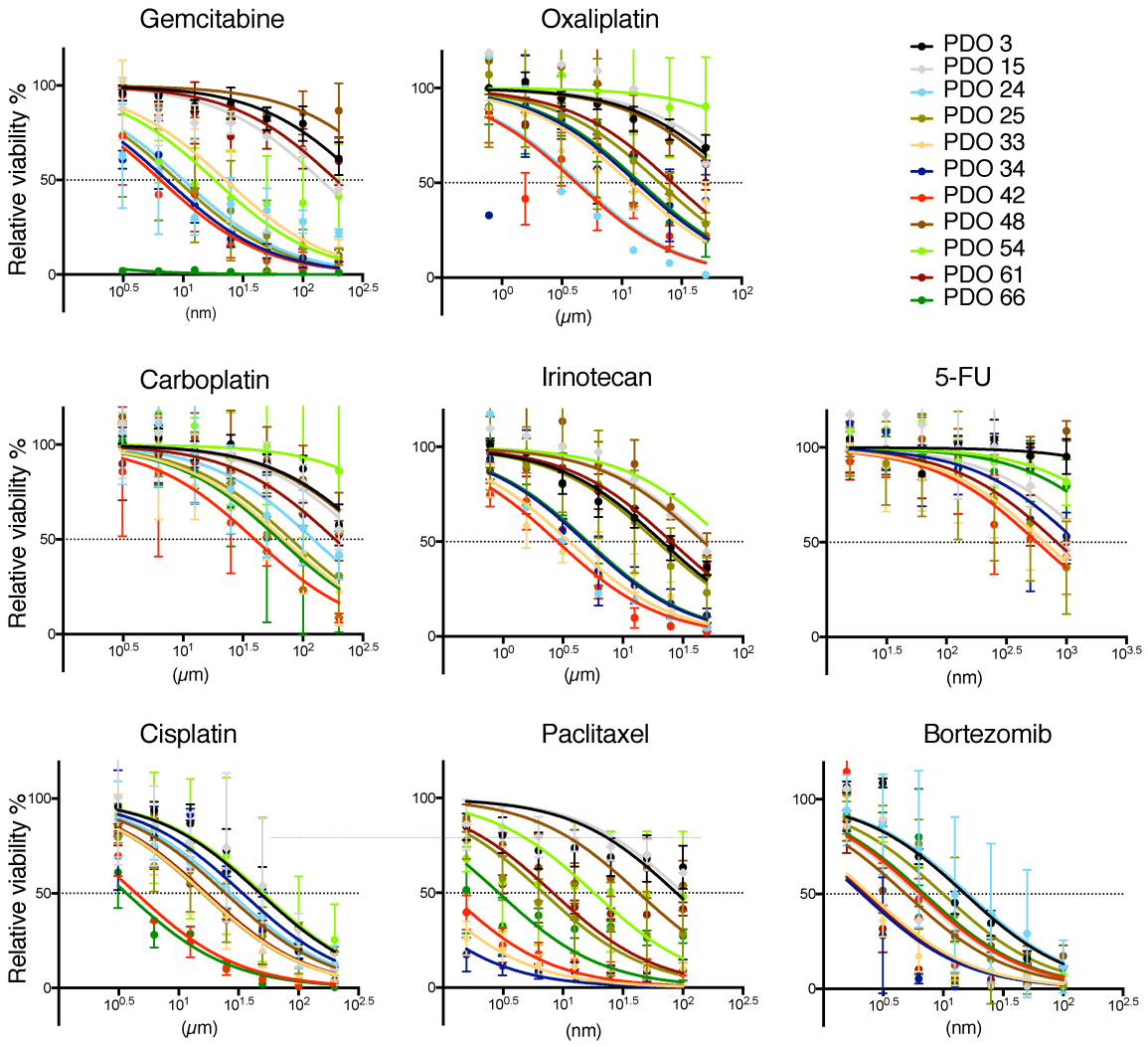

Figure 13. Dose-response curves of different PDO lines to indicated chemotherapeutic drugs.

By calculating the IC-50 value of PDOs treated with different chemotherapeutic drugs, a diverse range of IC-50 between PDOs was noticed illustrating the inter-tumoral heterogeneity (Fig. 14).

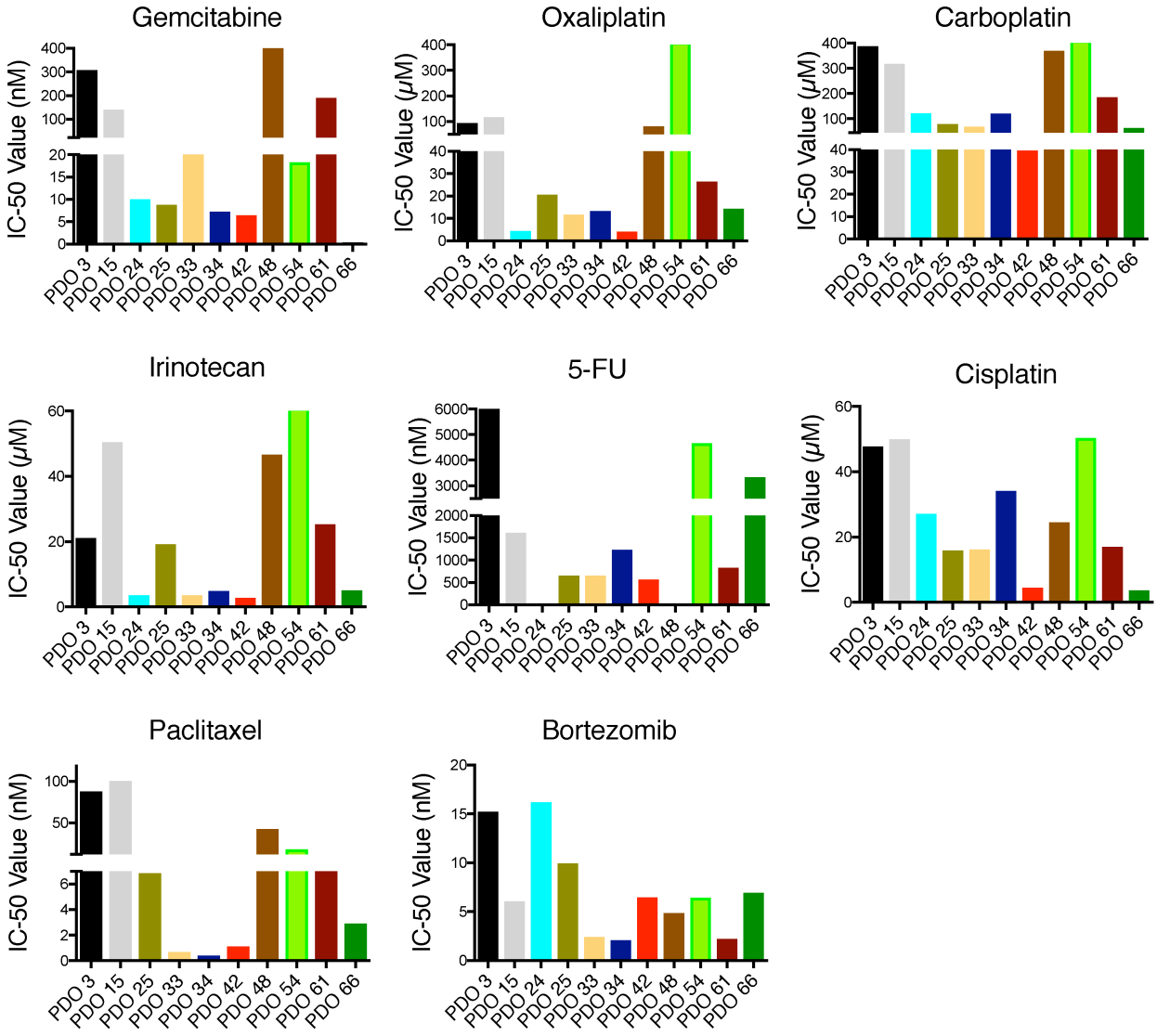

Figure 14. IC-50 of each organoid line regarding different drugs as indicated.

Based on calculation of IC-50, the PDOs were grouped into resistant (more than 75% percentile), intermediate (between 25% and 75%) and sensitive (less than 25% percentile) (Fig. 15). An intra-tumoral heterogeneity regarding drug response could be observed. For instance, PDO 61 showed an intermediate response towards most of the drugs as well as being highly resistant towards gemcitabine. In contrast to that, PDO 61 displayed a high sensitivity towards

bortezomib. On the other hand, PDO 54 showed a high sensitivity towards gemcitabine whereas being resistant towards platinum family as well as 5-FU and irinotecan (Fig. 15).

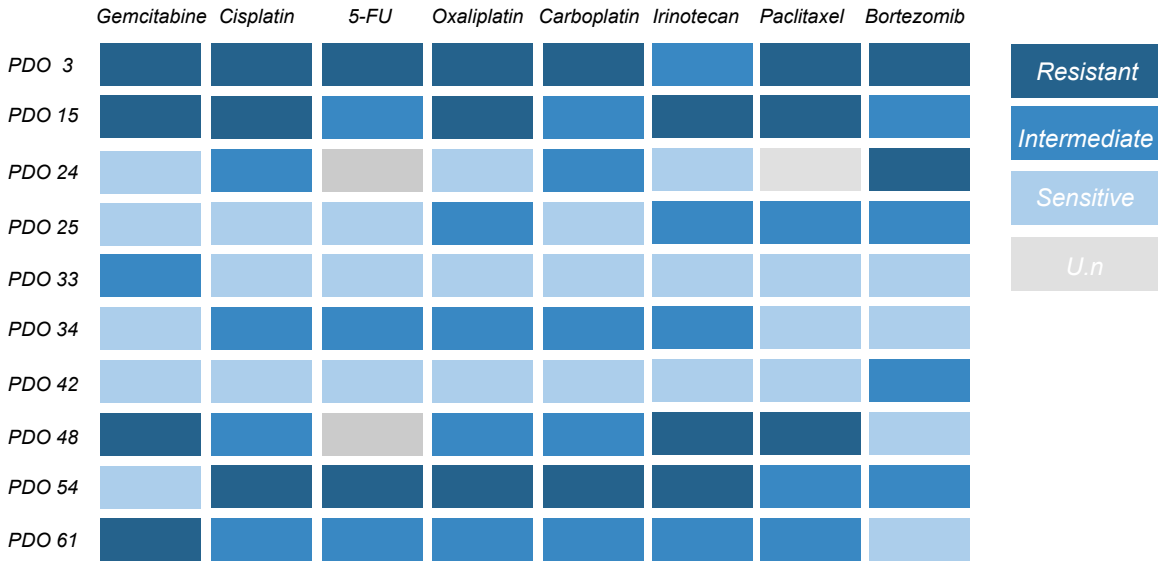

Figure 15. Heatmap illustrates the inter- and intra-tumoral heterogeneity of different PDOs regarding different chemotherapeutic drugs. U.n = Unknown. Resistant: IC-50 was higher than 75% percentile, Intermediate: IC-50 was between 25% and 75% and sensitive: IC-50 was lower than 25% percentile.

1.10. Pharmacogenetic analysis reveals gemcitabine dependent signatures

In order to investigate the difference between resistant and sensitive PDOs towards gemcitabine on the transcriptomic level, PDOs were subjected to RNA-sequencing. PDOs were screened for differential expression and the analysis showed that 27 genes were regulated at an alpha level of 0.05 (Fig. 16 A). Out of these 27 genes, twenty had a high expression in resistant PDOs, whereas 7 genes showed a high expression in sensitive PDOs (Fig. 16 A). To further characterize group differences on pathway level, gene set enrichment analysis (GSEA) was conducted. Testing within the KEGG, Reactome and GSEA Hallmark databases revealed several pathways being altered between resistant and sensitive PDOs including EMT signaling (Fig. 16 B)

A

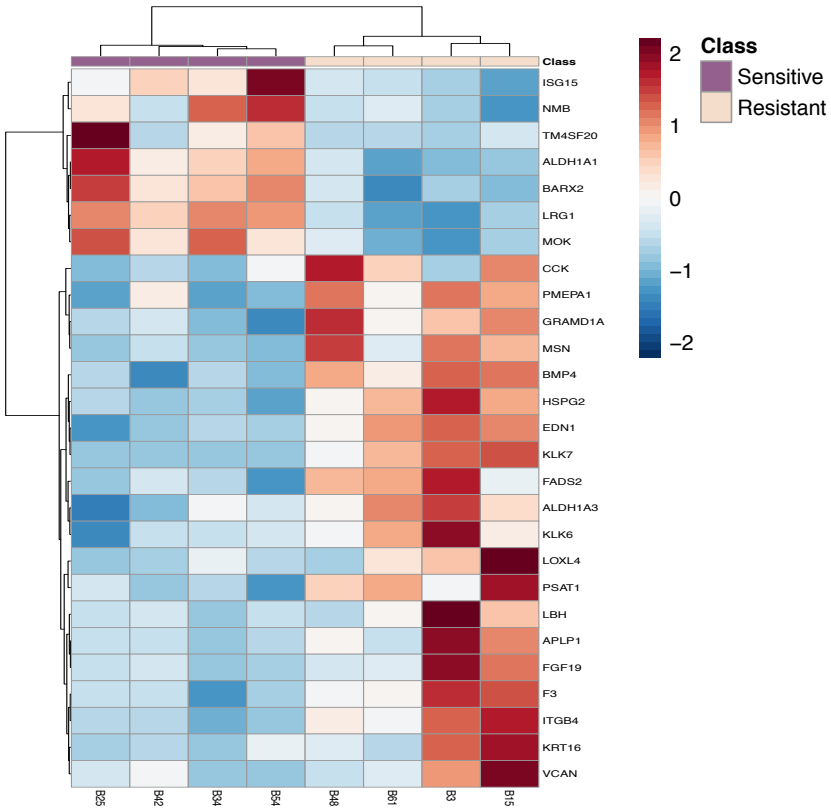

B

KEGG gene set	Genes overlap	p-value	FDR q-value
REGULATION_OF_ACTIN_CYTOSKELETON	3/216	2.46 e^{-4}	4.57 e^{-2}

REACTOME gene sets	Genes overlap	p-value	FDR q-value
A_TETRASACCHARIDE_LINKER_SEQU EQUENCE_IS_REQUIRED_FOR_GAG_SYNTHESIS	2/25	9.16 e^{-5}	3.55 e^{-2}
G_ALPHA_Q_SIGNALLING_EVENTS	3/184	1.53 e^{-4}	3.55 e^{-2}
PEPTIDE_LIGAND_BINDING_RECEPT EPTORS	3/188	1.63 e^{-4}	3.55 e^{-2}
GASTRIN_CREB_SIGNALLING_PATHW THWAY_VIA_PKC_AND_MAPK	3/205	2.11 e^{-4}	3.55 e^{-2}
CHONDROITIN_SULFATE_DERMATAN_ AN_SULFATE_METABOLISM	2/49	3.56 e^{-4}	4.51 e^{-2}
HEPARAN_SULFATE_HEPARIN_HS_GA _GAG_METABOLISM	2/52	4.01 e^{-4}	4.51 e^{-2}

HALLMARK gene sets	Genes overlap	p-value	FDR q-value
APICAL_JUNCTION	3/200	1.96 e^{-4}	3.27 e^{-3}
EPITHELIAL_MESENCHYMAL_TRANSI NSITION [200]	3/200	1.96 e^{-4}	3.27 e^{-3}
TNFA_SIGNALING_VIA_NFKB	2/101	1.96 e^{-4}	3.27 e^{-3}
ANDROGEN_RESPONSE	2/112	1.5 e^{-3}	1.84 e^{-2}
BILE_ACID_METABOLISM	2/200	1.84 e^{-3}	1.84 e^{-2}
INFLAMMATORY_RESPONSE	2/200	5.72 e^{-3}	3.57 e^{-2}
KRAS_SIGNALING_DN	2/200	5.72 e^{-3}	3.57 e^{-2}
MTORC1_SIGNALING	2/200	5.72 e^{-3}	3.57 e^{-2}

Figure 16. **A.** Heatmap illustrates the differentially expressed genes between resistant and sensitive PDOs. **B**. Gene set enrichment analysis results of differentially expressed genes between resistant and sensitive PDOs.

II. PDAC organoid technology: A model with predictive power for the clinic?

2.1. Does PDO response recapitulate the clinical response of patient?

In order to investigate whether PDOs recapitulate the treatment response of the corresponding patient's treatment, the treatment response of PDOs towards gemcitabine was compared with the progression-free survival (PFS) of the corresponding patient. Since a subset of patients who were enrolled in our PDO biobank received gemcitabine as a first-line therapy (Fig. 13, dose-response curves of PDOs towards gemcitabine), the clinical response (PFS) was compared with the corresponding PDO sensitivity towards gemcitabine. To this end, the area under the curve (AUC) of PDOs treated with gemcitabine was calculated (Fig. 17 A) and PDOs grouped into three subgroups including resistant PDOs (top 33% AUC), intermediate PDOs (middle 33% AUC) and sensitive PDOs (lowest 34% AUC) (Fig. 17 A). Interestingly, patients with gemcitabine-resistant PDOs displayed a mean progression-free survival (PFS) of 50 days compared to the expected PFS of 180 days (Conroy et al., 2011; Von Hoff et al., 2013; Tiriac et al., 2018a). Whereas, the patients with gemcitabine-sensitive PDOs showed a mean PFS of 200 days (Fig. 17 B).

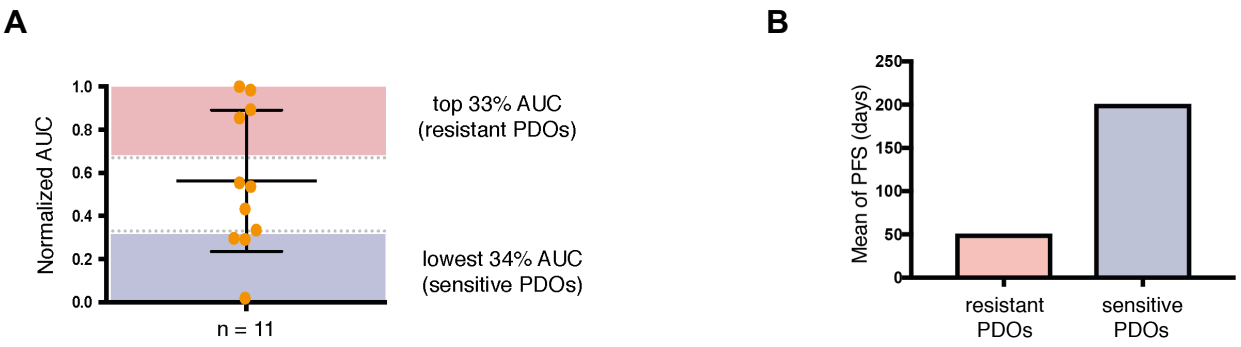

Figure 17. A. Calculation of area under the curve (AUC) of PDO lines treated with gemcitabine. **B.** Graph represents the mean of progression free survival (PFS) from patients treated with gemcitabine compared to the treatment response in corresponding PDOs.

Another proof of concept demonstrating that organoid technology is a model with predictive power for the clinic is represented by a patient with *PALB2* germline mutation, who was enrolled in our PDO biobank. It has been shown that 14% of PDAC patients are grouped as "*BRCAness*" having mutations in DNA maintenance genes (*BRCA1*, *BRCA2* and *PALB2*) and DNA repair machinery genes. These patients show a high sensitivity towards platinum base therapy and PARP inhibitor (Waddell et al., 2015). The patient received 6 cycles of FOLFIRINOX and following treatment a major reduction in tumor size and reduced diameter of the main pancreatic duct compared to the baseline scan was noted (Fig. 18 A). PDOs were generated from liver metastasis of this patient and treated with the PARP inhibitor olaparib, using another PDO as a control. Interestingly, the *PALB2* mutated PDO showed increased sensitivity to PARP inhibitor whereas the control PDO showed no response even with the highest concentration of 1000 nM (Fig. 18 B).

These results underscore the fact the organoids might be the first human model system with predictive value with regards to drug sensitivity.

A **B**

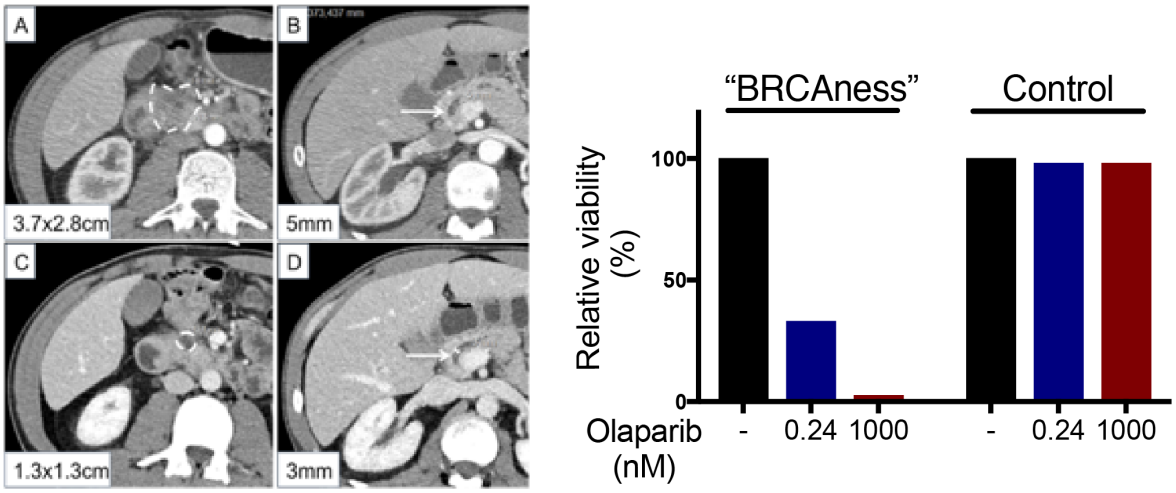

Figure 18. A. (A&B) Baseline arterial phase MSCT (multi-slice computed tomography): The size of the tumor (A) and main pancreatic duct (B) before treatment are shown. (C&D) post therapy arterial phase MSCT: The reduction of the tumor (C) and main pancreatic duct (D) after 6 cycles of FOLFIRINOX is shown. **B**. High sensitivity of *PALB2* mutated PDO towards olaparib versus control PDO.

III. Establishing a cost-effective culture method for human pancreatic organoids (NFMmodified)

The media supplements for PDOs as well as the matrix are expensive. Since the consistency of the matrix is extremely important to analyze the distinct biology, I decided to stay with Matrigel and modify the media supplements in order to make this culture technique affordable and therefore accessible to a larger group of scientists. Overall the established NFMm media is approximately 80% cheaper than the NFM media. The modified media (NFMmodified) was validated in comparison to the published NFM media by the group of Dr. Tuveson (Boj et al., 2015) using several assays to assess morphology, viability and most importantly sensitivity towards chemotherapy. PDOs were also compared *in vivo* (by orthotopic transplantation of PDOs and generation of PDOX), and on the transcriptomic and genomic level by performing RNA-seq. and WES respectively.

3.1. Comparing morphology and viability in PDOs cultured with NFM media versus PDOs cultured with NFMm media

Morphologically, PDOs cultured with NFM media look very similar with PDOs cultured with NFMm (Fig. 19 A). In the PDO repository, some PDOs grew better with NFM media, whilst some grew better with NFMm. For our further investigation exploring the effect of media on the growth of organoids, PDOs that grew with both media conditions have been selected. By comparing the passage number, PDOs treated with both media conditions showed the same passage number (Fig. 19 B).

A **B**

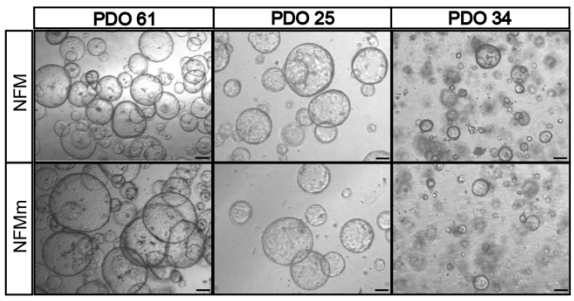

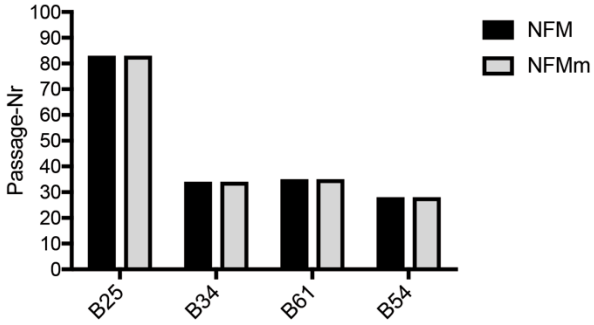

Figure 19. A. Representative phase-contrast images of PDOs cultured with NFM and NFMm media. The upper panel shows PDOs cultured with NFM media and the lower panel illustrates PDOs cultured with NFMm media. Scale bars, 50 µM. **B**. Comparing passage number in 4 different PDOs cultured with 2 different media (NFM and NFMm).

3.2. Analysis of proliferation as well as apoptosis in both media conditions by immunofluorescence staining (Ki67/ToPro and Cleaved-cas3/ToPro)

In order to validate whether there was a difference in proliferation as well as apoptosis between 2 media conditions, immunofluorescence (IF) staining for Ki-67 and cleaved-Cas 3 was performed (Fig. 20 A). The Ki-67 and Cleaved-Cas 3 positive cells were counted in 6 organoids in each individual PDO which was grown under both media conditions. In addition, ToPro (nuclear stain) positive nuclei were also counted in the corresponding organoids. Then the Ki-67 and Cleaved-Cas3 positive cells were divided by ToPro positive cells in each individual PDO that illustrates proliferation and apoptosis respectively (Fig. 20 B). Statistically there was no significant difference in proliferation and apoptosis between the 2 media conditions (Fig. 20 B).

A

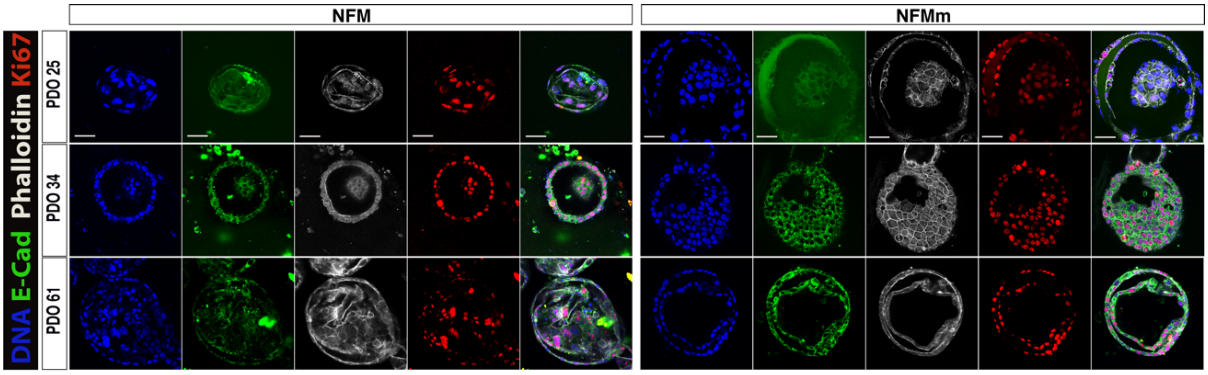

B

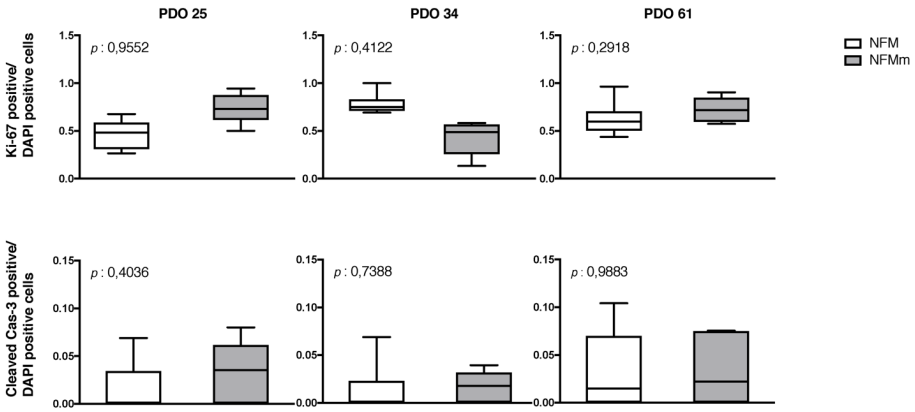

Figure 20. Immunofluorescence staining of PDOs cultured with NFM and NFMm. **A**. Comparing proliferation and apoptosis in 2 different culture media by Ki-67 and cleaved Cas-3 staining. Scale bars, 50 µM. **B**. IF analysis of proliferation and apoptosis, regarding the 2 different culture media. The positive Ki-67 and cleaved Cas-3 cells were counted in 6 different organoids in each conditioned media and normalized to TopRo positive cells. The mean ± SEM is shown, and p-value was determined by unpaired Student *t*-test.

3.3. Comparing sensitivity of PDOs cultured with NFM versus NFMm media towards chemotherapeutic drugs by performing drug screening

Different studies including our study have shown that PDOs offer a valuable platform for testing drugs *in vitro* which recapitulate the drug response of the corresponding patient *in vivo.* Therefore, the most important question was whether media has an effect on the therapeutic response of PDOs. In order to address this question, PDOs with different media conditions were treated with 8 different chemotherapeutic drugs. Morphologically, there was no difference between organoids treated with specific drug in the 2 media conditions (Fig. 21). By analyzing the viability using CellTitre-Glo Luminescent cell viability assay, there was no significant difference in drug response between the 2 media conditions (Fig. 22 A and B). However, there was a significant difference in the carboplatin and oxaliplatin response of PDO 61 although there were not any differences in other settings (Fig. 22 B).

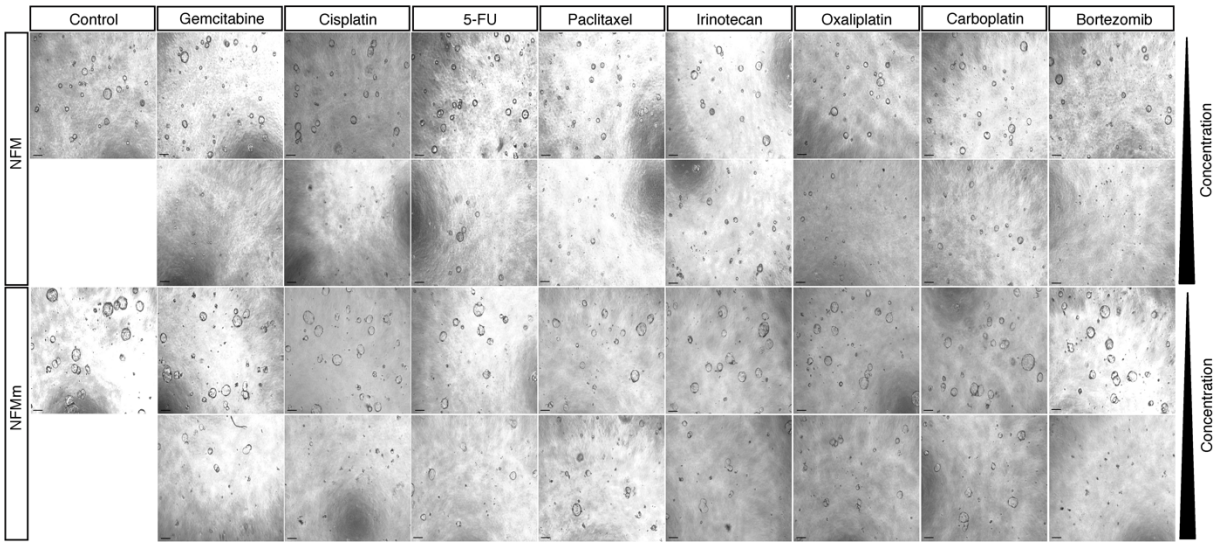

Figure 21. Drug screening of PDOs with 2 different media conditions. Phase-contrast images of PDOs under treatment with 8 different chemotherapeutic drugs. Representative images of the lowest and highest concentration of each drug is shown. Scale bars, 50 μM.

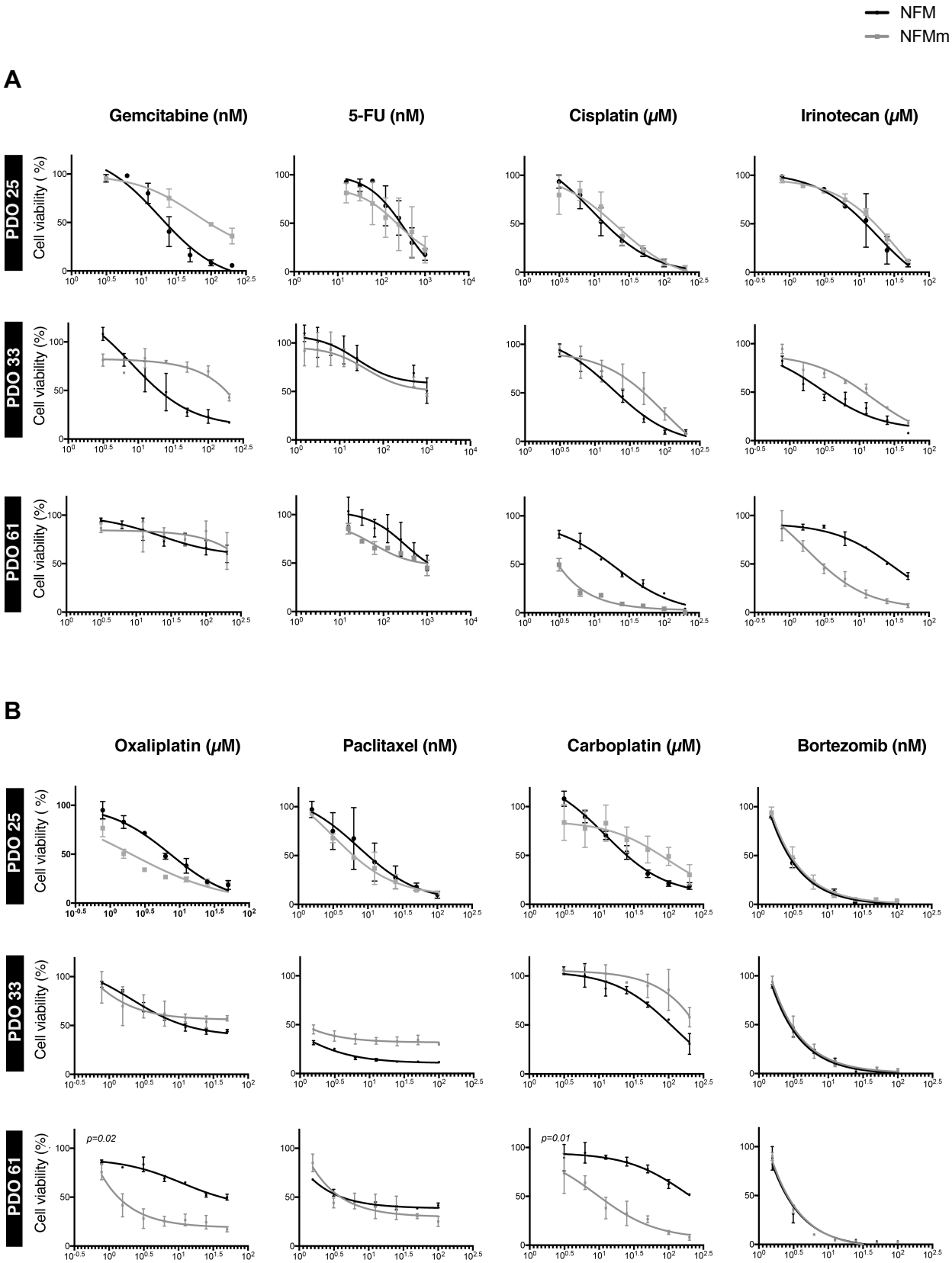

Figure 22. Drug screening of PDOs with 2 different media conditions. **A.** Statistically, regarding gemcitabine, 5-fu, cisplatin and irinotecan there was no significant difference observed between the 2 media conditions. The mean ± SEM was calculated, and p-value was determined by unpaired Student *t*-test. **B.** Statistically, regarding paclitaxel and bortezomib there was no significant difference between the 2 media conditions. In regard to oxaliplatin and carboplatin, there was only a significant difference seen in PDO 61, whereas in the other 2 PDOs no significant difference was observed. The mean ± SEM was calculated, and p-value was determined by unpaired Student *t*-test.

3.4. Comparing tumor initiation capacity of PDOs cultured with NFM versus NFMm by orthotopic transplantation

Additionally, in order to demonstrate the ability of PDOs to initiate tumor formation upon orthotopic transplantation in athymic nude mice, the PDOs treated with NFM and NFMm were orthotopically transplanted (intra-pancreatic). In all cases, except transplanted mice with PDO 54-NFM, the mice were imaged after 50 days with PET/MRI imaging modalities and euthanized (Fig. 23). The transplanted mice with PDO 54-NFM was euthanized after 35 days because of intestinal complications. All mice generated tumors except for transplanted mice with PDO 54-NFM. It is possible that this is due to the shorter time of transplantation.

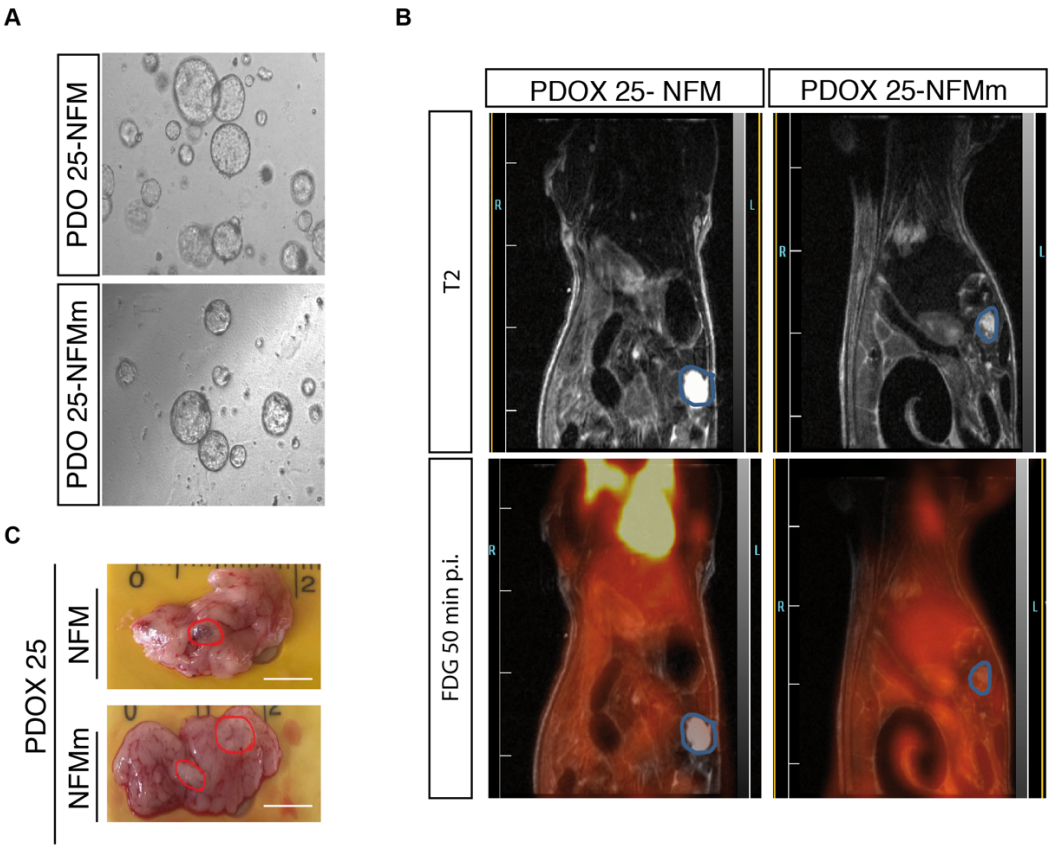

Figure 23. **A**. Representative phase contrast images of PDOs treated with NFM and NFMm. **B**. Monitoring of the tumor by PET/MRI imaging modalities. The upper panel shows the MRI images and the lower panel displays PET images. **C**. Macroscopic images of the PDOX**.**

3.5. Comparison of histology and IHC-subtyping in Patient-derived organoid xenografts (PDOXs) generated from PDOs cultured with NFM vs. NFMm media

Based on H&E staining, all embedded organoid samples (ID 25, 54 and 61, treated with NFM and NFMm (NFM-PDOs and NFMm-PDOs)) presented with a duct-like formation, with single to multilayered pleomorphic cells (Fig. 24 A).

Orthotopic tumor formation after implantation of organoid cultures into the athymic nude mice was morphologically consistent with pancreatic adenocarcinoma in PDOX (NFM: ID 25 and 61 and NFMm: ID 25, 54 and 61). No tumor formation was detectable in transplanted mice with PDO 54-NFM, as explained above. No metastasis was found in any organ for any of the PDOXs.

The subtyping according to the criteria of Muckenhuber et al, 2018 (Table 14), was performed on the PTs, PDOs and PDOXs. In addition, the NFM-PDOs were subtyped based on RNA-seq data (Moffitt subtyping). As shown in the color-coded chart (Fig. 24 B), the subtype is not consistent between PT, PDOs (NFM and NFMm) and corresponding PDOXs based on IHC staining and did not correspond with the Moffitt subtyping of NFM-PDOs. For example, ID-25 shows an HNF1A positive subtype in PT, NFM-PDO and PDOXs (NFM and NFMs), whereas the subtype was switched to KRT81 positive subtype in NFMm-PDO. Interestingly, the RNA-seq subtype of NFM-PDO based on Moffitt subtype showed a classical subtype which was different from IHC subtyping of both NFM- (HNF1A positive) and NFMm- (KRT81 positive) PDOs. On the other hand, ID-61 displayed a double-negative subtype in PT, PDOs (NFM and NFMm) and NFM-PDOX whereas the subtype was switched to HNF1A positive subtype in NFMm-PDOX which was in line with RNA-seq subtyping of NFM-PDO, which showed a basal-like subtype.

A

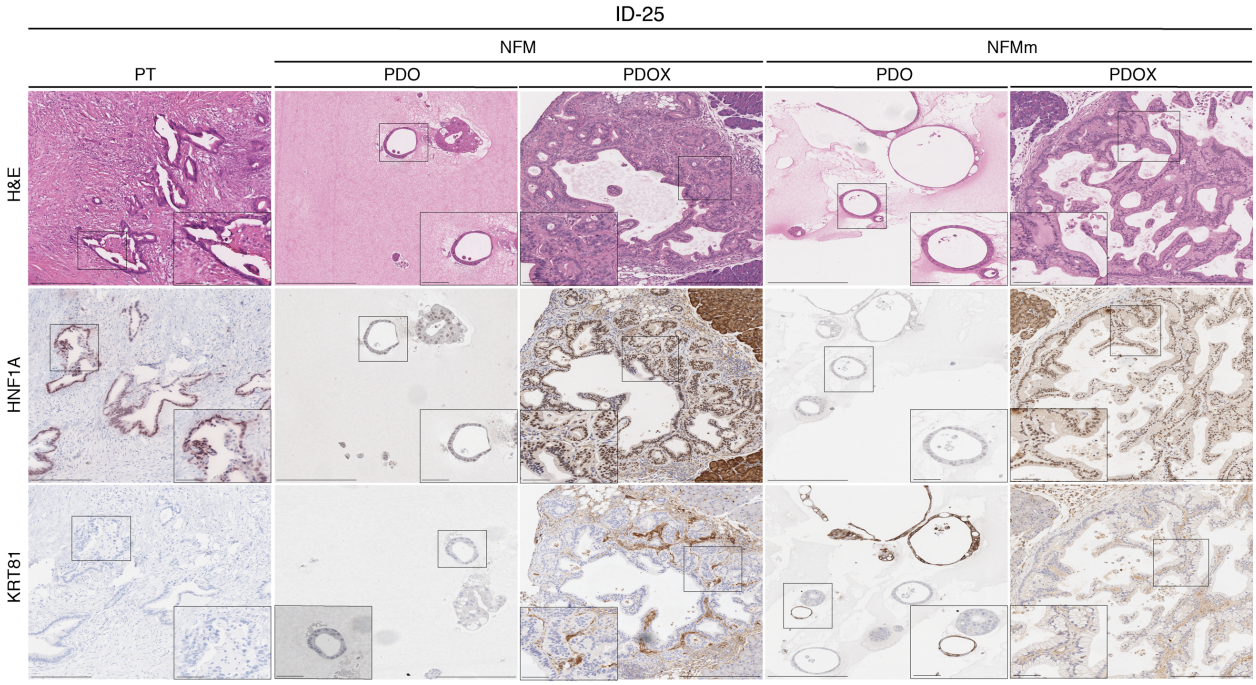

B

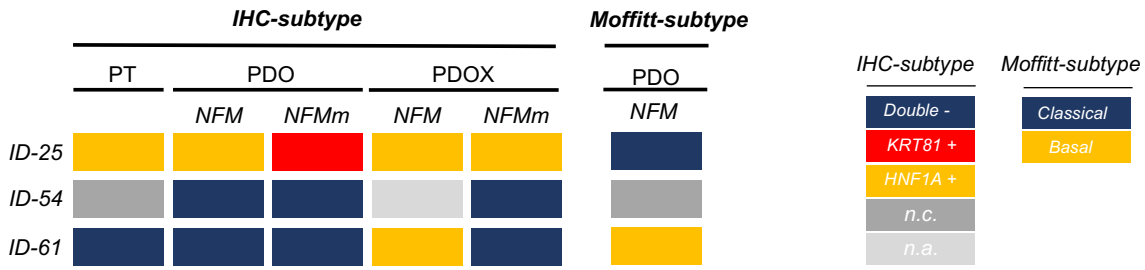

Figure 24 A. Representative images of H&E staining and IHC staining based on HNF1A and KRT81 in PT, PDO (NFM and NFMm) and PDOX (NFM and NFMm); ID-25. **B.** Color-coded chart illustrates the subtyping of PT, PDO (NFM and NFMm) and PDOX (NFM and NFMm) based on IHC subtype and subtyping of NFM-PDO based on RNA-seq. (Moffitt-subtype). n.c.: not classified, n.a.: not available.

3.6. Characterizing of PDOs with different media conditions on the transcriptomic level by performing RNA-sequencing

In order to investigate the impact of different media conditions on the transcriptomic level, the RNA from PDOs treated with NFM versus NFMm media was subjected to RNA-sequencing. The analysis of gene expression profiling revealed a homogeneous expression pattern which can be seen in the scatter plots (Fig. 25).

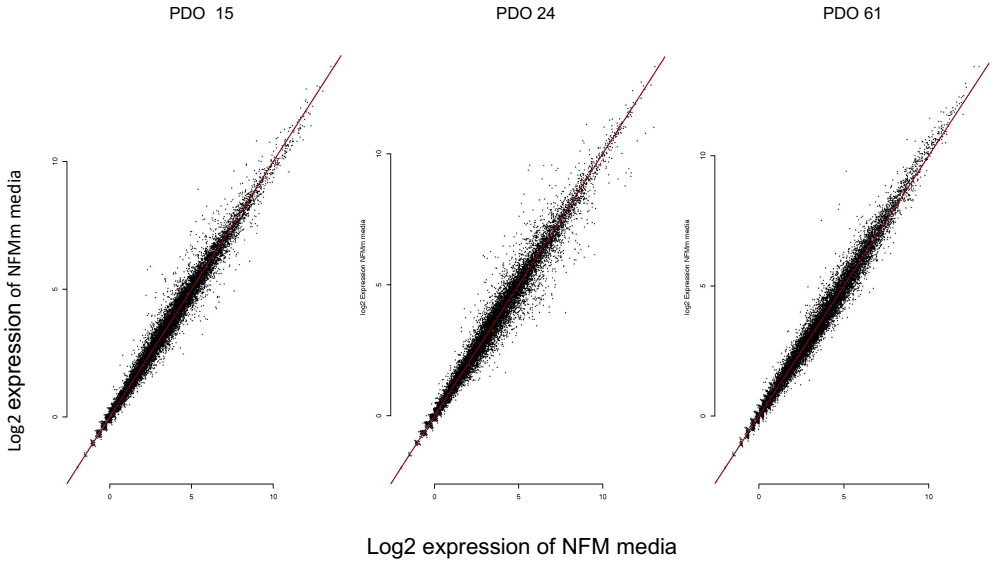

Figure 25. Scatter plots show a homogenous pattern based on comparing the log2 expression genes in NFM-PDOs (X-axis) versus NFMm-PDOs (Y-axis).

3.7. Comparison of PDOs with different media conditions based on whole-exome-sequencing (WES)

In order to see whether PDOs show a difference on the genomic level between media conditions, DNA from PDOs treated with NFM and NFMm was subjected to WES. There was no difference on the genomic level between NFM- and NFMm-PDOs. For example, on the copy number level, the same amplification and deletion of parts of chromosomes between NFM- and NFMm-PDOs could be seen (Fig. 26 A). When comparing MAF of *KRAS* and *TP53* in NFM-PDO versus NFMm-PDO (ID-61) no difference could be seen (Fig. 26 B). Furthermore, by filtering for missense and nonsense mutations between NFM-PDO and NFMm-PDO, 60% shared mutations

were identified, 21 % of genes were unique for NFM-PDO whereas 19% of genes were unique for NFMm-PDO (Fig. 26 C).

A

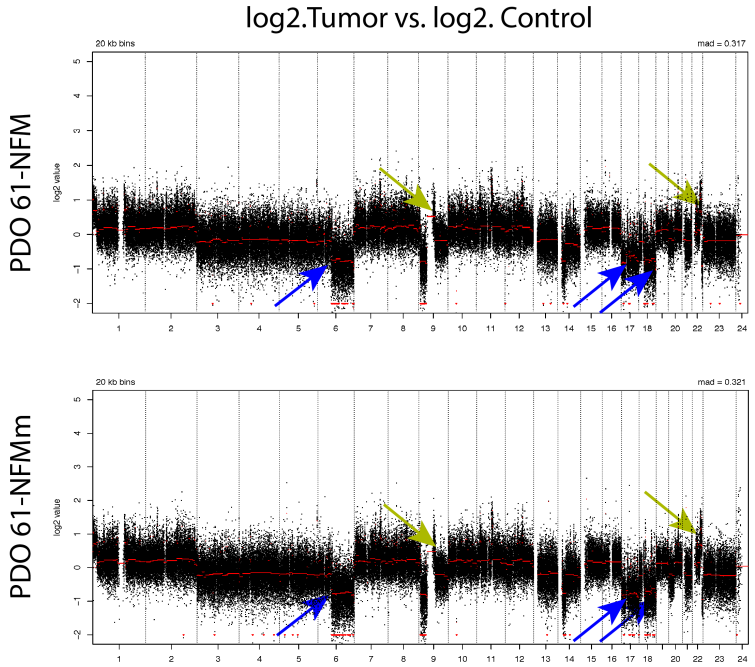

B

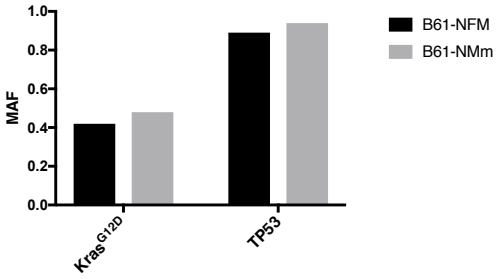

C

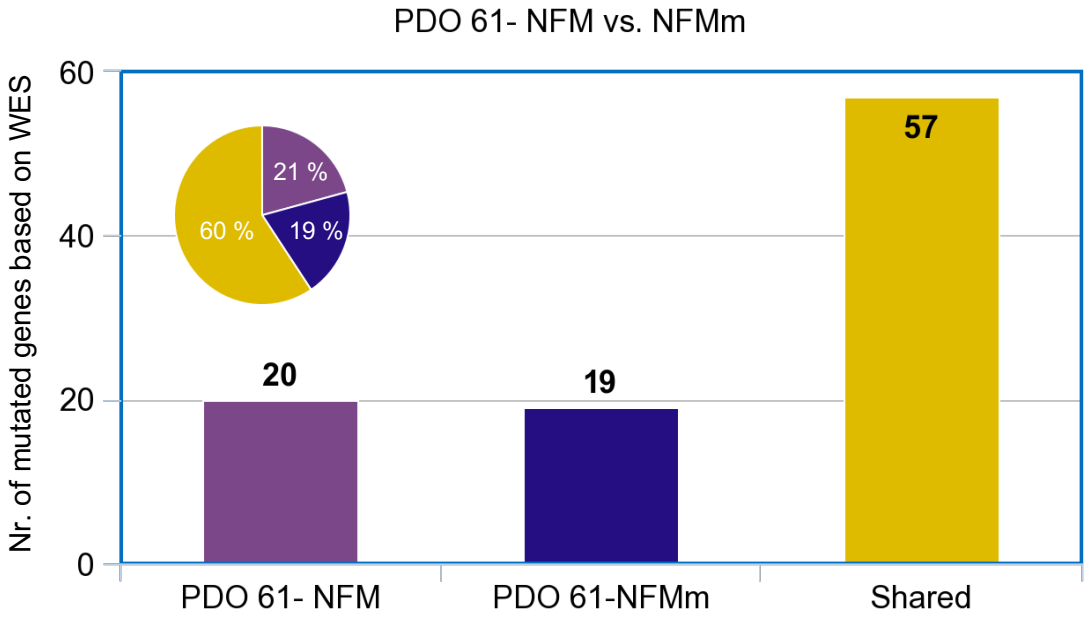

Figure 26. No difference neither in CNVs nor in MAFs between NFM-PDO versus NFMm-PDO was seen**. A**. Comparing copy number variations of NFM-PDO versus NFMm-PDO. Green arrows show amplification whereas the blue arrows show deletions of parts of the chromosomes. **B**. Similar MAF of *KRAS* (heterozygous mutation) and *TP53* (homozygous mutation) in NFM-PDO vs. NFMm-PDO. **C**. Illustration of the missense and nonsense mutations in NFM-PDO (purple bar), NFMm-PDO (blue bar) and number of mutations which are shared between NFM- and NFMm-PDOs (yellow bar). The pie chart displays the percentage of shared mutated genes (60%), unique mutated genes in NFM-PDO (21%) and unique mutated genes in NFMm-PDO (19%).

IV. Utilizing patient-derived organoids from fine needle aspiration as diagnostic and therapeutic research platforms for personalized medicine in pancreatic ductal adenocarcinoma

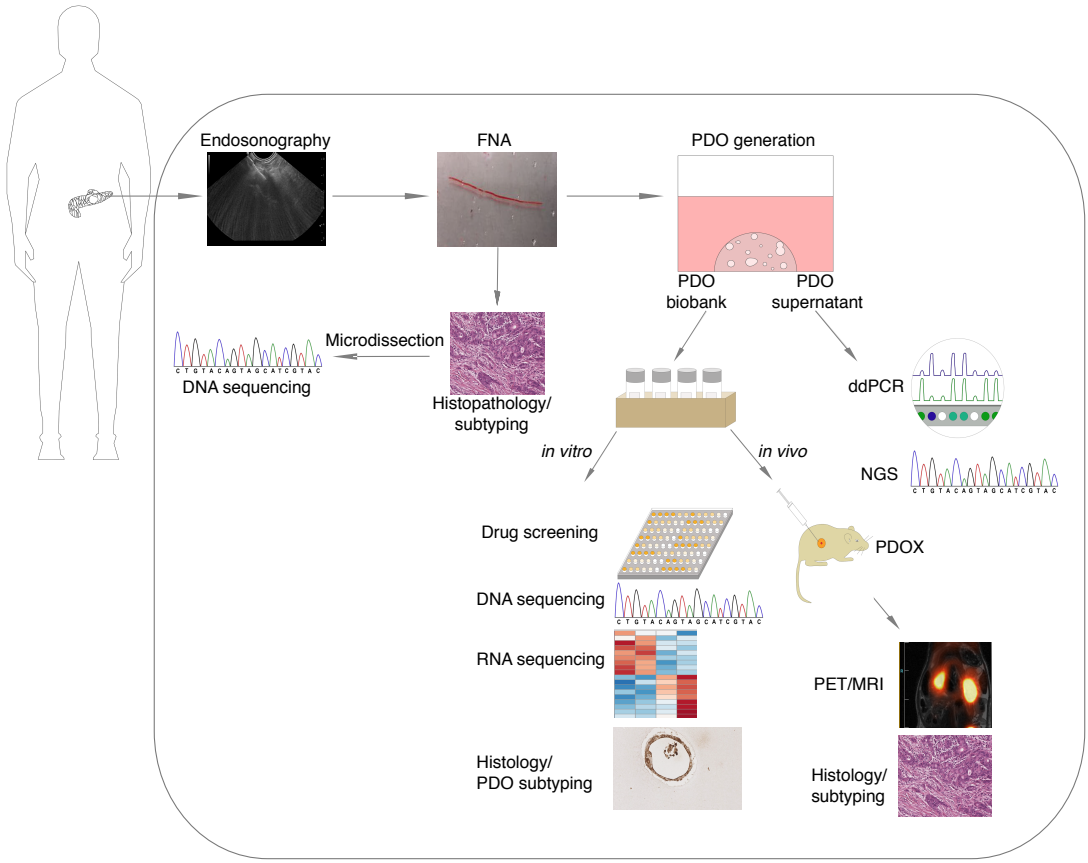

Figure 27. PDOs from EUS-FNA as diagnostic research platforms in PDAC

4.1. The success rate of established PDOs from EUS-FNAs and characterizing the cytology/histopathology status of EUS-FNAs

As it was mentioned in section 1.3, 80 patients were enrolled in this study. PDOs were derived from surgical specimens (n=39) or EUS-FNAs (n=41). The take rate from surgical resection specimens and EUS-guided FNAs was 97% and 75% respectively (Fig. 28 A). The PDOs withstand the freeze-thaw cycles and functional assays including sequencing and drug screens could be performed within 2-6 weeks post isolation. Frequently, interpreting the cytology from EUS-FNAs with very little material can be challenging. In this study for 58% of established PDOs from EUS-FNAs the histology/cytology was positive, whereas for 42% the cytology or histopathology was negative (Fig. 28 B). In order to overcome this issue, PDOs from EUS-FNAs with negative cytology/histopathology or from FNAs with very low tumor cell number (Supplementary Fig. 2 and Supplementary table 1) were established, expanded (Fig. 28 C) and further characterized.

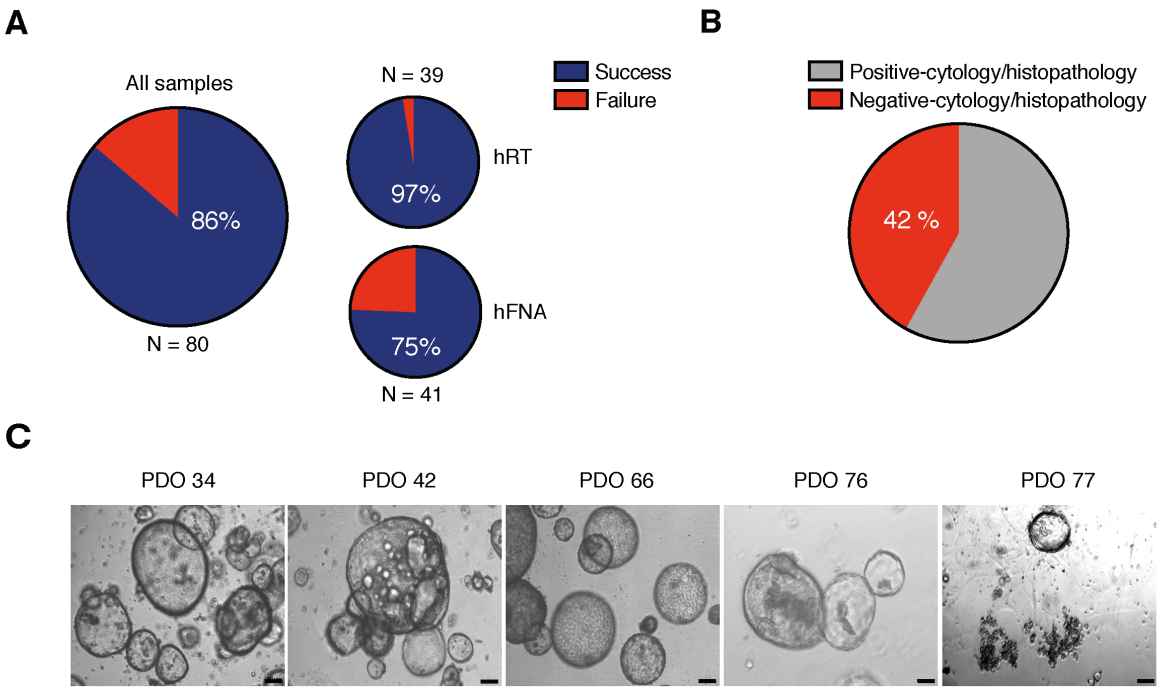

Figure 28. **A**. The overall take rate of PDOs isolated from both resection tumors and EUS-FNAs (the left pie-chart), take rate of PDOs from resection tumors (upper pie chart) and take rate of PDOs generated from EUS-FNAs (lower pie chart). **B.** The cytology/histopathology status of EUS-FNAs of established PDOs. **C.** Phase contrast images of PDOs established from cytology-negative FNAs or from FNAs with very low tumor cell number. Scale bars, 50 μM. hRT: human resected tumor, hFNA: human FNA.

4.2. Orthotopic transplantation of negative-cytology PDOs and generation of patient-derived-organoid xenografts (PDOXs)

In order to further characterize the negative-cytology PDOs and demonstrate the tumor initiating capacity of PDOs, two PDOs (ID 34 and 66) with negative-cytology and one PDO with few neoplastic cells in cytology (ID 42) were orthotopically transplanted into athymic nude mice (Nc (NCr)-Foxn1nu). The mice were monitored 50 days post transplantation by PET-MRI imaging modalities. The tumor was established in all transplanted mice and visualized by MRI and PET imaging modalities (Fig. 29).

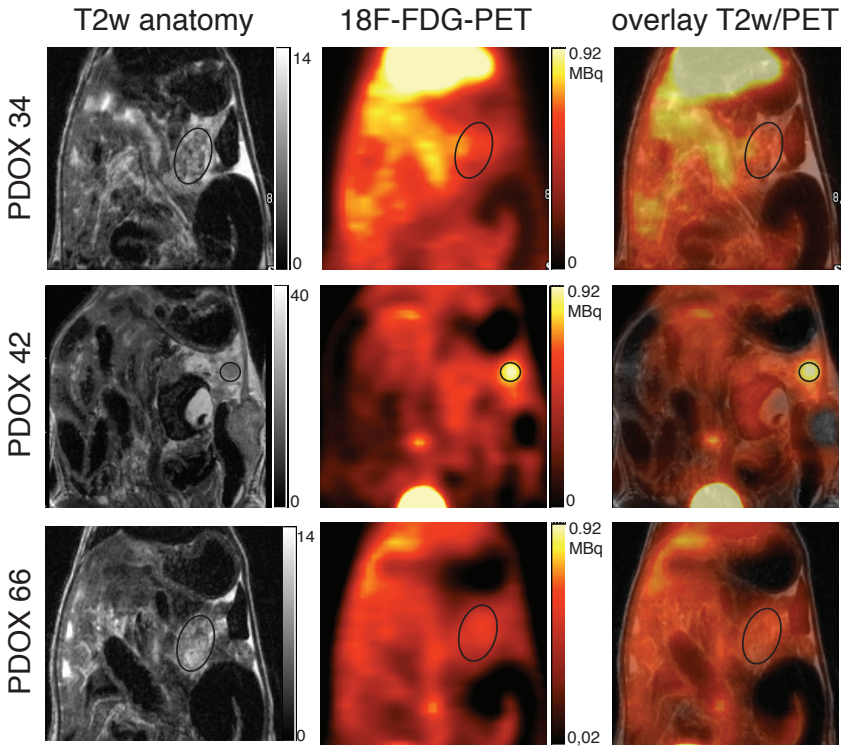

Figure 29. MRI/PET images of PDOXs**.** The left panel shows the MRI images, the middle panel displays PET images and the right panel indicates an overly of MRI and PET.

4.3. IHC subtyping of cytology-negative PDOs, corresponding PTs (when available) and PDOX based on HNF1A and KRT81 expression

After PET and MRI imaging, the animals were consequently euthanized. Macroscopically all transplanted mice demonstrated tumor burden. Hematoxylin & Eosin (H&E) and IHC staining was performed on PDO, PDOX (Fig. 30 and Fig 31 A) and primary tissue when available (FNA or resection tumor) (Fig. 31 A).

Following the embedding process and H&E staining of the PDOs and PDOXs, all PDOs displayed a multifocal duct-like formation with single to multilayered pleomorphic cells and PDOXs showed a solid or cystic phenotype (Fig. 30 and 31 A). Interestingly, in PDOX 42, which showed 5% dysplastic cells in the corresponding FNA- cytology, one small metastasis in the liver with ductal morphology was found (Fig. 31 B). In order to identify the subtyping, IHC staining based on KRT81 and HNF1A (Muckenhuber et al., 2018) was performed on the FNA (when available), and the corresponding PDOs and the PDOXs (Fig. 30 and 31 A).

Only in one case (ID 42), the cytology of FNA containing 5% dysplastic cells was available. For the other 2 cases (ID 34 and 66), no cytologic material of diagnostic quality was available. Since 2 patients (ID 76 and 77) underwent surgical resection, the resection tumor (Res.) was further analyzed (Supplementary Table 1 and Supplementary Fig. 2). Interestingly all PDOXs demonstrated a HNF1A-positive subtype (Fig. 30, 31 A and C).

In detail, the subtype for patient ID 42 switched from HNF1A-positive subtype in the primary sample to KRT81-positive subtype in the PDO and back to HNF1A-positive subtype in the PDOX (Fig. 31 C). The subtype of patient ID 66 switched from double-negative subtype in the PDO to HNF1A-positive subtype in the PDOX. In summary, both PDOXs 42 and 66, switched from other subtypes in corresponding PDO to HNF1A-positive subtype in PDOX, whilst PDOX 34 maintained the subtyping of the corresponding PDO (HNF1A-positive subtype) (Fig. 31 C).

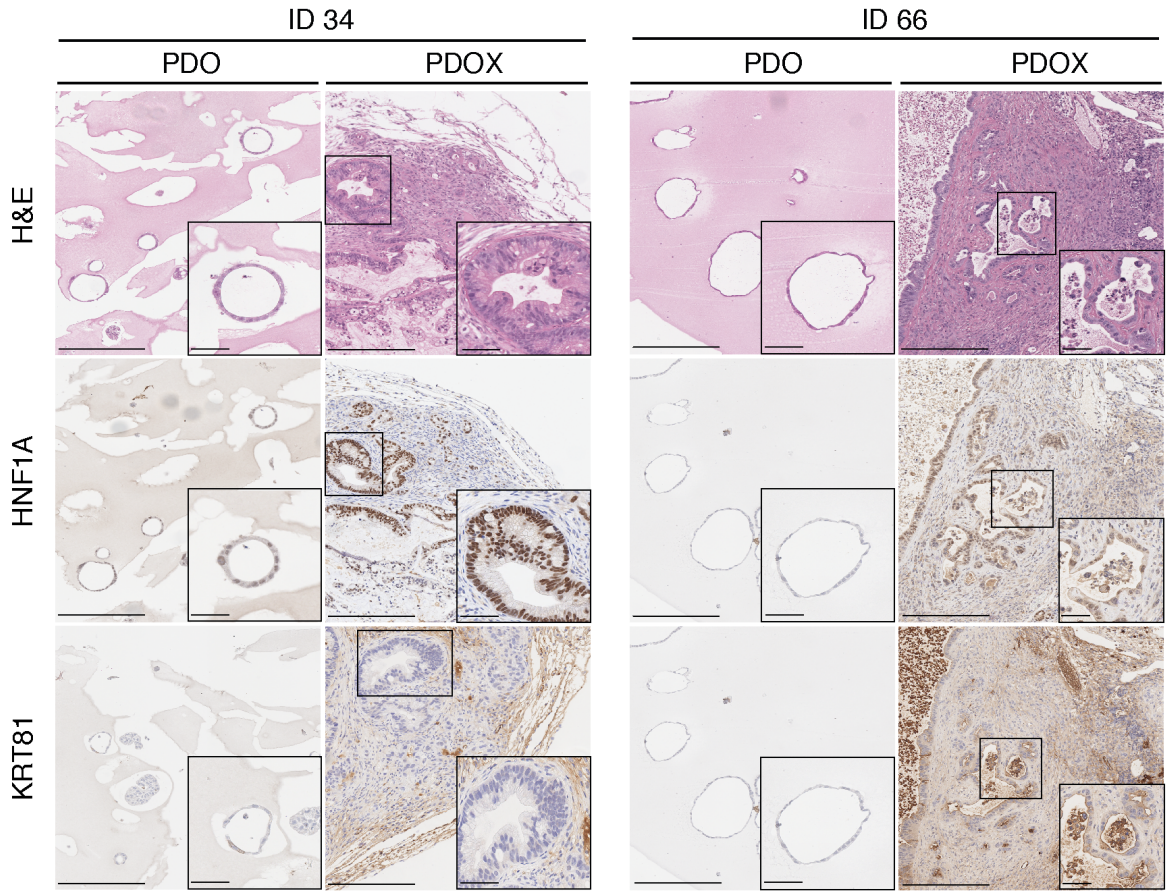

Figure 30. H&E staining and subtyping of PDO and PDOX from 2 patients with negative cytology/histopathology (ID 34 and ID 66). Upper panel: H&E staining of PDO and corresponding PDOX. Middle panel: HNF1A staining of PDO and PDOX. Lower panel: KRT81 staining of PDO and PDOX. Scale bars are 300µm for the main images and 60µm for the inset images.

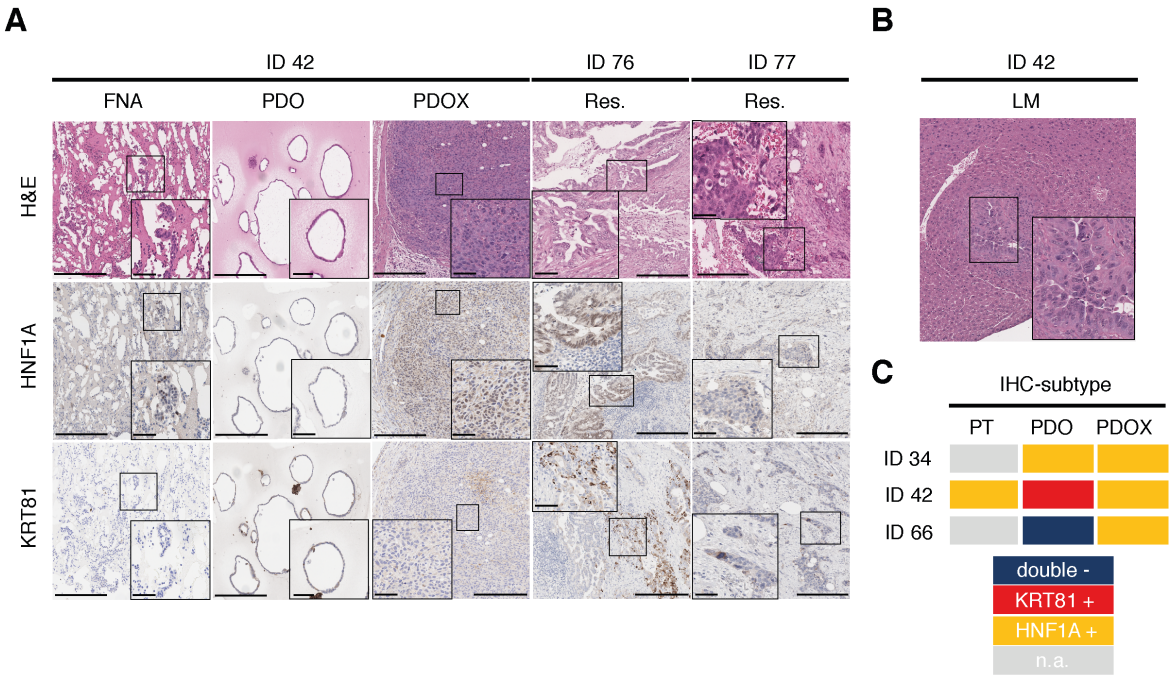

Figure 31. **A**. H&E staining and subtyping of PDO, PDOX and PT (FNA (ID 42) or resection tumor (Res.) (ID 76 and 77)). Upper panel: H&E staining of PT, PDO and corresponding PDOX. Middle panel: HNF1A staining of PT, PDO and PDOX. Lower panel: KRT81 staining of PT, PDO and PDOX. Scale bars are 300µm for the main images and 60µm for the inset images. **B**. H&E staining of the liver metastasis of PDOX 42. **C**. The color-coded chart illustrates the subtyping of PT, PDOs and corresponding PDOXs. n.a.: not available.

4.4. Characterizing of negative-cytology FNAs on the genomic level by performing next generation sequencing

In order to characterize the negative-cytology FNAs on the genomic level, the DNA from PT (FNA or Res. when available), PDO and PDOX (FFPE) was extracted and next generation sequencing (NGS) was performed. On the genomic level, PDOs displayed *KRAS* mutation and other frequent mutated candidates in PDAC (*TP53*, *CDKN2A* and *SMAD4*), and in addition other additional candidates such as *FLT4*, *NLRP1*, *ZNF521*, *WRN*, *KAT6A*, *KDM6A* and *COL1A1* (Fig. 32, 33 and Supplementary Table 2) were identified underscoring the tumor characteristic of the negative-cytology PDOs. Especially, a striking similarity between mutational profile of PDO with the corresponding PDOX could be identified (Fig. 32 A). Since PDOs have a high enrichment of tumor cells, they displayed a higher MAFs compared to the primary tumor. For example, a *MYC* amplification in PDO 42 based on NGS was detected that was not detectable in the corresponding PT (Supplementary Fig. 3 A). In addition, on the histopathology level based on MYC staining, the primary tumor (FNA) of ID 42 showed a very low cellularity whereas the IHC staining for MYC displayed high MYC-levels in PDOs

compared to the primary tumor (Supplementary Fig. 3 B). However, nearly identical MAFs regarding one PDO and corresponding PT (ID 76) could be observed (Fig. 32 B), therefore the tumor/stroma ratio in the micro-dissected area was analyzed and showed an exceptionally high tumor cellularity of the micro-dissected area (Supplementary Fig. 4).

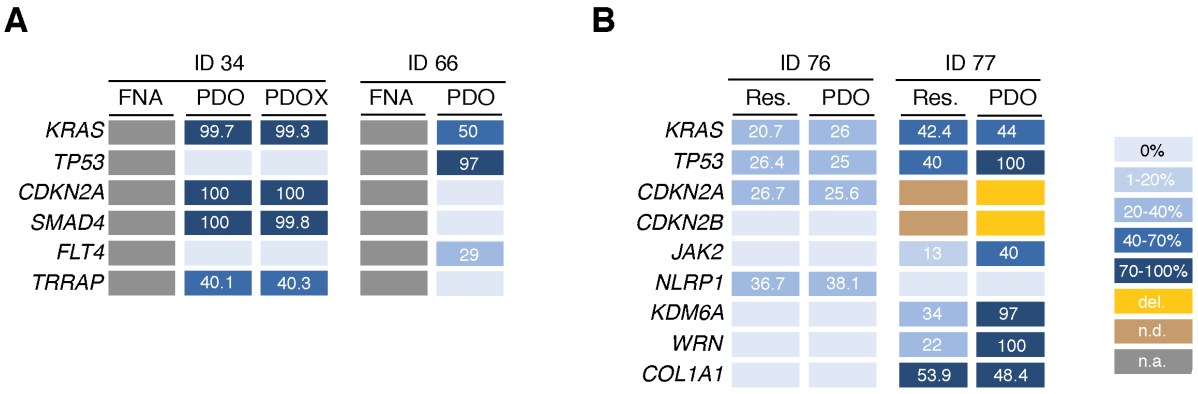

Figure 32. **A**. Detection of mutations in PDOs generated from negative-cytology FNAs (ID 34 and 66). Mutational profile of PDOX 34 shows a high similarity to the corresponding PDO. **B**. Detection of mutations in PDOs (ID 76 and 77) and corresponding primary tumor (Res.). del.: deletion; n.d.: not detectable; n.a.: not available.

4.5. Subjecting PDO-SN to ddPCR and NGS for identifying *KRAS* and other mutational profile in PDAC

In order to reduce the time for diagnosis of negative-cytology PDOs and facilitate further molecular characterization of PDAC, the supernatant of PDOs was harvested and subjected to digital droplet PCR (ddPCR) in order to detect mutations of $KRAS^{G12D}$, $KRAS^{G12V}$, and $KRAS^{G12R}$ (Fig. 33 A and B). In addition, the MAF of indicated *KRAS* mutations in PT (FNA and Res.), PDOs and PDOX was determined by NGS (Fig. 33 B).

Notably, almost identical MAFs of *KRAS* in PDO-SN compared to the PT, PDO and PDOX was observed. For example, performing ddPCR on the PDO-SN in ID 42 displayed 39% MAF of *KRAS*, whereas performing NGS on corresponding PT, PDO and PDO-SN showed MAF of 38%, 50% and 44% respectively. ID 34 showed a 74.5% MAF of *KRAS* in the PDO-SN (ddPCR) versus 99.7% and 99.3% in PDO and PDOX (NGS) respectively. ID 77 demonstrated almost the same MAF of *KRAS* in PDO-SN (44%) compared to the PT (42.4%) and PDO (44%) by NGS (Fig. 33 B). Most importantly, when NGS was applied to the PDO-SN, the matching results from PT and PDO could be obtained (Fig. 33 C). Interestingly, a shift from heterozygous mutation of *TP53* in the primary tumor (FNA) to a homozygous mutation in

PDO could be observed (Fig. 33 C), underscoring the pure epithelial phenotype of PDOs which amplify the signal compared to the primary tumor allowing deeper sequencing and therefore increasing detection of mutation.

Most importantly, the homozygous mutation of *TP53* could be detected in the corresponding PDO-SN as well. Regarding *JAK1* and *ZNF521*, the signal was even amplified in PDO-SN compared to corresponding FNA and PDO (44.4% MAF of *JAK1* in PDO-SN compared to 15.2% and 36.4% in FNA and PDO respectively; 81.8% MAF of *ZNF521* in PDO-SN compared to 53.9% and 56.7% in FNA and PDO respectively) (Fig. 33 C). *CDKN2A* mutation could be detected in the PDO and PDO-SN, while not being detected in the primary tumor (FNA) (Fig. 33 C). On the other hand, *KDM6A* could be detected in FNA and PDO while not being detected in the SN (Fig. 33 C).

A **B**

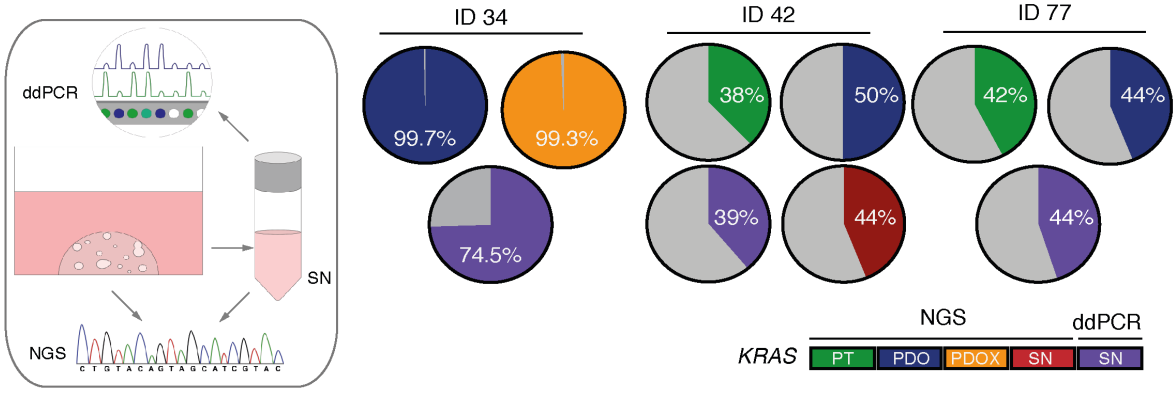

C

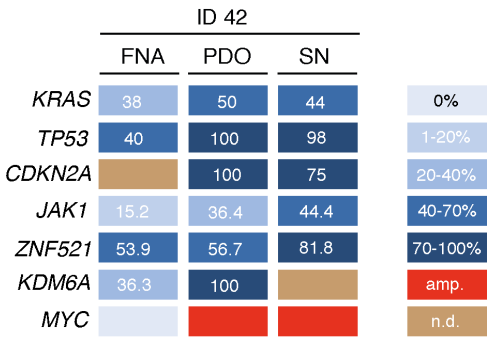

Figure 33. **A**. Workflow for analyzing PDO-supernatant (PDO-SN) by ddPCR. **B**. DdPCR of the PDO-supernatant and NGS of PT, PDO, PDOX and SN. Pie charts illustrate the MAF of *KRAS* (G12D, G12V and G12R) identified by NGS and ddPCR. **C**. Detection of the same mutations in PT (FNA), PDO and PDO-SN by NGS. amp.: amplification; n.d.: not detectable.

DISCUSSION

I. Establishing a PDAC patient-derived organoid (PDO) biobank and characterizing a subset of PDOs by performing drug screens and sequencing (WES and RNA)

In this project, 80 patients were enrolled into a living biobank of PDOs. PDOs were generated from both surgical resection specimens (n = 39) as well as EUS-FNAs (n = 41). The overall success rate of PDOs was 86% with 97% success rate from surgical resection specimens and 75% success rate from EUS-FNAs. Patient derived organoids (PDOs) preserving the architecture and the heterogeneity of the primary tissue offer a new platform for the testing of standard and targeted therapeutic drugs and the discovery of prognostic and predictive biomarkers. The advantages of creating organoids from PDAC patients include**:** (1) enabling basic scientific research on tumor biology in PDAC, and (2) testing different standard chemotherapeutic drugs as well as targeted therapeutics to discover individual patient sensitivities towards different drugs**.**

After generation of the PDOs, the successfully established PDOs could be expanded, indexed and stored. Interestingly, the number of organoids that could be generated from each patient as well as the growth rate of organoids varied between different patients. This variability illustrates the inter-tumoral heterogeneity of the PDOs and was responsible for the different time frames used for the functional assays. However, in most cases drug screens (using conventional as well as targeted therapeutic drugs) could be performed 2-6 weeks post isolation giving the opportunity to study each individual patient in a clinically relevant time frame. Overall, distinct PDOs responded differently to individual drugs, indicating a marked intertumoral heterogeneity similar to what has been shown by Tiriac et al. (Tiriac et al., 2018a). Importantly, the PDO's response to gemcitabine was correlated with clinical response of corresponding patients. For example, patients with gemcitabine-resistant PDOs displayed a shorter mean of progression-free survival compared to patients with gemcitabine-sensitive PDOs similar to the previous study by Tiriac and colleagues (Tiriac et al., 2018a).

Furthermore, the established PDOs could be subjected to whole-exome sequencing (WES) and RNA- sequencing. The high proportion of the stromal compartment in PDAC makes genetic sequencing of this disease more challenging. However, as PDOs harbor an epithelial phenotype, enriched for high tumor cell cellularity, this increases the sensitivity to detection of mutations. In general on the genomic level, there was a strong concordance between PDO

and primary tumor as has been shown in different studies (Boj et al., 2015; Tiriac et al., 2018a). Furthermore, on the CNV level there was an increase in amplifications as well as deletions in the PDO compared to the matched primary tumor, underscoring the high tumor cellularity of PDOs and therefore increasing sensitivity. Comparing mutant allele frequency (MAF) of most mutated candidates in PDAC in PDO versus primary tumor led to the same results (higher MAF in PDO versus primary tumor). In addition, whole exome sequencing of one PDO-line at different passages (interval of 30 passages) showed the same mutational profile over passages of PDOs, suggesting that they preserve their genomic characteristics over passages. This is especially critical for drug screening, since PDOs were subjected to the drug screening at different passages.

The differences on the gene expression level as well as drug sensitivity between 2D (monolayer cell lines) and corresponding primary tumor has been shown (Stein et al., 2004). In this study, by comparing the primary tumor, matched PDO and 2D cultures based on gene expression, a high concordance between PDO and primary tumor could be observed as it has been also shown in previous studies (Boj et al., 2015; Tiriac et al., 2018a). All known mutated candidates in PDAC were shared between PDO and primary tumor, whereas there were either no shared mutated genes between 2D culture and PDO or primary tumor (ID-48) or very low number of shared mutated genes between 2D culture and PDO (ID-3), suggesting that PDOs shared the genomic characteristics of the primary tumor, whereas 2D cultures failed to preserve the mutational profile of the primary tumor. Several explanations might address the different expression profiles observed between 2D cultures and primary tumor. Firstly, genetic drift may occur in 2D cultures, or alternatively, the loss of genetic heterogeneity of the primary tumor may occur during the growth of the culture (Deer et al., 2010; Gillet et al., 2013). Additionally the growth of a sub-population of clones may contribute to the observed differences in expression (Gillet et al., 2013). The possibilty of outgrowth of the cells from the tumor microenvironment could also be possible, however since identification of mutations in non-tumor cells is unlikely, this concern could be excluded. However, based on our study a definitive conclusion is not possible, since only two samples comparing 2D and PDO were analyzed based on the genomic level.

On the transcriptomic level, there were many genes that were differentially expressed between PDOs and matched 2D culture. At the top of the list were EMT markers, which were significantly upregulated in 2D versus 3D (PDOs), suggesting the type of culture per se might influence the RNA expression profiling of cells. Since in 3D culture cells grow in a matrix, the cell-cell interaction as well as cell-matrix interaction can be mimicked better than in 2D culture.

PDOs were subtyped based on RNA-sequencing. The transcriptomic data of PDOs was used to determine the classical and basal-like subtype of PDOs based on Moffitt signatures (Moffitt et al., 2015). Based on Moffitt signature, 59% of PDOs showed a classical subtype whereas 41% displayed a basal-like subtype which is in line with the findings of Tiriac et al. which reported 70% classical PDOs versus 30% basal-like PDOs (Tiriac et al., 2018a). This demonstrates a new finding, since very few cell line models of classical subtype in PDAC are available (Tiriac et al., 2018a; Moffitt et al., 2015). Combining the drug response of individual patients with genomic and transcriptomic information may represent a new scheme of precision medicine in pancreatic cancer (Pauli et al., 2017; Tiriac et al., 2018b).

II. Establishing a cost-effective culture method for human pancreatic organoids (NFMmodified)

Although PDO technology represents a valuable and powerful *in vitro* model system to study pancreatic cancer biology as well as inter-patient tumor heterogeneity regarding drug response, it is an expensive technology due to the matrix (Matrigel) and to the very high costs of established organoid media supplements. The expensive medium is especially critical for a large-scale application such as biobanking of organoids. However, the consistency of the matrix is extremely important to analyze the distinct biology. Therefore, one aim of this project was to establish a more cost-effective culture media that could be used in in order to generate patient-derived organoids successfully and therefore provide an affordable and accessible alternative to the wider scientific community. To this end, modifications on the media components was performed and a new modified media (Normal-Feeding-Media modified; NFMm) was established.

The NFMm media was validated in comparison to the basic organoid media (Normal-Feeding-Media; NFM), which was established by the group of Dr. Tuveson (Boj et al., 2016), using multilayered bioassays assessing morphology, proliferation and take rate. PDOs were also compared based on orthotopic transplantation (patient-derived organoid xenografts; PDOX), whole-exome and RNA sequencing and most importantly sensitivity towards chemotherapy.

PDOs generated with NFM and NFMm showed similar morphology and growth rate. There was not any difference in proliferation nor in rates of apoptosis between PDOs cultured with NFM versus PDOs cultured with NFMm.

Most importantly, the effect of both media conditions on the chemotherapeutic response of PDOs was investigated. In general, there was not any significant difference between PDOs cultured with NFM versus NFMm media towards different conventional chemotherapeutic drugs (gemcitabine, oxaliplatin, cisplatin, carboplatin, 5-flurouracil, paclitaxel, irinotecan and bortezomib).

It should be mentioned that there were some organoid-lines that could only grow with one type of medium, either with NFM or NFMm. A variety of factors could contribute to the difference in growth rate. One important aspect could be the inter-tumoral heterogeneity of PDOs, which makes them dependent on different growth factors in the media that are responsible for activating different signaling pathways.

III. Utilizing patient-derived organoids from fine needle aspiration as diagnostic and therapeutic research platforms for personalized medicine in pancreatic ductal adenocarcinoma

As most mutations occur at a frequency lower than 5% in pancreatic cancer, in addition to the noticeable inter- and intra-patient heterogeneity and existing definite morphologic and molecular subtypes in pancreatic cancer (Waddell et al., 2015), it is necessary to analyze large patient cohorts for definition as well as characterization of clinically relevant pancreatic cancer subgroups. Unfortunately, more than 80% of pancreatic cancer patients are not eligible for surgery which is the only curative option (Ryan et al., 2014). Therefore, these patients with advanced pancreatic cancer are an understudied population of PDAC patients due to the insufficient amount of tumor material available. Accordingly, new diagnostic and therapeutic approaches are urgently needed.

In addition, PDOs harbor a pure epithelial phenotype and therefore maintain a decreased signal-to-noise ratio allowing deeper sequencing compared to the primary tumor and thereby increasing sensitivity. In addition, mutations which have been identified in PDOs showed the potential implications for the development of novel therapeutic approaches in the context of personalized medicine (Tiriac et al., 2018a).

Recently, the potential use of organoid technology for generation of PDOs from a small amount of starting material using EUS-guided fine needle aspiration and biopsy (EUS-FNA

and FNB) (Tiriac et al., 2018b) was established to foster discovery of a previously undiscovered genomic and molecular population of PDAC patients with advanced disease. Similarly, in this study PDOs have been generated not only from surgical specimens but also from fine needle aspirations (FNAs). The take rate from fine needle aspiration (FNA) samples was 75% comparable to 72% success rate by Tiriac et al., (Tiriac et al., 2018a). In our study, the success rate was higher in surgical specimens (97%) compared to EUS-FNAs (75%). The higher take rate of surgical specimens argues for a larger starting material and probably more viable cells, as it has been also described by Tiriac and colleagues (Tiriac et al., 2018b). They also described that EUS-guided fine needle biopsy (EUS-FNB) leads to more starting material over FNA (Tiriac et al., 2018b). Most importantly, the potential value of PDOs in predicting therapeutic responses in PDAC has been indicated (Tiriac et al., 2018a). However, the utility of FNA-PDOs as a resource to establish diagnosis and allow molecular characterization of PDAC patients in a reasonable timeframe, even prior to therapy, has not been investigated so far.

Even in a high-volume comprehensive cancer center interpreting the cytology from EUS-guided FNAs of patients with pancreatic masses can be challenging. In one part of this project, I was interested in characterizing PDOs that have been generated from negative EUS-FNAs based on cytological and/or histopathology findings, to establish the patient derived organoid system, not only to predict treatment response, but also as a supportive diagnostic tool. However, even biopsies containing low tumor cellularity that allow making definitive diagnoses, most frequently suffer from lack of sufficient material required for further molecular profiling. Therefore, in addition to PDO generation from negative-cytology FNAs, PDOs were also generated from EUS-FNAs which could lead to a definitive diagnosis but didn't harbor enough material for additional molecular profiling. PDOs were expanded for further characterization such as sequencing and functional downstream applications. Performing molecular characterization of PDOs, drug screens and further functional assays is highly valuable, since it has been shown that 40% of PDAC patients harbor mutations that are potentially druggable (Cancer Genome Atlas Research Network., 2017). Negative-cytology PDOs could initiate tumor upon orthotopic transplantation into nude mice (PDOX).

Primary tumor, matched PDO and corresponding PDOX were also subtyped based on HNF1A and KRT81 expression by IHC subtyping. From the pathological point of view, organoids of EUS-FNA samples can be successfully established with patient derived organoids showing morphological alterations consistent with neoplasia. Patient derived organoid xenografts (PDOXs) show a variable growth pattern, which might be due to different growth patterns of the primary tumors. Based on findings of this study, a direct comparison of

PDO subtype to patient subtype and PDOX requires further exploration. Since the IHC-subtyping was not consistent between PT, PDO and corresponding PDOX, surrogate markers of PDAC subtyping would be recommended. Next, we aimed to determine the PDAC subtype based on gene expression signatures. Therefore, RNA-sequencing was performed in a larger cohort of PDOs. As it has been mentioned before, based on Moffitt signature on RNA-sequencing, 59% of PDOs showed a classical subtype whereas 41% displayed a basal-like subtype.

Similar to previous studies (Boj et al., 2016; Tiriac et al., 2018a), the organoid repository reproduced the genetic information of the patient tumor, and drug testing of PDOs displayed a high concordance to the therapeutic response of patients.

Importantly, one of the main focuses in this part of the project was reduction of the time required for the PDO-augmented diagnosis of PDAC, which is one of the most challenging tasks in this field. The hypothesis was that cell-free DNA (cfDNA) might be released from PDOs in the supernatant even at the very beginning after PDO isolation in vitro and could be used as a valuable source for detection of potentially targetable mutations of the corresponding PDAC patient. To this end, the harvested supernatant was subjected to ddPCR and mutations of $KRAS^{G12D}$, $KRAS^{G12V}$, and $KRAS^{G12R}$ were detected. In addition, submitting PDO supernatant (cfDNA) to next-generation-sequencing could detect the same mutational landscape of the corresponding primary tumor and PDO. These findings illustrate the diagnostic value of PDO technology even during the initial expansion of a given PDO line without disturbing the PDO expansion process which could be used for further functional assays and drug screens.

For future studies, from methodological point of view, the different protocols for isolation, expansion as well as drug screens of PDOs should be compared and standardized. Most importantly, in order to create a more realistic *ex vivo* culture system, developing and optimizing co-culturing of PDOs with tumor-microenvironment cells such as immune cells, fibroblasts as well as nerve and vasculature compartments should be taken into consideration. From clinical aspect, expansion of PDO biobank and performing drug screens combined with PDO profiling on the genomic and transcriptomic level might predict responses in PDAC patients to develop individualized therapy concept and improve patient survival.

ZUSAMMENFASSUNG

Die Zahl der Todesursachen bedingt durch das duktale Adenokarzinom des Pankreas wird prognostiziert, im Jahre 2030 die beiden führenden Krebstodesursachen, das kolorektales Karzinom sowie Brustkrebs, zu überholen. Eine der Hauptursachen dieser Entwicklung, neben den demographischen Veränderungen, ist vor allem die Resistenz gegenüber Chemotherapie. Aufgrund der molekularen und morphologischen Tumorheterogenität, welche zu schlechtem Ansprechen auf chemotherapeutische Ansätze und somit unterschiedlichen klinischen Erfolgen führt, werden dringend effiziente Strategien für personalisierte Assays benötigt. Zu diesem Zweck wurde eine Organoidbiobank (PDO) etabliert, welche mittels einer dreidimensionalen Organoidkultur von 39 Operationsbiopsien und 41 endoskopischen ultraschallgeführten Feinnadelaspirationen (EUS-FNA) mit Erfolgsrate von 97% beziehungsweise 75% generiert wurde.

Aufgrund der immensen Kosten von Supplementen für das bereits publizierte NFM Organoidmedien (Boj et al., 2015) wurde eine kostengünstige Alternative etabliert, welche zur erfolgreichen Generierung von PDOs aus pankreatischem Tumorgewebe verwendet werden kann. Dieses modifizierte Medium (NFMm) wurde gegenüber dem NFM Medium mittels vielschichtiger Bioassays zum Erfassen der Generierungsrate, Proliferation, Viabilität und Morphologie validiert. Des Weiteren wurden die PDOs, kultiviert in den verschiedenen Medien, basierend auf orthotopischer Transplantation (PDOX), Whole-Exom- und RNA-Sequenzierung und am wichtigsten aber auf Basis ihrer Sensitivität gegenüber Chemotherapie miteinander verglichen. Interessanterweise waren die PDOs, welche mit dem NFMm Medium generiert wurden, in allen Parametern vergleichbar mit den korrespondierenden, in NFM Medium-generierten PDOs.

Die etablierten PDO-Linien überstehen mehrere Einfrier-Auftau-Zyklen und ab 2 bis 6 Wochen nach Isolierung können funktionale Experimente mit ihnen durchgeführt werden. Screenings mit verschiedenen konventionellen Chemotherapeutika wie Gemcitabin, 5-Fluoruracil (5-FU), Oxaliplatin, Cisplatin, Carboplatin, Irinotecan, Paclitaxel und Bortezomib konnten aufzeigen, dass PDOs die intertumorale Heterogenität wiederspiegeln und zudem mit den Parametern in der Klinik korrelieren. Zum Bespiel haben Patienten, deren korrespondierende PDOs resistent gegenüber Gemcitabin waren, ein mittleres progressionsfreies Überleben (PFS) von 50 Tagen verglichen mit den zu erwartenden 180 Tagen. Im Gegensatz dazu zeigten Patienten mit Gemcitabin-sensitiven PDOs ein mittleres PFS von 200 Tagen.

Ein weiterer Beweis dafür, dass PDOs als Applikation zur Vorhersage von Therapieansprechen und Nachahmung der Biologie von PDAC *in situ* dienen, war ein Patient mit einer *PALB2* Keimbahnmutation. Wie schon aus der Literatur bekannt, weisen DNA-Reparaturgene (*BRCA1*, *BRCA2*, *PALB2*) eine höhere Sensitivität gegenüber Platinum-basierten Chemotherapeutika und PARP-Inhibition auf. In der Tat konnten bei einem Studienpatienten, diagnostiziert mit familiärem Pankreaskrebs, aufgrund der *PALB2* Keimbahnmutation hervorragende Resultate mittels Platinum-basierter Chemotherapie erzielt werden. Bemerkenswerterweise zeigten PDOs, die nach Therapie generiert wurden, mit einer *PALB2* Mutation signifikantes Ansprechen auf PARP-Inhibitoren wie Olaparib mit einem IC50-Wert von 0,16 nM, während *PALB2* Wildtyporganoide auch bei einer Konzentration von 1000 nM in keinster Weise reagierten.

In dieser Studie wurden die PDOs als Modellsystem für die Diagnose, genetische Charakterisierung und Plattform für Behandlungen mit Chemotherapeutika in einem kurzen und klinisch-relevanten Zeitfenster verwendet.

In 42% der EUS-FNA Biopsien, aus denen PDOs etabliert wurden, konnten anhand der Cytologie und/oder Histologie keine eindeutige Diagnose gestellt werden. Das nächste Ziel war es, das Potenzial der PDO-Technologie als diagnostisches Tool zu untersuchen, um die Informationen, welche man von einer einzigen Biopsie erhält, zu vermehren. Die Ergebnisse deuten klar auf das enorme Potenzial dieser Technologie hin. Aus nur wenigen in der Biopsie enthaltenen Tumorzellen, welche in der cytologischen Analyse jedoch unentdeckt blieben, und aus EUS-FNAs mit einer negativen Cytologie (Cytologie-negative PDOs) konnte genug Material gewonnen werden, um funktionale *in vivo* Experimente durchzuführen. Zum Beispiel führten die Cytologie-negativen PDOs, welche orthotop in Nude-Mäuse transplantiert wurden (PDOX), zur Entstehung eines Pankreastumors. Des Weiteren konnten die Primärtumore (PT), PDOs und PDOXs anhand IHC Färbungen basierend auf HNF1A- und KRT81-Expression in verschiedene Subtypen unterteilt werden. Insbesondere aber zeigten die Cytologie-negativen PDOs das PDAC-Mutationsprofil sowie zusätzliche genetische Mutationen auf.

Noch wichtiger allerdings war es, die Zeit, welche zur Diagnose mittels der PDO-Technologie und zur molekularen Charakterisierung von PDAC notwendig ist, zu verringern, was derzeit eine der anspruchsvollsten Aufgaben in diesem Gebiet darstellt. Der Hypothese nach wird Zell-freie DNA (cfDNA) von den PDOs direkt nach der Isolierung freigesetzt, welche zur Detektion von möglicherweise behandelbaren Mutationen des Patienten verwendet werden kann. Zu diesem Zweck wurde die cfDNA des PDO-Überstandes (PDO-SN) mittels

digital-droplet PCR (ddPCR) und Next-Generation-Sequenzierung (NGS) zur genomischen Charakterisierung untersucht. Interessanterweise konnte die Sequenzierung der cfDNA des PDO-SNs das gleiche Mutationsprofil erzielen wie der korrespondierende PT und PDO. Diese Daten wiederum suggerieren, dass die cfDNA im PDO-SN als wertvolle Ressource in der Medizin gegen Pankreaskrebs dienen kann.

Zusammengefasst lässt sich sagen, dass dieses neu etablierte Organoidkultursystem das klinische Ansprechen der Patienten vorhersagen könnte. Zusätzlich wird diese Technologie durch das modifizierte und bezahlbare Protokoll zugänglich für die gesamte wissenschaftliche Community auf dem Gebiet des Pankreaskrebses und könnte somit in großem Umfang nützlich für die Klinik sein. Die Ergebnisse dieser Studie deuten ebenso darauf hin, dass die Generierung der PDOs von einer einzigen EUS-FNA die diagnostische Genauigkeit erhöht und auch molekulare Subtypisierung und Medikamentenscreenings ermöglicht, was in kurzer Zeit auch in der Klinik Anwendung finden kann.

ACKNOWLEDGEMENTS

I dedicate this work to the memory of our patients. I thank all patients and their families.

I would like to thank my supervisor Dr. med. Maximilian Reichert for his great mentoring, valuable support, trust and for giving me the opportunity to develop my own ideas and improve my research skills as well as giving me the chance to attend many national and international conferences. I owe my gratitude to Prof. Dr. med. Roland M. Schmid for giving me the opportunity to work in his department. I also would like to thank Prof. Dr. med. Roland M. Schmid and Prof. Dr. med. Güralp O. Ceyhan for their valuable input, advice and support during Thesis Committee Meetings.

Special gratitude goes to Prof. Dr. med. Jens Siveke for his valuable support.

I am especially grateful to TUM graduate school for the financial support to attend AACR conference. With a special mention to Dr. Nicole Abbrederis, Dr. Katrin Offe, Bettina Kratzer and Desislava Zlatanova from TUM Medical Graduate Center for their great support and assistance.

Special gratitude goes to AGA Moti L. & Kamla Rustgi for giving me the international travel Award.

I would like to acknowledge the support of my laboratory members including Katja Peschke, Reiner Dunkl, Karin Feldmann, Aristeidis Papargyriou. Jana Grosz, Yukio Iwamoto, Charlotte Spitzner and Lukas Zottl.

I owe my gratitude to my friend, Dr. Laura Jacob for all of her support during my PhD as well as her diligent revision of my thesis.

Special thanks go to Thomas Engleitner, Dr. Sebastian Lange, Dr. Rupert Öllinger, Dr. rer. nat. Clara Lubeseder-Martellato, Dr. Jennifer Altomonte, Dr. Ana Hidalgo-Sastre, Dr. Alexander Muckenhuber, Dr. Katja Steiger, Dr. His-Yu Yen for fruitful scientific discussions. I also would like to thank the technical contribution of Olga Josefina Seelbach, Marion Mielke, Thomas Wochnig, Sybille Reder, Markus Mittelhäuser, Julia Horstmann and Jens-Peter Zimmermann.

Finally, I am tremendously grateful to my lovely family and my friends especially Ms. Sadaf Dabirian for their constant support.

APPENDIX

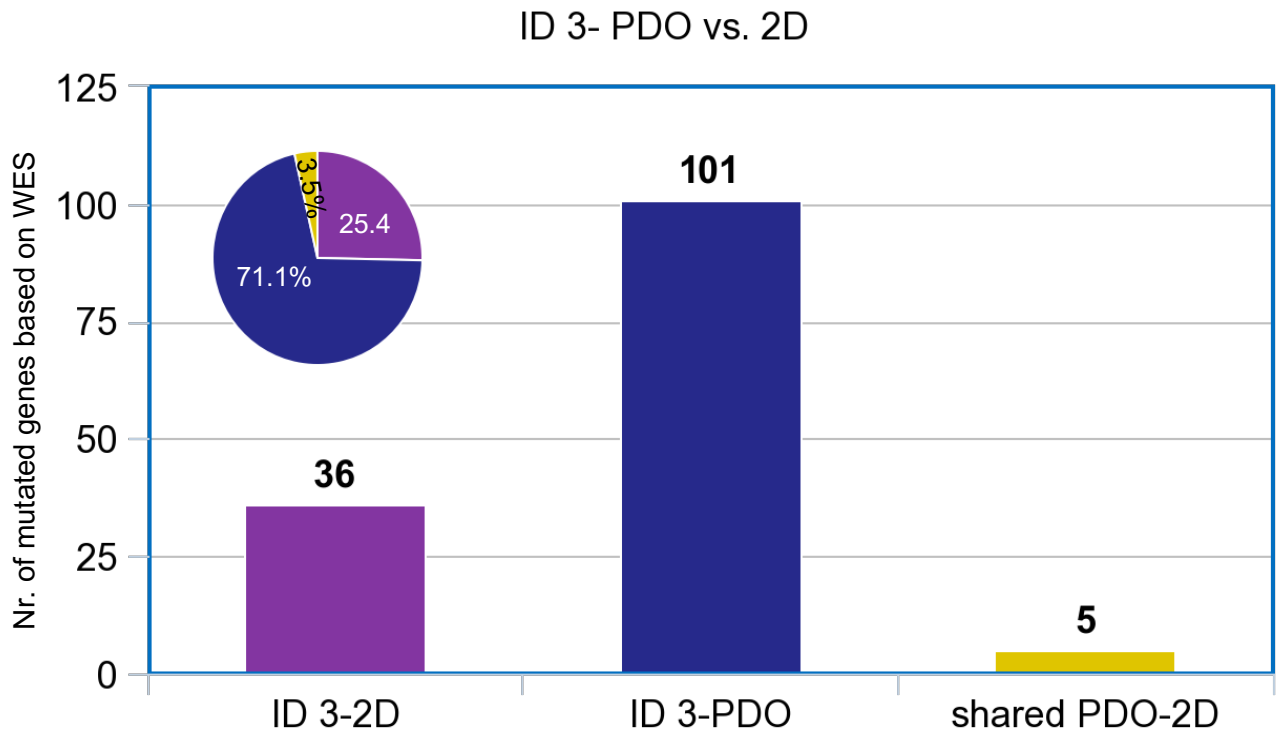

Supplementary figure 1. Number of missense and nonsense mutations in PDO and paired 2D culture. The pie chart shows the percentage of missense and nonsense mutations for PDO (71.1%), 2D culture (25.4%) as well as shared genes between PDO and 2D (3.5%). The bar graphs show the number of missense and nonsense mutations for 2D culture (36), PDO (101), shared PDO-2D (5).

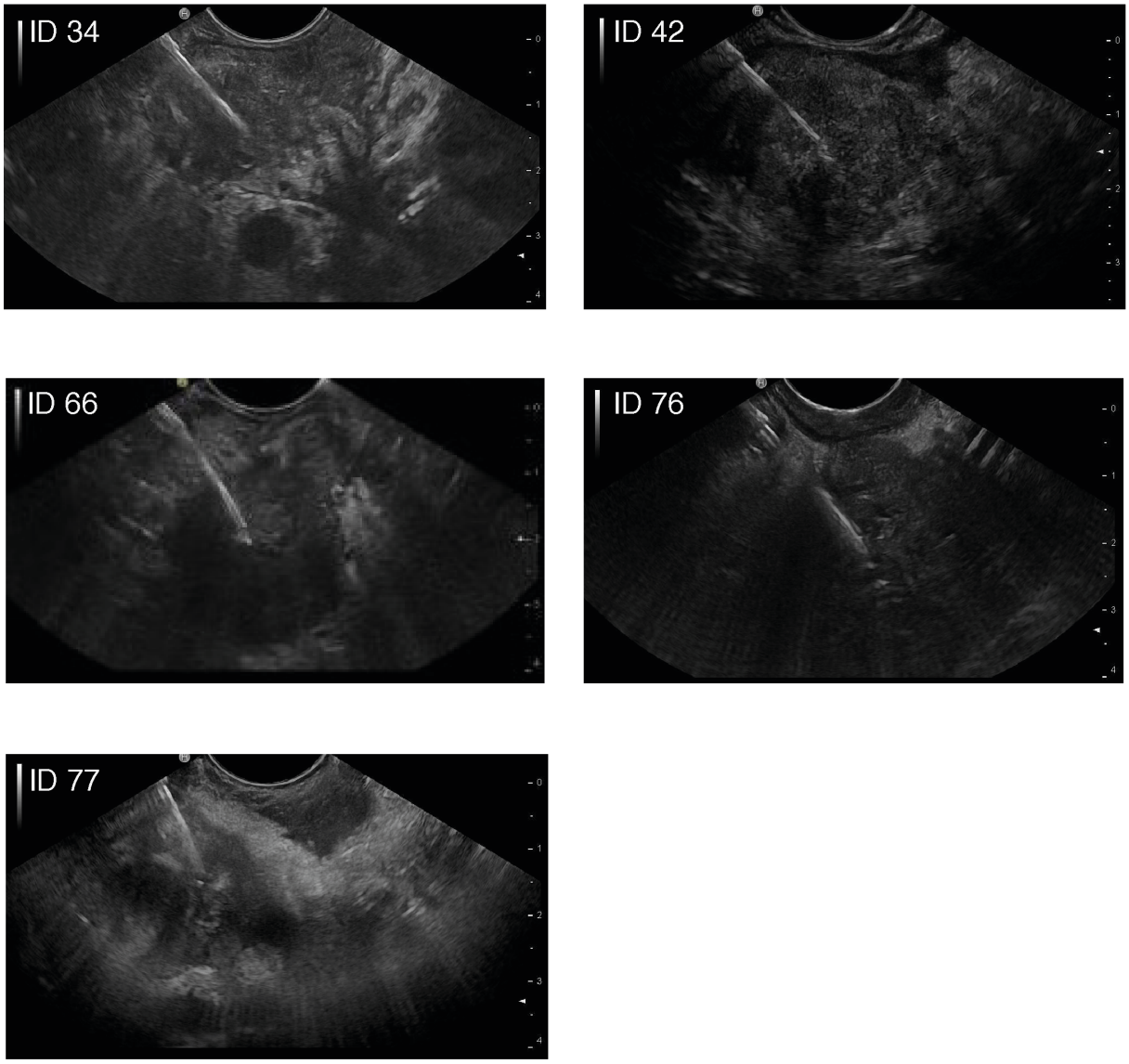

Supplementary figure 2. Endoscopic ultrasound (EUS) images of pancreatic mass and biopsy needle of indicated patients.

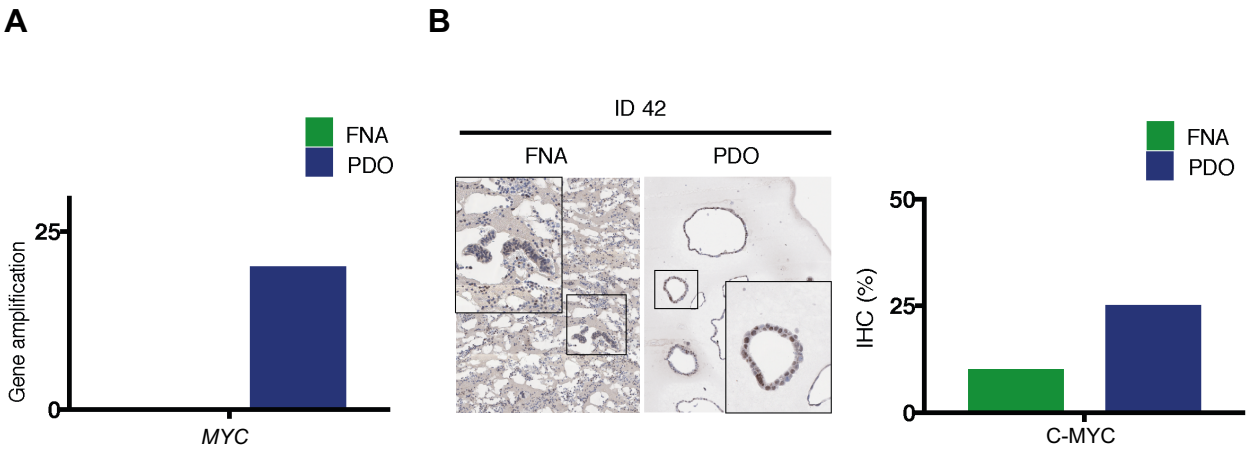

Supplementary figure 3. PDOs illustrate a high tumor cell enrichment. **A.** *MYC* expression on the genomic level based on NGS in PT and PDO. **B.** C-MYC staining of primary tumor (FNA) and corresponding PDO.

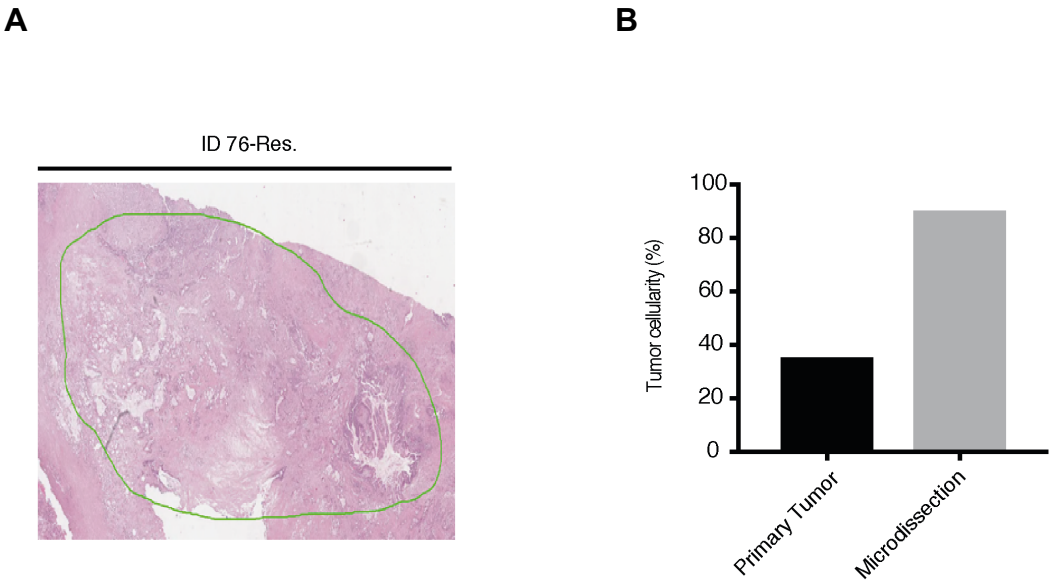

Supplementary figure 4. A. Representative image of primary tumor in patient ID 76 illustrating the tumor/stroma ratio. **B.** Comparison of tumor cellularity in the primary tumor versus microdissected area in patient 76.

Patient-ID	Gender	Age	Needle	PDO growth rate*	Histopathology/Cytology	Invasion/ Metastasis	Therapy
PDO 34	F	84	22G	***	Negative	-	gemcitabine
PDO 42	F	81	22G	***	Positive-few tumor cells	V. linealis	gemcitabine and nab-paclitaxel
PDO 66	M	75	22G	***	Negative	-	n.a.
PDO 76	F	68	20G	**	Suspicious	-	Surgery/ gemcitabine and nab-paclitaxel
PDO 77	M	74	20G	*	Suspicious	Liver	Surgery/ gemcitabine and nab-paclitaxel

*PDO growth rate: *<1 passage/week, ** 1-2 passages/week, ***>2 passages/week).

Supplementary Table 1. Patients with EUS-FNA for initial diagnosis and PDO generation.

PDO-Nr	Gene	Acc-No	Mutation			Percentage PDO	Percentage PT	Percentage PDOX	Percentage SN
PDO 34	*KRAS*	NM_004985	exon 2	c.35G>A	p.G12D	99,7%	n.a.	99,3%	
	TRRAP	NM_003496	exon 36	c.5131A>G	p.M1711V	40,1%		40,3%	
	CDKN2A	NM_000077	exon 1	c.132C>G	p.Y44*	100,0%		100,0%	
	SMAD4	NM_005359	exon 12	c.1585delT	p.L529Yfs*8	100,0%		99,8%	
PDO 42	*KRAS*	NM_004985	exon 2	c.35G>T	p.G12V	50,0%	38,0%		44,0%
	JAK1	NM_002227	exon 15	c.2050G>C	p.D684H	36,4%	15,2%		44,4%
	CDKN2A	NM_000077	exon 1	c.47_50delTGGC	p.L16Pfs*9	100,0%	not present		75%
	TP53	NM_000546	exon 5	c.469G>T	p.V157F	100,0%	40,0%		98,0%
	ZNF521	NM_015461	exon 4	c.1078G>C	p.D360H	56,7%	53,2%		81,8%
	ZNF521	NM_015461	exon 4	c.1992G>C	p.L664F	68,2%	53,9%		75,3%
	KDM6A	NM_021140	exon 17	c.2049delC	p.T684Pfs*7	100,0%	36,3%		not analyzable
	MYC	gene amplification				>20 gene copies	not present		>20 gene copies
PDO 66	*KRAS*	NM_004985	exon 2	c.35G>A	p.G12D	50,0%	n.a.		
	FLT4	NM_182925	exon 3	c.247G>A	p.D83N	29,0%			
	TP53	NM_000546	exon 6	c.662_665dup	p.P223Afs*3	97%			
PDO 76	*KRAS*	NM_004985	exon 2	c.35G>A	p.G12D	26,0%	20,7%		
	CDKN2A	NM_000077	exon 1	c.126T>A	p.N42K	25,6%	26,7%		
	NLRP1	NM_033004	exon 4	c.658A>G	p.R220G	38,1%	37,6%		
	TP53	NM_000546	exon 5	c.395A>G	p.K132R	25,0%	26,4%		
PDO 77	*KRAS*	NM_004985	exon 2	c.35G>T	p.G12V	44,0%	42,4%		
	WRN	NM_000553	exon 17	c.1975G>T	p.D659Y	100,0%	22,2%		
	TP53	NM_000546	exon 6	c.637C>T	p.R213*	100,0%	39,8%		
	COL1A1	NM_000088	exon 35	c.2420C>A	p.P807H	48,4%	53,9%		
	JAK3	NM_000215	exon 18	c.2398G>T	p.D800Y	40,0%	13,2%		
	KDM6A	NM_021140	exon 16	c.1824_1827dup	p.Q611Pfs*11	97,7%	34,7%		
	KAT6A	gene amplification				~8-10 gene copies	~4-8gene copies		
	CDKN2A	full gene deletion				homozygous	not present		
	CDKN2B								

Supplementary Table 2. Summary of type of mutations in PDO, PT, PDOX and SN.
n.a.: not available.

REFERENCES

Bailey, P., Chang, D.K., Nones, K., Johns, A.L., Patch, A.M., Gingras, M.C., Miller, D.K., Christ, A.N., Bruxner, T.J., Quinn, M.C.*, et al.* (2016). Genomic analyses identify molecular subtypes of pancreatic cancer. Nature *531*, 47-52.

Baker, L.A., Tiriac, H., Clevers, H., and Tuveson, D.A. (2016). Modeling pancreatic cancer with organoids. Trends Cancer *2*, 176-190.

Barker, N., Huch, M., Kujala, P., van de Wetering, M., Snippert, H.J., van Es, J.H., Sato, T., Stange, D.E., Begthel, H., van den Born, M.*, et al.* (2010). Lgr5(+ve) stem cells drive self-renewal in the stomach and build long-lived gastric units in vitro. Cell Stem Cell *6*, 25-36.

Blokzijl, F., de Ligt, J., Jager, M., Sasselli, V., Roerink, S., Sasaki, N., Huch, M., Boymans, S., Kuijk, E., Prins, P.*, et al.* (2016). Tissue-specific mutation accumulation in human adult stem cells during life. Nature *538*, 260-264.

Boj, S.F., Hwang, C.I., Baker, L.A., Chio, II, Engle, D.D., Corbo, V., Jager, M., Ponz-Sarvise, M., Tiriac, H., Spector, M.S.*, et al.* (2015). Organoid models of human and mouse ductal pancreatic cancer. Cell *160*, 324-338.

Boj, S.F., Hwang, C.I., Baker, L.A., Engle, D.D., Tuveson, D.A., and Clevers, H. (2016). Model organoids provide new research opportunities for ductal pancreatic cancer. Mol Cell Oncol *3*, e1014757.

Breslin, S., and O'Driscoll, L. (2013). Three-dimensional cell culture: the missing link in drug discovery. Drug Discov Today *18*, 240-249.

Broutier, L., Andersson-Rolf, A., Hindley, C.J., Boj, S.F., Clevers, H., Koo, B.K., and Huch, M. (2016). Culture and establishment of self-renewing human and mouse adult liver and pancreas 3D organoids and their genetic manipulation. Nat Protoc *11*, 1724-1743.

Burris, H.A., 3rd, Moore, M.J., Andersen, J., Green, M.R., Rothenberg, M.L., Modiano, M.R., Cripps, M.C., Portenoy, R.K., Storniolo, A.M., Tarassoff, P.*, et al.* (1997). Improvements in survival and clinical benefit with gemcitabine as first-line therapy for patients with advanced pancreas cancer: a randomized trial. J Clin Oncol *15*, 2403-2413.

Cancer Genome Atlas (2017). Integrated Genomic Charakterization of Pancreatic Ductal Adenocarcinoma. Cancer Cell *32*, 185-203.

Cantrell, M.A., and Kuo, C.J. (2015). Organoid modeling for cancer precision medicine. Genome Med *7*, 32.

Caponigro, G., and Sellers, W.R. (2011). Advances in the preclinical testing of cancer therapeutic hypotheses. Nat Rev Drug Discov *10*, 179-187.

Cho, H., Ackerstaff, E., Carlin, S., Lupu, M.E., Wang, Y., Rizwan, A., O'Donoghue, J., Ling, C.C., Humm, J.L., Zanzonico, P.B.*, et al.* (2009). Noninvasive multimodality imaging of the tumor microenvironment: registered dynamic magnetic resonance imaging and positron

emission tomography studies of a preclinical tumor model of tumor hypoxia. Neoplasia *11*, 247-259, 242p following 259.

Clevers, H. (2016). Modeling Development and Disease with Organoids. Cell *165*, 1586-1597.

Collisson, E.A., Sadanandam, A., Olson, P., Gibb, W.J., Truitt, M., Gu, S., Cooc, J., Weinkle, J., Kim, G.E., Jakkula, L.*, et al.* (2011). Subtypes of pancreatic ductal adenocarcinoma and their differing responses to therapy. Nat Med *17*, 500-503.

Colucci, G., Giuliani, F., Gebbia, V., Biglietto, M., Rabitti, P., Uomo, G., Cigolari, S., Testa, A., Maiello, E., and Lopez, M. (2002). Gemcitabine alone or with cisplatin for the treatment of patients with locally advanced and/or metastatic pancreatic carcinoma: a prospective, randomized phase III study of the Gruppo Oncologia dell'Italia Meridionale. Cancer *94*, 902-910.

Colucci, G., Labianca, R., Di Costanzo, F., Gebbia, V., Carteni, G., Massidda, B., Dapretto, E., Manzione, L., Piazza, E., Sannicolo, M.*, et al.* (2010). Randomized phase III trial of gemcitabine plus cisplatin compared with single-agent gemcitabine as first-line treatment of patients with advanced pancreatic cancer: the GIP-1 study. J Clin Oncol *28*, 1645-1651.

Conroy, T., Desseigne, F., Ychou, M., Bouche, O., Guimbaud, R., Becouarn, Y., Adenis, A., Raoul, J.L., Gourgou-Bourgade, S., de la Fouchardiere, C.*, et al.* (2011). FOLFIRINOX versus gemcitabine for metastatic pancreatic cancer. N Engl J Med *364*, 1817-1825.

Cowley, M.J., Chang, D.K., Pajic, M., Johns, A.L., Waddell, N., Grimmond, S.M., and Biankin, A.V. (2013). Understanding pancreatic cancer genomes. J Hepatobiliary Pancreat Sci *20*, 549-556.

Daniel, V.C., Marchionni, L., Hierman, J.S., Rhodes, J.T., Devereux, W.L., Rudin, C.M., Yung, R., Parmigiani, G., Dorsch, M., Peacock, C.D.*, et al.* (2009). A primary xenograft model of small-cell lung cancer reveals irreversible changes in gene expression imposed by culture in vitro. Cancer Res *69*, 3364-3373.

Deer, E.L., Gonzalez-Hernandez, J., Coursen, J.D., Shea, J.E., Ngatia, J., Scaife, C.L., Firpo, M.A., and Mulvihill, S.J. (2010). Phenotype and genotype of pancreatic cancer cell lines. Pancreas *39*, 425-435.

Dekkers, J.F., Wiegerinck, C.L., de Jonge, H.R., Bronsveld, I., Janssens, H.M., de Winter-de Groot, K.M., Brandsma, A.M., de Jong, N.W., Bijvelds, M.J., Scholte, B.J.*, et al.* (2013). A functional CFTR assay using primary cystic fibrosis intestinal organoids. Nat Med *19*, 939-945.

Dobrynin, Y.V. (1963). Establishment and Characteristics of Cell Strains from Some Epithelial Tumors of Human Origin. J Natl Cancer Inst *31*, 1173-1195.

Drost, J., and Clevers, H. (2018). Organoids in cancer research. Nat Rev Cancer *18*, 407-418.

Drost, J., Karthaus, W.R., Gao, D., Driehuis, E., Sawyers, C.L., Chen, Y., and Clevers, H. (2016). Organoid culture systems for prostate epithelial and cancer tissue. Nat Protoc *11*, 347-358.

Drost, J., van Boxtel, R., Blokzijl, F., Mizutani, T., Sasaki, N., Sasselli, V., de Ligt, J., Behjati, S., Grolleman, J.E., van Wezel, T.*, et al.* (2017). Use of CRISPR-modified human stem cell organoids to study the origin of mutational signatures in cancer. Science *358*, 234-238.

Drost, J., van Jaarsveld, R.H., Ponsioen, B., Zimberlin, C., van Boxtel, R., Buijs, A., Sachs, N., Overmeer, R.M., Offerhaus, G.J., Begthel, H.*, et al.* (2015). Sequential cancer mutations in cultured human intestinal stem cells. Nature *521*, 43-47.

Du, Y., Zhao, B., Liu, Z., Ren, X., Zhao, W., Li, Z., You, L., and Zhao, Y. (2017). Molecular Subtyping of Pancreatic Cancer: Translating Genomics and Transcriptomics into the Clinic. J Cancer *8*, 513-522.

Dutta, D., Heo, I., and Clevers, H. (2017). Disease Modeling in Stem Cell-Derived 3D Organoid Systems. Trends Mol Med *23*, 393-410.

Endris, V., Penzel, R., Warth, A., Muckenhuber, A., Schirmacher, P., Stenzinger, A., and Weichert, W. (2013). Molecular diagnostic profiling of lung cancer specimens with a semiconductor-based massive parallel sequencing approach: feasibility, costs, and performance compared with conventional sequencing. J Mol Diagn *15*, 765-775.

Forbes, S.A., Beare, D., Gunasekaran, P., Leung, K., Bindal, N., Boutselakis, H., Ding, M., Bamford, S., Cole, C., Ward, S.*, et al.* (2015). COSMIC: exploring the world's knowledge of somatic mutations in human cancer. Nucleic Acids Res *43*, D805-811.

Frese, K.K., and Tuveson, D.A. (2007). Maximizing mouse cancer models. Nat Rev Cancer *7*, 645-658.

Froeling, F.E., Marshall, J.F., and Kocher, H.M. (2010). Pancreatic cancer organotypic cultures. J Biotechnol *148*, 16-23.

Fujii, M., Shimokawa, M., Date, S., Takano, A., Matano, M., Nanki, K., Ohta, Y., Toshimitsu, K., Nakazato, Y., Kawasaki, K.*, et al.* (2016). A Colorectal Tumor Organoid Library Demonstrates Progressive Loss of Niche Factor Requirements during Tumorigenesis. Cell Stem Cell *18*, 827-838.

Gadaleta, E., Cutts, R.J., Kelly, G.P., Crnogorac-Jurcevic, T., Kocher, H.M., Lemoine, N.R., and Chelala, C. (2011). A global insight into a cancer transcriptional space using pancreatic data: importance, findings and flaws. Nucleic Acids Res *39*, 7900-7907.

Garrido-Laguna, I., and Hidalgo, M. (2015). Pancreatic cancer: from state-of-the-art treatments to promising novel therapies. Nat Rev Clin Oncol *12*, 319-334.

Gelse, K., Poschl, E., and Aigner, T. (2003). Collagens--structure, function, and biosynthesis. Adv Drug Deliv Rev *55*, 1531-1546.

Gillet, J.P., Varma, S., and Gottesman, M.M. (2013). The clinical relevance of cancer cell lines. J Natl Cancer Inst *105*, 452-458.

Gurski, L.A., Petrelli, N.J., Jia, X., Farach-Carson, M.C. (2010) 3D matrices for anti-cancer drug testing and development. Oncology issues. Jan-Feb, 20–25

Heinemann, V., Quietzsch, D., Gieseler, F., Gonnermann, M., Schonekas, H., Rost, A., Neuhaus, H., Haag, C., Clemens, M., Heinrich, B.*, et al.* (2006). Randomized phase III trial of gemcitabine plus cisplatin compared with gemcitabine alone in advanced pancreatic cancer. J Clin Oncol *24*, 3946-3952.

Hidalgo, M., Cascinu, S., Kleeff, J., Labianca, R., Lohr, J.M., Neoptolemos, J., Real, F.X., Van Laethem, J.L., and Heinemann, V. (2015). Addressing the challenges of pancreatic cancer: future directions for improving outcomes. Pancreatology *15*, 8-18.

Hingorani, S.R., Petricoin, E.F., Maitra, A., Rajapakse, V., King, C., Jacobetz, M.A., Ross, S., Conrads, T.P., Veenstra, T.D., Hitt, B.A.*, et al.* (2003). Preinvasive and invasive ductal pancreatic cancer and its early detection in the mouse. Cancer Cell *4*, 437-450.

Hingorani, S.R., Wang, L., Multani, A.S., Combs, C., Deramaudt, T.B., Hruban, R.H., Rustgi, A.K., Chang, S., and Tuveson, D.A. (2005). Trp53R172H and KrasG12D cooperate to promote chromosomal instability and widely metastatic pancreatic ductal adenocarcinoma in mice. Cancer Cell *7*, 469-483.

Huang, L., Holtzinger, A., Jagan, I., BeGora, M., Lohse, I., Ngai, N., Nostro, C., Wang, R., Muthuswamy, L.B., Crawford, H.C.*, et al.* (2015). Ductal pancreatic cancer modeling and drug screening using human pluripotent stem cell- and patient-derived tumor organoids. Nat Med *21*, 1364-1371.

Huch, M., Boj, S.F., and Clevers, H. (2013a). Lgr5(+) liver stem cells, hepatic organoids and regenerative medicine. Regen Med *8*, 385-387.

Huch, M., Bonfanti, P., Boj, S.F., Sato, T., Loomans, C.J., van de Wetering, M., Sojoodi, M., Li, V.S., Schuijers, J., Gracanin, A.*, et al.* (2013b). Unlimited in vitro expansion of adult bi-potent pancreas progenitors through the Lgr5/R-spondin axis. EMBO J *32*, 2708-2721.

Huch, M., Gehart, H., van Boxtel, R., Hamer, K., Blokzijl, F., Verstegen, M.M., Ellis, E., van Wenum, M., Fuchs, S.A., de Ligt, J.*, et al.* (2015). Long-term culture of genome-stable bipotent stem cells from adult human liver. Cell *160*, 299-312.

Hwang, C.I., Boj, S.F., Clevers, H., and Tuveson, D.A. (2016). Preclinical models of pancreatic ductal adenocarcinoma. J Pathol *238*, 197-204.

Jin, K., Teng, L., Shen, Y., He, K., Xu, Z., and Li, G. (2010). Patient-derived human tumour tissue xenografts in immunodeficient mice: a systematic review. Clin Transl Oncol *12*, 473-480.

Jin, M.Z., Han, R.R., Qiu, G.Z., Ju, X.C., Lou, G., and Jin, W.L. (2018). Organoids: An intermediate modeling platform in precision oncology. Cancer Lett *414*, 174-180.

Jung, J., Lee, C.H., Seol, H.S., Choi, Y.S., Kim, E., Lee, E.J., Rhee, J.K., Singh, S.R., Jun, E.S., Han, B.*, et al.* (2016). Generation and molecular characterization of pancreatic cancer patient-derived xenografts reveals their heterologous nature. Oncotarget *7*, 62533-62546.

Khoshnoodi, J., Pedchenko, V., and Hudson, B.G. (2008). Mammalian collagen IV. Microsc Res Tech *71*, 357-370.

Kleinman, H.K., and Martin, G.R. (2005). Matrigel: basement membrane matrix with biological activity. Semin Cancer Biol *15*, 378-386.

Kondo, J., Endo, H., Okuyama, H., Ishikawa, O., Iishi, H., Tsujii, M., Ohue, M., and Inoue, M. (2011). Retaining cell-cell contact enables preparation and culture of spheroids composed of pure primary cancer cells from colorectal cancer. Proc Natl Acad Sci U S A *108*, 6235-6240.

Kumar, K., Chow, C.R., Ebine, K., Arslan, A.D., Kwok, B., Bentrem, D.J., Eckerdt, F.D., Platanias, L.C., and Munshi, H.G. (2016). Differential Regulation of ZEB1 and EMT by MAPK-Interacting Protein Kinases (MNK) and eIF4E in Pancreatic Cancer. Mol Cancer Res *14*, 216-227.

Lek, M., Karczewski, K.J., Minikel, E.V., Samocha, K.E., Banks, E., Fennell, T., O'Donnell-Luria, A.H., Ware, J.S., Hill, A.J., Cummings, B.B.*, et al.* (2016). Analysis of protein-coding genetic variation in 60,706 humans. Nature *536*, 285-291.

Li, X., Nadauld, L., Ootani, A., Corney, D.C., Pai, R.K., Gevaert, O., Cantrell, M.A., Rack, P.G., Neal, J.T., Chan, C.W.*, et al.* (2014). Oncogenic transformation of diverse gastrointestinal tissues in primary organoid culture. Nat Med *20*, 769-777.

Louvet, C., Labianca, R., Hammel, P., Lledo, G., Zampino, M.G., Andre, T., Zaniboni, A., Ducreux, M., Aitini, E., Taieb, J.*, et al.* (2005). Gemcitabine in combination with oxaliplatin compared with gemcitabine alone in locally advanced or metastatic pancreatic cancer: results of a GERCOR and GISCAD phase III trial. J Clin Oncol *23*, 3509-3516.

Macosko, E.Z., Basu, A., Satija, R., Nemesh, J., Shekhar, K., Goldman, M., Tirosh, I., Bialas, A.R., Kamitaki, N., Martersteck, E.M.*, et al.* (2015). Highly Parallel Genome-wide Expression Profiling of Individual Cells Using Nanoliter Droplets. Cell *161*, 1202-1214.

Matano, M., Date, S., Shimokawa, M., Takano, A., Fujii, M., Ohta, Y., Watanabe, T., Kanai, T., and Sato, T. (2015). Modeling colorectal cancer using CRISPR-Cas9-mediated engineering of human intestinal organoids. Nat Med *21*, 256-262.

Moffitt, R.A., Marayati, R., Flate, E.L., Volmar, K.E., Loeza, S.G., Hoadley, K.A., Rashid, N.U., Williams, L.A., Eaton, S.C., Chung, A.H.*, et al.* (2015). Virtual microdissection identifies

distinct tumor- and stroma-specific subtypes of pancreatic ductal adenocarcinoma. Nat Genet *47*, 1168-1178.

Moreira, L., Bakir, B., Chatterji, P., Dantes, Z., Reichert, M., and Rustgi, A.K. (2018). Pancreas 3D Organoids: Current and Future Aspects as a Research Platform for Personalized Medicine in Pancreatic Cancer. Cell Mol Gastroenterol Hepatol *5*, 289-298.

Muckenhuber, A., Berger, A.K., Schlitter, A.M., Steiger, K., Konukiewitz, B., Trumpp, A., Eils, R., Werner, J., Friess, H., Esposito, I.*, et al.* (2018). Pancreatic Ductal Adenocarcinoma Subtyping Using the Biomarkers Hepatocyte Nuclear Factor-1A and Cytokeratin-81 Correlates with Outcome and Treatment Response. Clin Cancer Res *24*, 351-359.

Noll, E.M., Eisen, C., Stenzinger, A., Espinet, E., Muckenhuber, A., Klein, C., Vogel, V., Klaus, B., Nadler, W., Rosli, C.*, et al.* (2016). CYP3A5 mediates basal and acquired therapy resistance in different subtypes of pancreatic ductal adenocarcinoma. Nat Med *22*, 278-287.

Oberstein, P.E., and Olive, K.P. (2013). Pancreatic cancer: why is it so hard to treat? Therap Adv Gastroenterol *6*, 321-337.

Oettle, H., Richards, D., Ramanathan, R.K., van Laethem, J.L., Peeters, M., Fuchs, M., Zimmermann, A., John, W., Von Hoff, D., Arning, M.*, et al.* (2005). A phase III trial of pemetrexed plus gemcitabine versus gemcitabine in patients with unresectable or metastatic pancreatic cancer. Ann Oncol *16*, 1639-1645.

Parekh, S., Ziegenhain, C., Vieth, B., Enard, W., and Hellmann, I. (2016). The impact of amplification on differential expression analyses by RNA-seq. Sci. Rep *6*, 25533.

Pauli, C., Hopkins, B.D., Prandi, D., Shaw, R., Fedrizzi, T., Sboner, A., Sailer, V., Augello, M., Puca, L., Rosati, R.*, et al.* (2017). Personalized In Vitro and In Vivo Cancer Models to Guide Precision Medicine. Cancer Discov *7*, 462-477.

Perez-Mancera, P.A., Guerra, C., Barbacid, M., and Tuveson, D.A. (2012). What we have learned about pancreatic cancer from mouse models. Gastroenterology *142*, 1079-1092.

Peterson, J.K., and Houghton, P.J. (2004). Integrating pharmacology and in vivo cancer models in preclinical and clinical drug development. Eur J Cancer *40*, 837-844.

Pfarr, N., Darb-Esfahani, S., Leichsenring, J., Taube, E., Boxberg, M., Braicu, I., Jesinghaus, M., Penzel, R., Endris, V., Noske, A.*, et al.* (2017a). Mutational profiles of Brenner tumors show distinctive features uncoupling urothelial carcinomas and ovarian carcinoma with transitional cell histology. Genes Chromosomes Cancer *56*, 758-766.

Pfarr, N., Penzel, R., Endris, V., Lier, C., Flechtenmacher, C., Volckmar, A.L., Kirchner, M., Budczies, J., Leichsenring, J., Herpel, E.*, et al.* (2017b). Targeted next-generation sequencing enables reliable detection of HER2 (ERBB2) status in breast cancer and provides ancillary information of clinical relevance. Genes Chromosomes Cancer *56*, 255-265.

Philip, P.A., Benedetti, J., Corless, C.L., Wong, R., O'Reilly, E.M., Flynn, P.J., Rowland, K.M., Atkins, J.N., Mirtsching, B.C., Rivkin, S.E.*, et al.* (2010). Phase III study comparing gemcitabine plus cetuximab versus gemcitabine in patients with advanced pancreatic adenocarcinoma: Southwest Oncology Group-directed intergroup trial S0205. J Clin Oncol *28*, 3605-3610.

Poplin, E., Feng, Y., Berlin, J., Rothenberg, M.L., Hochster, H., Mitchell, E., Alberts, S., O'Dwyer, P., Haller, D., Catalano, P.*, et al.* (2009). Phase III, randomized study of gemcitabine and oxaliplatin versus gemcitabine (fixed-dose rate infusion) compared with gemcitabine (30-minute infusion) in patients with pancreatic carcinoma E6201: a trial of the Eastern Cooperative Oncology Group. J Clin Oncol *27*, 3778-3785.

Quante, A.S., Ming, C., Rottmann, M., Engel, J., Boeck, S., Heinemann, V., Westphalen, C.B., and Strauch, K. (2016). Projections of cancer incidence and cancer-related deaths in Germany by 2020 and 2030. Cancer Med *5*, 2649-2656.

Rahib, L., Smith, B.D., Aizenberg, R., Rosenzweig, A.B., Fleshman, J.M., and Matrisian, L.M. (2014). Projecting cancer incidence and deaths to 2030: the unexpected burden of thyroid, liver, and pancreas cancers in the United States. Cancer Res *74*, 2913-2921.

Reichert, M., Takano, S., Heeg, S., Bakir, B., Botta, G.P., and Rustgi, A.K. (2013). Isolation, culture and genetic manipulation of mouse pancreatic ductal cells. Nat Protoc *8*, 1354-1365.

Rimann, M., and Graf-Hausner, U. (2012). Synthetic 3D multicellular systems for drug development. Curr Opin Biotechnol *23*, 803-809.

Rocha Lima, C.M., Rizvi, N.A., Zhang, C., Herndon, J.E., 2nd, Crawford, J., Govindan, R., King, G.W., Green, M.R., and Cancer Leukemia Group, B. (2004). Randomized phase II trial of gemcitabine plus irinotecan or docetaxel in stage IIIB or stage IV NSCLC. Ann Oncol *15*, 410-418.

Rubio-Viqueira, B., Jimeno, A., Cusatis, G., Zhang, X., Iacobuzio-Donahue, C., Karikari, C., Shi, C., Danenberg, K., Danenberg, P.V., Kuramochi, H.*, et al.* (2006). An in vivo platform for translational drug development in pancreatic cancer. Clin Cancer Res *12*, 4652-4661.

Ruckert, F., Aust, D., Bohme, I., Werner, K., Brandt, A., Diamandis, E.P., Krautz, C., Hering, S., Saeger, H.D., Grutzmann, R.*, et al.* (2012). Five primary human pancreatic adenocarcinoma cell lines established by the outgrowth method. J Surg Res *172*, 29-39.

Ruess, D.A., Gorgulu, K., Wormann, S.M., and Algul, H. (2017). Pharmacotherapeutic Management of Pancreatic Ductal Adenocarcinoma: Current and Emerging Concepts. Drugs Aging *34*, 331-357.

Russo, M., Siravegna, G., Blaszkowsky, L.S., Corti, G., Crisafulli, G., Ahronian, L.G., Mussolin, B., Kwak, E.L., Buscarino, M., Lazzari, L.*, et al.* (2016). Tumor Heterogeneity and

Lesion-Specific Response to Targeted Therapy in Colorectal Cancer. Cancer Discov *6*, 147-153.

Ryan, D.P., Hong, T.S., and Bardeesy, N. (2014). Pancreatic adenocarcinoma. N Engl J Med *371*, 2140-2141.

Sato, T., and Clevers, H. (2013). Growing self-organizing mini-guts from a single intestinal stem cell: mechanism and applications. Science *340*, 1190-1194.

Sato, T., Vries, R.G., Snippert, H.J., van de Wetering, M., Barker, N., Stange, D.E., van Es, J.H., Abo, A., Kujala, P., Peters, P.J.*, et al.* (2009). Single Lgr5 stem cells build crypt-villus structures in vitro without a mesenchymal niche. Nature *459*, 262-265.

Schutte, M., Risch, T., Abdavi-Azar, N., Boehnke, K., Schumacher, D., Keil, M., Yildiriman, R., Jandrasits, C., Borodina, T., Amstislavskiy, V.*, et al.* (2017). Molecular dissection of colorectal cancer in pre-clinical models identifies biomarkers predicting sensitivity to EGFR inhibitors. Nat Commun *8*, 14262.

Shields, M.A., Dangi-Garimella, S., Redig, A.J., and Munshi, H.G. (2012). Biochemical role of the collagen-rich tumour microenvironment in pancreatic cancer progression. Biochem J *441*, 541-552.

Siegel, R.L., Miller, K.D., and Jemal, A. (2018). Cancer statistics, 2018. CA Cancer J Clin *68*, 7-30.

Stathopoulos, G.P., Syrigos, K., Aravantinos, G., Polyzos, A., Papakotoulas, P., Fountzilas, G., Potamianou, A., Ziras, N., Boukovinas, J., Varthalitis, J.*, et al.* (2006). A multicenter phase III trial comparing irinotecan-gemcitabine (IG) with gemcitabine (G) monotherapy as first-line treatment in patients with locally advanced or metastatic pancreatic cancer. Br J Cancer *95*, 587-592.

Stein, W.D., Litman, T., Fojo, T., and Bates, S.E. (2004). A Serial Analysis of Gene Expression (SAGE) database analysis of chemosensitivity: comparing solid tumors with cell lines and comparing solid tumors from different tissue origins. Cancer Res *64*, 2805-2816.

Taub, M., Wang, Y., Szczesny, T.M., and Kleinman, H.K. (1990). Epidermal growth factor or transforming growth factor alpha is required for kidney tubulogenesis in matrigel cultures in serum-free medium. Proc Natl Acad Sci U S A *87*, 4002-4006.

Tentler, J.J., Tan, A.C., Weekes, C.D., Jimeno, A., Leong, S., Pitts, T.M., Arcaroli, J.J., Messersmith, W.A., and Eckhardt, S.G. (2012). Patient-derived tumour xenografts as models for oncology drug development. Nat Rev Clin Oncol *9*, 338-350.

Tiriac, H., Belleau, P., Engle, D.D., Plenker, D., Deschenes, A., Somerville, T., Froeling, F.E.M., Burkhart, R.A., Denroche, R.E., Jang, G.H.*, et al.* (2018a). Organoid profiling identifies common responders to chemotherapy in pancreatic cancer. Cancer Discov.

Tiriac, H., Bucobo, J.C., Tzimas, D., Grewel, S., Lacomb, J.F., Rowehl, L.M., Nagula, S., Wu, M., Kim, J., Sasson, A.*, et al.* (2018b). Successful creation of pancreatic cancer

organoids by means of EUS-guided fine-needle biopsy sampling for personalized cancer treatment. Gastrointest Endosc *87*, 1474-1480.

Torres, C., and Grippo, P.J. (2018). Pancreatic cancer subtypes: a roadmap for precision medicine. Ann Med *50*, 277-287.

van de Wetering, M., Francies, H.E., Francis, J.M., Bounova, G., Iorio, F., Pronk, A., van Houdt, W., van Gorp, J., Taylor-Weiner, A., Kester, L.*, et al.* (2015). Prospective derivation of a living organoid biobank of colorectal cancer patients. Cell *161*, 933-945.

Vlachogiannis, G., Hedayat, S., Vatsiou, A., Jamin, Y., Fernandez-Mateos, J., Khan, K., Lampis, A., Eason, K., Huntingford, I., Burke, R.*, et al.* (2018). Patient-derived organoids model treatment response of metastatic gastrointestinal cancers. Science *359*, 920-926.

Von Figura, G. & Reichert, M. (2018). Pankreaskarzinom - neue Konzepte? Gastroenterologe *13*, 450-454.

Von Hoff, D.D., Ervin, T., Arena, F.P., Chiorean, E.G., Infante, J., Moore, M., Seay, T., Tjulandin, S.A., Ma, W.W., Saleh, M.N.*, et al.* (2013). Increased survival in pancreatic cancer with nab-paclitaxel plus gemcitabine. N Engl J Med *369*, 1691-1703.

Voskoglou-Nomikos, T., Pater, J.L., and Seymour, L. (2003). Clinical predictive value of the in vitro cell line, human xenograft, and mouse allograft preclinical cancer models. Clin Cancer Res *9*, 4227-4239.

Vukicevic, S., Kleinman, H.K., Luyten, F.P., Roberts, A.B., Roche, N.S., and Reddi, A.H. (1992). Identification of multiple active growth factors in basement membrane Matrigel suggests caution in interpretation of cellular activity related to extracellular matrix components. Exp Cell Res *202*, 1-8.

Waddell, N., Pajic, M., Patch, A.M., Chang, D.K., Kassahn, K.S., Bailey, P., Johns, A.L., Miller, D., Nones, K., Quek, K.*, et al.* (2015). Whole genomes redefine the mutational landscape of pancreatic cancer. Nature *518*, 495-501.

Walsh, A.J., Castellanos, J.A., Nagathihalli, N.S., Merchant, N.B., and Skala, M.C. (2016). Optical Imaging of Drug-Induced Metabolism Changes in Murine and Human Pancreatic Cancer Organoids Reveals Heterogeneous Drug Response. Pancreas *45*, 863-869.

Wang, K., Li, M., and Hakonarson, H. (2010). ANNOVAR: functional annotation of genetic variants from high-throughput sequencing data. Nucleic Acids Res *38*, e164.

Wang, S., Gao, D., and Chen, Y. (2017). The potential of organoids in urological cancer research. Nat Rev Urol *14*, 401-414.

Weeber, F., Ooft, S.N., Dijkstra, K.K., and Voest, E.E. (2017). Tumor Organoids as a Pre-clinical Cancer Model for Drug Discovery. Cell Chem Biol *24*, 1092-1100.

Weeber, F., van de Wetering, M., Hoogstraat, M., Dijkstra, K.K., Krijgsman, O., Kuilman, T., Gadellaa-van Hooijdonk, C.G., van der Velden, D.L., Peeper, D.S., Cuppen, E.P.*,*

et al. (2015). Preserved genetic diversity in organoids cultured from biopsies of human colorectal cancer metastases. Proc Natl Acad Sci U S A *112*, 13308-13311.

Westphalen, C.B., and Olive, K.P. (2012). Genetically engineered mouse models of pancreatic cancer. Cancer J *18*, 502-510.

Ychou, M., Conroy, T., Seitz, J.F., Gourgou, S., Hua, A., Mery-Mignard, D., and Kramar, A. (2003). An open phase I study assessing the feasibility of the triple combination: oxaliplatin plus irinotecan plus leucovorin/ 5-fluorouracil every 2 weeks in patients with advanced solid tumors. Ann Oncol *14*, 481-489.

PUBLICATIONS, PRESENTATIONS AND AWARDS

Parts of this thesis was included in the following publication

Dantes Z, Yen HS, Pfarr N, Winter C, Steiger K, Muckenhuber A, Hennig A, Heid I, Kaissis G, Shi K, Topping G, Lange S, Engleitner T, Öllinger R, Wirth M, Peschke K, Rezaee-Oghazi M, Feldmann K, Lubeseder-Martellato C, Stange DE, Welsch T, Martignoni M, Ceyhan G, Friess H, Herner A,Liotta L, Treiber M, Von Figura G, Abdelhafez M, Klare P, Schlag C, Siveke J, Braren R, Weirich G, Weichert W, Saur D, Rad R, Schmid R, Schneider G and Reichert M. (2018). Utilizing Patient-Derived Organoids from Fine Needle Aspiration as Diagnostic Research Platforms for Personalized Medicine in Pancreatic Ductal Adenocarcinoma. **Manuscript under revision in Gut**.

Submitted for publications

Lesch S, Blumenberg V, Stoiber S, Ogonek J, Cadilha B, **Dantes Z**, Rataj F, Dorman K, Lutz J, Karches C. H, Heise C, Kurzay M, Grassmann S, Rapp M, Megens R.T, Janssen K.P, Jastrosch M, Lamp D, Ruehland S, Pilato M.D., Pruessmann J.N, Ormanns S, Reischer A, Hristov M, Rothenfusser S, Duewell P, Schnurr M, Subklewe M, Reichert M, Mempel T.R, Endres S and Kobold S. Arming T cells with C-X-C-motive receptor 6 enables adoptive T cell therapy of cancer. Manuscript under preparation for submission.

Hidalgo-Sastre*, **Dantes Z***, Desztics J*, Schulte K*, Kabadayi H, Ollinger R, Engleitner E, Blessing B, Lyndsay R , Daniel J, Steiger K, Lesina M, Rad R, Reichert M, Von Figura G, Siveke J , Schmid R, Lubeseder-Martellato C. Loss of Wasl improves pancreatic cancer outcome. Manuscript under preparation for submission. ***These authors contributed equally to this work**.

Biederstädt A, Hassan Z, Schneider L, Muckenhuber A, Hong Y, Schick M, Nilsson L, Wirth M, **Dantes Z**, Schneeweis C, Steiger K, Kunz K, Siegers G, , Langston S, Lenhof, H.-P, Saur D, Müller S, Rad R, Weichert W, Nilsson J, Reichert M, Schneider G, Keller U. he SUMO Pathway as a Therapeutic Option in Pancreatic Cancer. Manuscript under revision in Gut.

Publications

Renz BW, Tanaka T, Sunagawa M, Takahashi R, Jiang Z, Macchini M, **Dantes Z**, Valenti G, White RA, Middelhoff MA, Ilmer M, Oberstein PE, Angele MK, Deng H, Hayakawa Y, Westphalen CB, Werner J, Remotti H, Reichert M, Tailor YH, Nagar K, Friedman RA, Iuga AC, Olive KP, Wang TC. Cholinergic Signaling via Muscarinic Receptors Directly and Indirectly Suppresses Pancreatic Tumorigenesis and Cancer Stemness. **Cancer Discov**. 2018 Sep 5. pii: CD-18-0046. doi: 10.1158/2159-8290.CD-18-0046.

Ruess D, Heynen GJ, Ciecielski KJ , Ai J , Berninger A , Kabacaoglu D , Görgülü K , **Dantes Z**, Wörmann SM , Diakopoulos KN , Karpathaki A , Kowalska M, Kaya-Aksoy E , Song L , van der Laan EAZ , López-Alberca MP , Nazaré M , Reichert M , Saur D , Erkan M , Hopt UT , Sainz Jr B , Birchmeier W , Schmid R , Lesina M, Algül H. Mutant KRAS-

driven cancers depend on PTPN11/SHP2 phosphatase. **Nat Med**. 2018 Jul;24(7):954-960. doi: 10.1038/s41591-018-0024-8.

Hassan Z, Schneeweis C, Wirth M, Veltkamp C, **Dantes Z**, Feuerecker B, Ceyhan GO, Knauer SK, Weichert W, Schmid RM, Stauber R, Arlt A, Krämer OH, Rad R, Reichert M, Saur D, Schneider G. MTOR inhibitor-based combination therapies for pancreatic cancer. ***Br J Cancer***. 2018 Feb 6;118(3):366-377. doi: 10.1038/bjc.2017.421.

Renz BW, Takahashi R, Tanaka T, Macchini M, Hayakawa Y, **Dantes Z**, Maurer HC, Chen X, Jiang Z, Westphalen CB, Ilmer M, Valenti G, Mohanta SK, Habenicht AJR, Middelhoff M, Chu T, Nagar K, Tailor Y, Casadei R, Di Marco M, Kleespies A, Friedman RA, Remotti H, Reichert M, Worthley DL, Neumann J, Werner J, Iuga AC, Olive KP, Wang TC. β2 Adrenergic-Neurotrophin Feed forward Loop Promotes Pancreatic Cancer. **Cancer Cell**. 2018 Jan 8;33(1):75-90.e. doi: 10.1016/j.ccell.2017.11.007.

Moreira L, Bakir B, Chatterji P, **Dantes Z**, Reichert M, Rustgi AK. Pancreas 3D Organoids: Current and Future Aspects as a research Platform for Personalized Medicine in Pancreatic Cancer. **Cell Mol Gastroenterol Hepatol**. 2017 Dec 16;5(3):289-298. doi: 10.1016/j.jcmgh.2017.12.004.

Oral presentations

- Integration of Genomics and High-Throughput Drug Screening on a Living PDAC Organoid Biobank in pure Tumor and in Micro-environmentally Enriched Cultures. 38. Jahrestagung Deutscher Pankreasclub e.V. (DPC). January 2018, Ulm, Germany.

- A Novel Predictive Organoid Culture System from Pancreatic Cancer Patients - Personalized Medicine in Realtime. Digestive Disease Week (DDW) meeting. April 2017, Chicago, USA.

- Using pancreatic cancer patient-derived organoid culture technology to develop novel diagnostics and therapeutic approaches. 71. DGVS. September 2016, Hamburg, Germany.

- Investigating the impact of genetic heterogeneity of pancreatic cancer on chemotherapeutic resistance in highthroughput drug screens. 36. Jahrestagung.Deutscher Pankreasclub e.V. (DPC). February 2016, Munich, Germany.

- Pancreatic cancer patient-derived organoids, Personalized medicine in real-time. Retreat II. Medical Department, Klinikum rechts der Isar. TUM. October 2016, Herrsching, Germany.

- Isolation and expansion of pancreatic cancer cells for molecular and functional analysis. 70. DGVS. September 2015, Leipzig, Germany.

Poster presentations

- Patient-derived organoids from endoscopic fine needle as a personalized diagnostic and prognostic tool in pancreatic ductal adenocarcinoma. AACR. Pancreatic cancer: Advances in Science and Clinical Care. September 2018, Boston, USA.

- Advanced Organoid Culture Technology in Pancreatic Cancer and its Translational Applications. 33. Deutscher Krebskongress. February 2018, Berlin, Germany.

- Translational Application of a Modified Organoid Culture System from Pancreatic Cancer Patients. First Pancreas Spring Meeting. June 2017, Göttingen, Germany.

- Patient-derived organoids to model intra- and intertumoral heterogeneity of pancreatic cancer in high-throughput drug screens. 32. Deutscher Krebskongress February 2016, Berlin, Germany.

Awards/ research funding

- Abraham-Vater-Award for ‘best talk’ category. 38. Jahrestagung des Deutschen Pankreasclubs. February 2018, Ulm, Germany.

- AGA-Moti L and Kamla Rustgi International Travel Award. Digestive Disease Week (DDW). May 2017, Chicago, USA.

- Second Award in ‘best poster’ category. Life Science Community. November 2016, Munich, Germany.